ADDIS ABABA UNIVERSITY
COLLEGE OF NATURAL SCIENCE
SCHOOL OF EARTH SCIENCES

GEOLOGICAL AND GEOTHERMAL MAPPING OF BUTAJIRA GEOTHERMAL PROSPECT, CENTRAL MAIN ETHIOPIAN RIFT (CMER); ETHIOPIA

BY

AMARE KASSIE ANDARGE

ADVISORS

GEZHAGN YIRGU (Prof.)

SOLOMON KEBEDE

A Thesis Submitted to the School of Graduate Studies of Addis Ababa University, in Partial Fulfillment of the Requirements for the Degree of Master of Science in resource geology (geothermal energy)

JAN, 2019

ADDIS ABEBA, ETHIOPIA

ADDIS ABABA UNIVERSITY

COLLEGE OF NATURAL SCIENCES

SCHOOL OF EARTH SCIENCES

SURFACE GEOLOGICAL AND GEOTHERMAL MAPPING OF BUTAJIRA GEOTHERMAL PROSPECT, CENTRAL MAIN ETHIOPIAN RIFT (CMER)

BY

AMARE KASSIE ANDARGE

ADVISORS
Prof. GEZHAGN YIRGU
Mr. SOLOMON KEBEDE

A Thesis Submitted to the School of Graduate Studies of Addis Ababa University, in Partial Fulfillment of the Requirements for the Degree of Master of Science in Resource Geology (Geothermal Energy)

Jan , 2018

ADDIS ABABA, ETHIOPIA

Abstract

Butajira geothermal prospect is located in Central Main Ethiopian Rift nearby Western escarpment associated with SDZFZ and geographically bounded between UTM 427000-437000E, 882000-891000 N with area coverage of 90 Km^2. This is among **23** geothermal prospects in Ethiopia which has undergone limited geological and geothermal investigations. The main objective of the study is to assess the existence of promising geothermal system components at the Butajira geothermal prospect through investigating the geology and surface geothermal manifestations. To achieve the desired objectives various methodologies were adopted including review of secondary data, geological field observation, Petrographic study, and XRD geochemical analysis. As a result, geological and geothermal mapping was carried out at the scale of 1:50,000, promising sites were identified and a preliminary conceptual model was presented to related identified geothermal play type.

The main lithological units encompassed in the area are Basaltic Scoria, Basaltic lava flow, unwelded Tuff, welded Ignimbrite, Phreatomagmatic deposits comprising rock fragments of trachyte and Diorite as well as alluvial and reworked pyroclastic deposits. Cinder cones, Crater Lake, faults, lineaments, fractures, and joints were noticed with general fault orientation NNE-SSW, and NE-SW which dip 60^0-65^0 SE. Surface geothermal manifestations such as hot spring, mud pool, altered ground, and hot drill well and Abandoned well sites were identified. They prominent distributed in the south-west and apparently aligned in NE-SW direction around Ashute and Gerbi Ber villages, suggesting they are manifested along fault planes and at their intersection point. Moreover, high degree of hydrothermal alterations is vigorous predominantly associated with those structures. The recognized mineral assemblage consists of Titanite, Actinolite, Chlorite, Rutile, Albite, Adularia, Biotite, Calcite, Quartz, Stishovite, Cristoblite, Trydimite, and, Sulfur.

A preliminary geothermal conceptual model has been developed which resemble convective dominated geothermal play type and consistence with CV1b: Extinct Magmatic Play Type. This accommodates surface manifestations and geological structures and elucidates the expected geothermal system components like heat source, reservoir, recharge and discharge area, and an impermeable cap rock. Regarding to the local heat source anomaly that expressed by numerous surface manifestations two possible scenarios could be put forward related to the intrusive body. The first one is a series of mantle-derived basaltic dyke intrusions emplaced at shallow depths. The second one is a series of elongate and interconnected basaltic sills or magma chambers related to dyke intrusions emplaced beneath the young basaltic scoria cones and lava flows. Alteration minerals and fluid geothermometer estimate suggests that the expected reservoir temperature lies between 150^0C-200^0C indicating sufficient heat-generating capability and warrant further exploration work to assess their suitability for energy generation. The source of permeability of the system has apparently related with tectonic structures while impermeable layer found in upper 1km depth resulted from hydrothermal alterations. Hence, two promising areas were identified to execute next exploration phase on Ashute and Gerbi Ber villages.

ADDIS ABABA UNIVERSITY

COLLEGE OF NATURAL SCIENCES

SCHOOL OF EARTH SCIENCES

SURFACE GEOLOGICAL AND GEOTHERMAL MAPPING OF BUTAJIRA GEOTHERMAL PROSPECT, CENTRAL MAIN ETHIOPIAN RIFT (CMER)

BY

AMARE KASSIE ANDARGE

Approved by the Examining Committee

Dr. Balemwal Atnafu	_____	_____
Head, School of Earth Sciences	**Signature**	**Date**
Prof. Gezhagn Yirgu	_____	_____
Advisor	**Signature**	**Date**
Solomon Kebede	_____	_____
Advisor	**Signature**	**Date**
Prof. Dereje Ayalew	_____	_____
Examiner	**Signature**	**Date**
Dr . Ameha Atnafu	_____	_____
Examiner	**Signature**	**Date**

Jan, 2019

ADDIS ABABA, ETHIOPIA

Acknowledgement

First of all I would like to acknowledge the Almighty God for the guidance and the good overall performance throughout the thesis work. I would like to thank my advisors **Prof. Gezhagn Yirgu** and **Mr. Solomon Kebede** for their kindness support, encouragement and supervision. They offered a continuous and valuable comments, follow up and guidance from the pre-proposal formulation until the end of my thesis work.

I would like also thank Addis Ababa University and School of Earth Sciences for providing me the opportunity and necessary support to pursue my master study. Special thanks go to Dilla University for giving me an opportunity and being a sponsorship to study my master's degree in Addis Ababa University.

My greatest appreciation also goes to my colleagues at AAU, School of Earth Science, especially to those who helped and assisted me in Arc GIS part: **Mr. Belete Baycheken; Mr. Teshome Beyene and Mr. Wendiferaw Negussie.** My acknowledgement spirits to my family for giving me courage and unforgettable support while I'm in the project work. The last but not the least my gratitude goes to government officials and local people of **Kibet** town and the surrounding for permitting and helping me during the field work.

Declaration of originality

I hereby declare that this is my original work prepared for the partial fulfillment of the Degree of Master of Science in the School of Earth Sciences, Addis Ababa University during 2018 under the supervision of Prof. Gezahagn Yirgu and Ato Solomon Kebede. In addition, I am assuring that this work is not presented and published anywhere else. All sources are well referenced and acknowledged.

Amare Kassie _____ _____

Student **Signature** **date**

This is to certify that the above declaration made by the candidate is correct to the best of my knowledge as part of his Master of Science in resource geology (Geothermal energy).

Prof. Gezahagn Yirgu _____ _____

Signature **date**

Ato Solomon Kebede _____ _____

Signature **date**

Table of contents

Contents

List of figures and table

List of acronyms

CMER- Central Main Ethiopian Rift.

DEM- Digital elevation model

EAR- East African Rift

EARS- East African Rift System

ESE- East South East

ESE-WNW – East southeast – West northwest

E-W- East west

GSE-Geological Survey of Ethiopia

IGA-International Geothermal Association

JICA-Japan International Cooperation Agency

Km- Kilometer

Kms - Kilometers

m- Meter

MER- Main Ethiopian Rift

NE- North east

NE-SW – North east- South west

NG- Nazreth Group

NMER- Northern Main Ethiopian Rift

NNE-SSW- North north east- South south east

N-S- North south

NW- North West

NW-SE- North West - South east

PPL – Plane Polarized Light

SES- School of Earth Sciences

SMER- Southern Main Ethiopian Rift

SW- Southwest

UNDP- United nation development program

UNU-GTP-United Nation University Geothermal Training Program

MOWS-Ministry of Water Resources Ethiopian Water Technology Centre

WFB- Wonji fault belt

Wt%- Weight percent

XPL- Cross polarized light

YTVL- Yerer- Tulu Welel volcano tectonic lineament

CHAPTER ONE

1. INTRODUCTION

1.1 Background

Geothermal energy is the energy stored in the form of heat beneath the earth's surface that can, or could be, recovered and exploited (Wouter, V., 2006). It is a clean (carbon- free), renewable, and sustainable form of energy that provides a continuous, uninterrupted supply of heat. It used to generate electricity and for direct heat utilization in various applications like greenhouse, agriculture, aquaculture purpose as well as heating and cooling of buildings (Mary, H. & Fanell M.,2003). Geothermal energy is essential energy supply components that play a vital role to satisfy future energy demands. However, it requires the development of new geothermal sites and improves the performance of existing systems to satisfy this demand (Stober,I. & Bucher,K., 2013). The productivity of a geothermal field mainly depends on the geological and tectonic setting of the area preferred by adequate subsurface fluid flow within the system. Thus different geoscientific approaches should be combined to assess the favorability and potential of a new geothermal field as well as to improve the efficiency of existing geothermal systems (Moeck, 2014).

The East African Rift System is the volcano-tectonically active region where heat energy from the Earth's interior escapes to the surface in the form of volcanic eruptions and geothermal surface manifestations like hot springs, fumaroles, geysers, and mud pools(Pürschel,M., 2013: Teklemariam,M., 2008). In addition, the presence of shallow heat sources, intense faulting as well as the circulation abundant of water with high geothermal gradient indicates the presence of high-temperature geothermal systems in the rift valley (Abiye, 2003; Omenda,P., and Teklemariam,M. 2010).

Ethiopia has an enormous capacity to generate electricity from geothermal energy and geothermal investigation was began since 1969 by GSE with the collaboration of United Nations research project UNDP (UNDP, 1973; Peter Omenda and Meseret Teklemariam, 2010; Madlen Pürschel, *et al.*, 2013; Abebe et.al., 20016). Geothermal surface manifestations are more pronounced and vigorous within the axis of the rifts than on the flanks due to the favorable hydrology and relatively shallow heat sources (Tadiwos Chernet, 2011). Currently, there are about 22 geothermal prospects and only 7.2 MW is generating from the Aluto-Langano geothermal power plant (Omenda and Teklemariam, M., 2010; JICA, 2015;

Solomon Kebede, 2015). In the short term a total of 675 MW geothermal powers is planned to be developed from six selected prospects by 2018 and in the long term, 2000 MW is to be developed by 2030 (Meseret T. 2008; 2012; Solomon Kebede, 2015; 2016). The exploration were focused on the selection of potential geothermal sites in the Lakes District and the Tendaho Graben using remote sensing, geological, geochemical as well as geophysical methods (Madlen Pürschel, et al, 2013; JICA,2015).

According to JICA (2015) Project Team report the geothermal reservoir and target sites in Ethiopia are grouped into three categories namely; Volcano type, Caldera type and Graben type based on the analysis and interpretation of satellite image and site survey. These were determined with reference to the characteristics of the existing detail information of Aluto-Langano, Corbetti and Tendaho-Dubti areas where detail survey was already conducted. Volcano type is assumed to have a geothermal reservoir with a maximum plane area equivalent to the area coverage of young volcanic body identified in Dallol, Boina, Damali, Meteka (Ayelu and Amoissa), Dofan, Tulu Moye, Aluto (Langano, Finkilo, Bobesa), Abaya , Fantale and Boset geothermal areas. Caldera type is assumed to have a geothermal reservoir equivalent to the inner area of caldera comprising Gedemsa, Kone, Nazareth, and Corbetti areas; whereas graben type has equivalent to the area of geothermal manifestations in graben structure including area in Tendaho-(Allalobeda, Ayrobeda, Dubti), Teo, Danab, Meteka, Arabi and Butajira geothermal areas.

The present study was applied in a new area of Butajira geothermal prospect that found in the western part of central main Ethiopian rift nearby Silite Debre Zeit fault zone (SDZF). Even though limited geological and geothermal knowledge available previously, there are promising geothermal features in the area to conduct the study. Thus, the primary focus of the study presented here is to assess the geothermal system components of the surveyed area through surface geological and geothermal investigations that leads to the preparation of preliminary conceptual model and selection of the promising site for further exploration.

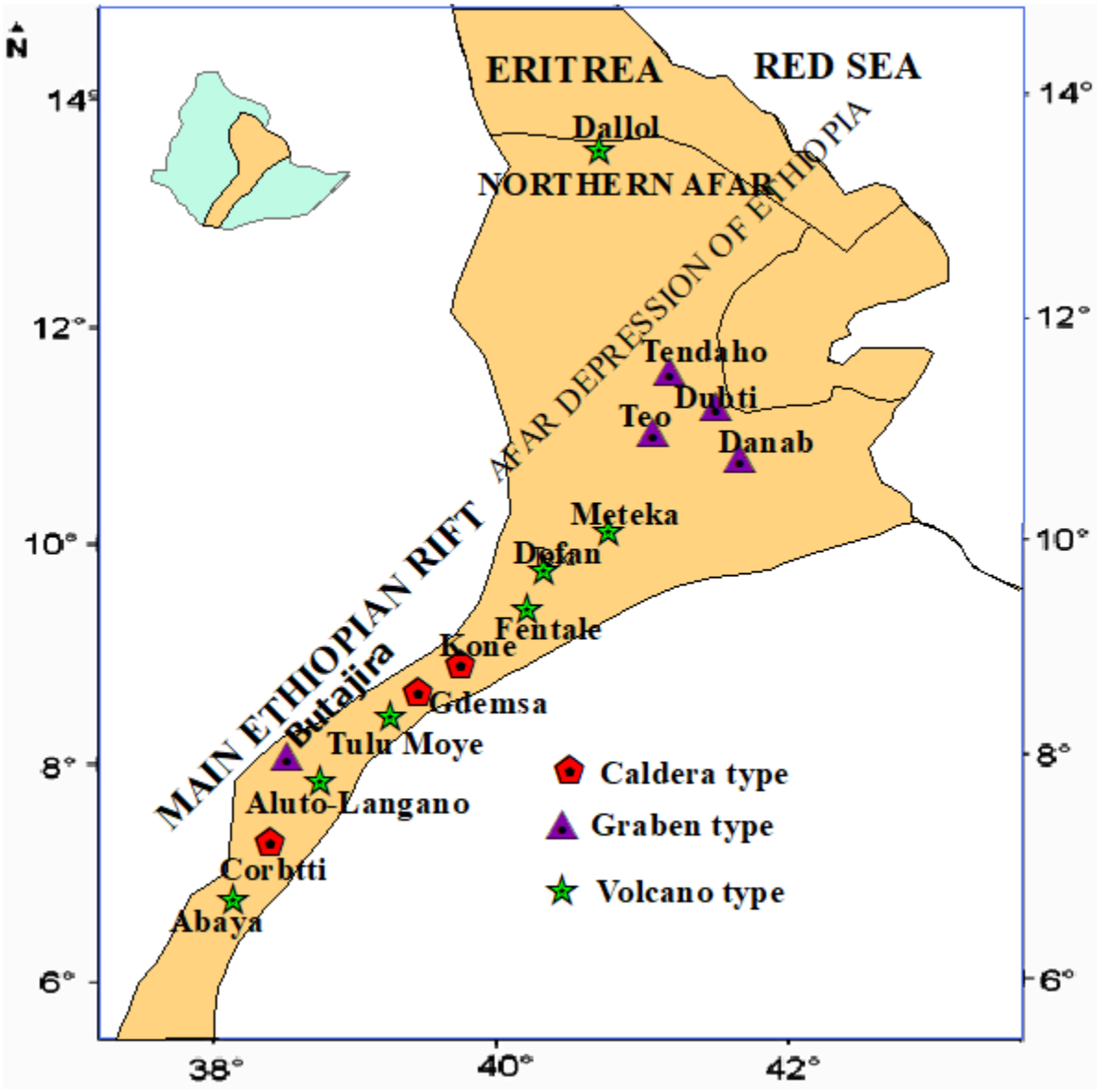

Figure1.1. Location of the study area with other geothermal fields in Ethiopia modified from (Meseret Teklemariam and Kibret Beyene, 2005)

1.2 General overview of geothermal resource

Geothermal exploration and exploitation is a multidisciplinary science, starting with surface exploration followed by collection of drill-hole data and finally reservoir engineering modelling and utilization monitoring. Each discipline looks at the geothermal system from a certain view of point, having a tendency to define the geothermal system from that perspective. Geothermal exploration is an examination of the subsurface of an area in pursuit of viable active geothermal regions with the goal of building a geothermal power plant or/and

various utilizations (Charles Wanjie, 2012).The following features are essential for the existence of viable a hydrothermal geothermal system for worth exploitation.

- **Heat source**: could be shallow magmatic body, decaying radioactive elements or heat from overburdened pressures. In most cases high temperature geothermal areas show a close connection with eruptive centers that have produced silicic lava (Moeck, 2014).
- **Chemical composition of the fluids:** sufficient amount of fluid will be obtained from rainfall and percolate through geological structures to a permeable rock layer. Thus portions of the Earth's thermal energy may be extracted from natural or artificially induced circulating fluids transported through production well to a point of use.
- **Recharge system:** As hot geothermal fluids are withdrawn from wells or from surface manifestations the hydrological balance of the system is restored or partially restored by the inflow of new recharge water.
- **Permeable formation(s)**: that accumulate the geothermal fluid which in turn the circulating fluids extract heat through Structures that allow water to percolate to deeper levels and also host the gas, vapor and water found within the reservoir
- **Cap rock** is a layer of rock of low permeability overlying the reservoir that allows the retention of heat and restricts the upward movement of fluids from a reservoir. It may be produced by self-sealing due to deposition of minerals from the solution mainly silica or by hydrothermal alteration of rocks to clays and/or zeolites.

1.2.1 Geothermal play types

The key to the successful exploration, development (including drilling) and utilization of any type of geothermal system is a clear definition and understanding of the nature and characteristics of the system in question, based on all available information and data (Kristján S., 2009; IGA , 2014). This is best achieved through the development of a conceptual model. A conceptual model is descriptive or qualitative model incorporating, and unifying, the essential physical features of the systems in question (Grant and Bixley, 2011) more prominence in cooperation of the different disciplines rather than each discipline developing their own models or ideas independently. Conceptual models are an important basis of field development plans, i.e. in selecting locations and targets of test wells to be drilled and

ultimately the foundation for all geothermal resource assessments, particularly volumetric assessments and geothermal reservoir modelling (Axelsson, 2013, Cumming 2009).

A geothermal play is defined as the model which comprises the geological factors controlling a technically and economically recoverable geothermal resource (Moeck, 2013, Wouter A., 2016). It represents a geological setting that includes a heat source, heat migration pathway, heat/fluid storage capacity, and the potential for economic recovery of the heat (Moeck, 2014). The aim of the geothermal play concept is to group similar geological settings that might host exploitable geothermal resources, and to develop site-specific exploration strategies that may lead to resource discovery and estimates of reserves independent of the subsequent heat recovery strategy. The characteristics of individual geothermal systems are a function of site-specific variables such as the nature and depth of the heat source; the dominant heat transfer mechanism; permeability and porosity distribution; rock mechanical properties; fluid/rock chemistry; and fluid recharge rates/sources. According to plate tectonic setting, the nature of the heat source (magmatic or non-magmatic), and whether the dominant heat-transfer mechanism is convection or conduction , geothermal systems can largely be grouped into Convection-dominated plays; Extensional domain type and Conduction-dominated play type (Moeck, 2014).

A) Convection-Dominated Play Types (CD)

In this plays type, heat is transported efficiently from depth to shallower reservoirs or the surface by the upward movement of fluid along permeable pathways. Laterally extensive, porous high-permeability formations act as the primary reservoirs with temperature greater than 200°C at shallower depth < 3 Km. These invariably lie in regions of high tectonic activity (Nukman and Moeck, 2013; Hickman et al., 2004), high volcanic activity (Bogie et al., 2005), young plutonism (less than three million years old), or regions with elevated heat flow due to crustal thinning during the extension of the crust (Faulds et al., 2009; 2010).The age of magmatism is an important indicator of the presence of a heat source and heat accumulations. Active and recent magmatism often indicates an excellent underlying heat source (McCoy-West et al., 2011), while inactive or extinct magmatism may be associated

with large-scale intrusions of igneous rock (plutons) at greater depth (>5 km depth) with remnant heat and additional heating by radioactive decay in granitic rock.

CV play type are subgrouped in to CV1a, CV1b and CV2.

CV1a: Magmatic Play Type, Active or Recent Magmatic Intrusion: in this play type fluid movement occurs in two zones: the outflow is generally modified from the original fluid, and has a lower temperature and higher pH than the upflow due to lateral migration (with associated heat loss) and loss of gases (during boiling) towards the flank of the volcano (Hochstein, 1988). Vertically extensive, low- permeability, clay-rich layers in steep terrain, such as andesitic stratovolcanoes, can cap high temperature reservoirs. A vapor-dominated zone may develop in regions of a high heat-generating, localized magma body and moderate to high topographic relief. Steam heated discharge at higher elevation and chloride spring discharge at lower elevation are typical surface manifestations of these vapor dominated plays. In areas influenced by active faulting, deep rooted magmas can intrude beneath flat terrain with no volcanism. It can lead to the upflow of liquid and the formation of hot springs, fumaroles, boiling mud pools, and other geothermal surface manifestations (Bogie et al., 2005).

CV1b: Magmatic Play Type, non-active /Extinct Magmatic Intrusion: it incorporates a heat source in the form of a pluton consisting of crystalline rock enriched in radioactive elements or a young, crystallized but still cooling, intrusive igneous body . Such play types are located where surrounding mountain ranges provide high recharge rates of circulating meteoric water, driving a hydrothermal system with possible vapor partition above the hot rock. The system includes a vapor-dominated layer above a fluid-dominated layer (Bertani et al., 2006). Faults and fractures control the recharge of meteoric water into the system and a low permeability barrier may act as cap-rock preventing the escape of steam or hot fluids to the surface.

B) CV2: Extensional Domain geothermal Play Type: In CV2 type the uprising mantle is the principal source of heat for geothermal systems due to crustal extension and thinning. The resulting high thermal gradients facilitate the heating of meteoric water circulating through deep faults or permeable formations. These non-magmatic play types are either “fault zone controlled” or “fault-leakage controlled” at the system scale. In first case,

meteoric water infiltrates down a shallow fault, circulates and heats through deep-seated faults, and rises along other faults (Reed, 1983). In later case, water circulates through a combination of faults and permeable buried formations, typically recharging and discharging along fault zones. In general, segmented faults are more favorable for geothermal systems than large faults with large offsets. The local stress regime and its orientation relative to fault geometry has a controlling impact on permeability pathways, with faults oriented perpendicular to the minimum compressive stress direction more likely to be permeable (Barton et al., 1997).

C) Conduction-Dominated Geothermal Play Types (CD): In CD play type the dominant heat transfer mechanism is conduction due to an absence of fast convective flow of fluids or short-term variations in fluid dynamics within passive tectonic settings .Geothermal gradient increases steadily and higher values can be detected in regions of high heat flow due to elevated concentrations of heat generating elements in the crust, or where overlying strata are thermally insulating (Beards more and Cull, 2001). Favorable geological settings for CD include extensional, divergent margins and grabens, or lithospheric subsidence basins. Faults do not naturally channel heat in CD while they serve as a fluid conduit or barrier during production from geothermal reservoirs associated with these play types, and may cause compartmentalization of the reservoir into separate fault blocks. Conduction-dominated geothermal play types with naturally low permeability reservoirs such as tight sandstones, carbonates, or crystalline rock can only be developed using engineered geothermal systems (EGS) technology. Inga Moeck (2014) subdivided CD into Intracratonic Basin Type (CD1), Orogenic Belt Type (CD2), and Basement Type (CD3).

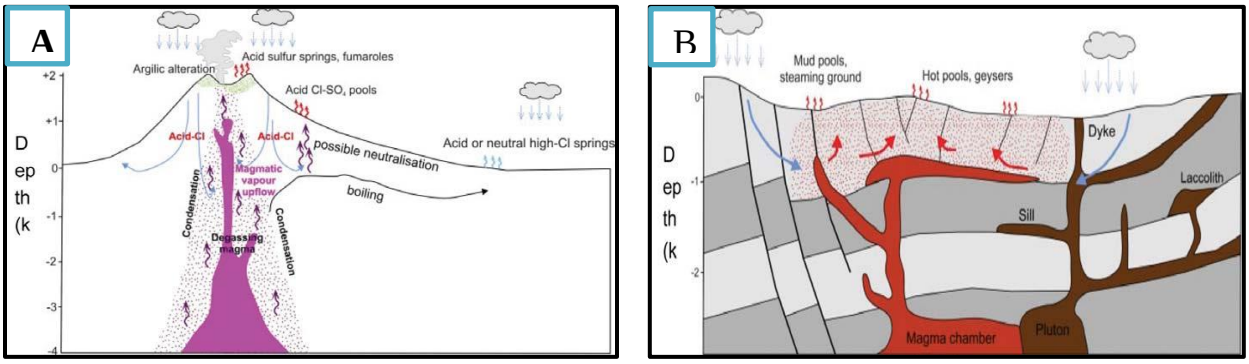

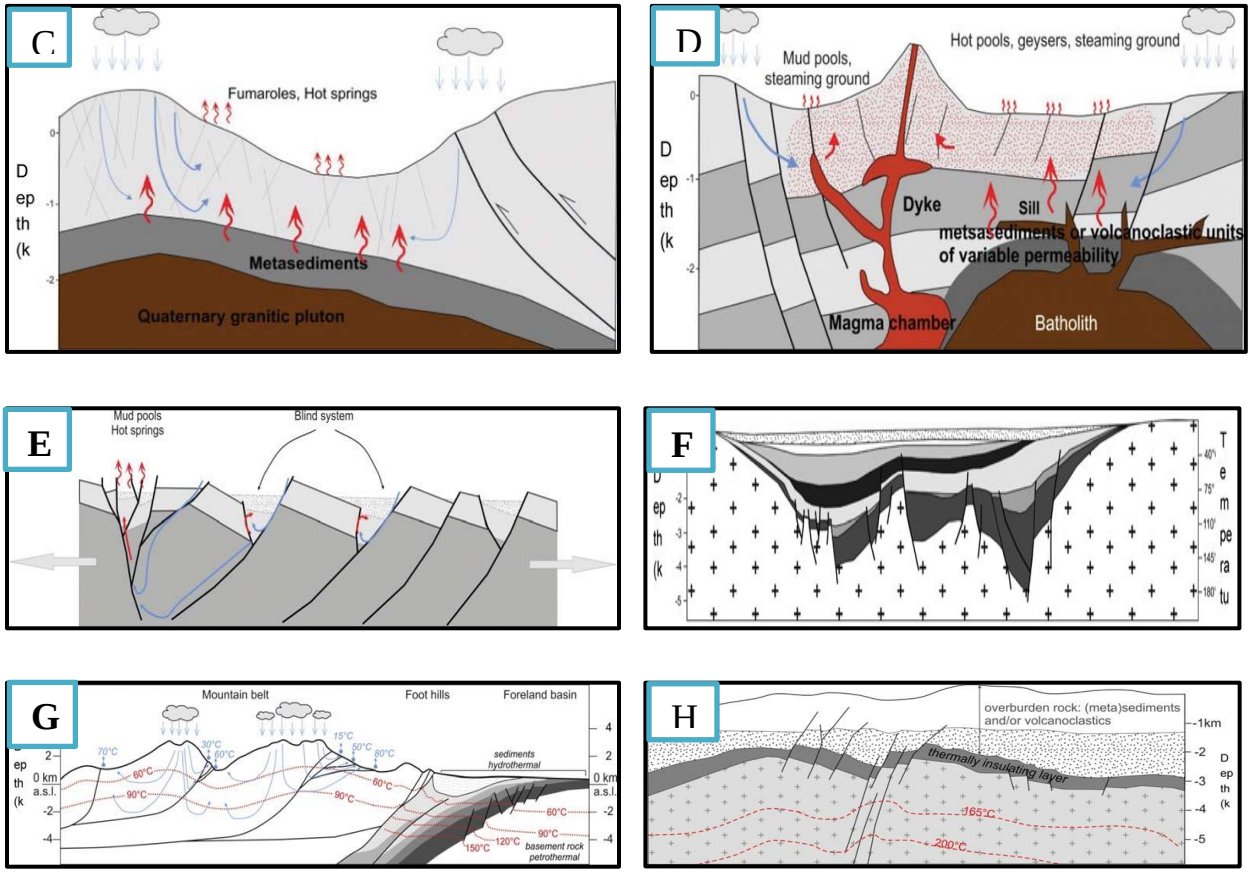

Figure1.2. Generalized conceptual models geothermal play type: (A) CV1a with eruptive magma chamber; (B) CV1a; (C) CV1b ;(D) CV1b; (E) CV2 (F) CD1 an intracratonic sedimentary (G) CD2 Orogenic Belt Type i.e. conductive; (H) Moeck, 2014

1.3 General descriptions of the study area

1.3.1 Location and accessibility

The study area "Butajira geothermal prospect" is found in Southern Nations Nationalities and Peoples of Ethiopia (SNNP) Regional state within Siliti zone that lies just south of Butajira town, east of Kibet town, south-west of Inseno town and west of Koshe , north of Lake Abaya and north-west of Tora and north of Lake Abaya. Its geological setting is placed within central main Ethiopian rift valley 145 km south west of Addis Ababa. Geographically it is bounded between UTM 37 882000N- UTM 910000N and UTM 37 42700E- UTM 437000E with total area coverage 90 Km^2. The area is accessible through Addis Ababa-Alem Gena-Butajira –Werabey asphalt main road until Kibet town. Numerous concrete roads as well as foot trials are available to perform fieldwork activities.

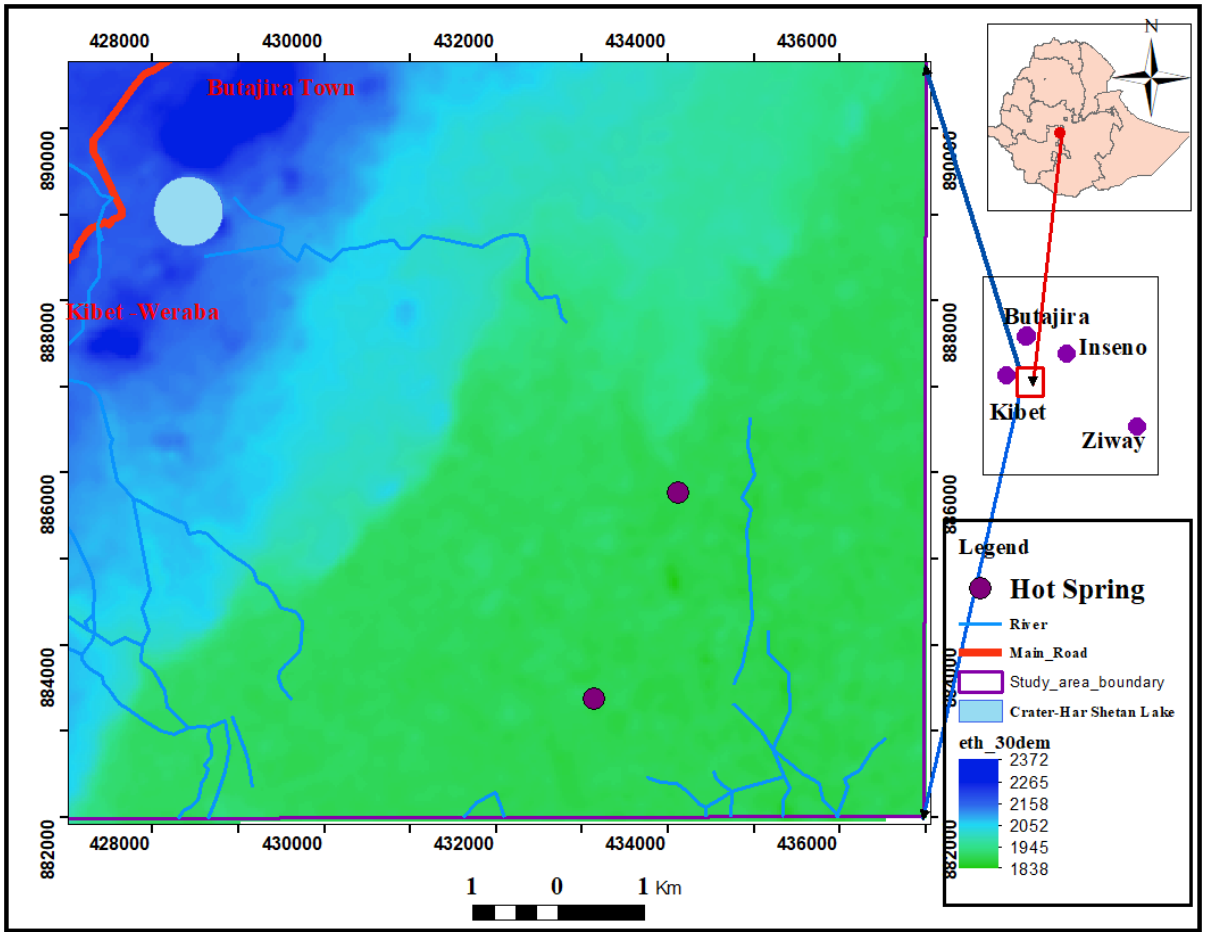

Figure1.3 Location map of the study area

1.3.2 Physiography and drainage pattern

The study area covers a small sector adjacent to western portions of the CMER that featured by various landscapes resulted by major faulting, volcano-tectonic activities, and lacustrine sedimentation. The main landscapes observed in the area are cinder cones, crater, fault escarpments, and fault-controlled depressions. The elevated topography is commonly observed at aligned scoria cones and along fault escarpments in western and northwestern corner whereas alluvial sediments have tended to flatten out and forms relatively flat plain areas in the eastern, southeastern portion of the mapped area. The highest elevation is measured about 2065 meter above mean sea level north of Har Shetan Lake and the lowest elevation is 1810 meter above mean sea level at Kontane Marsh that found the southeast corner of the study area. The area found inside the western parts of Meki River basin which shows low drainage density indicating the presence of high permeable strata or week zone that favors the infiltration of surface water. The highest river is Lebu River which flows from northern highland

areas towards the southern flat plain and eventually it changes its name to Garore River and drains to the flat plain of Kontane Marsh and Abaya Lake. The tributaries of Waja River, which found nearby East and South East of the study area, drain towards Kontane Marsh in north and northwest direction as well as minor in East-West and North East directions. The Kontane Marsh got water from runoff of North-West highland and South-East fault Controlled Waja River in addition to the contributions from groundwater and precipitation that makes it always wet. Consequently, the dominant surface water flow is from cinder cones to plain land area towards lower topography. In some localities the flowing river deviate its direction sharply and dry out follows the orientation of geological structures. The presence of this features leads to an expectation of internal lineament beneath that serve as the main recharge zone for the geothermal system if linked to the reservoir.

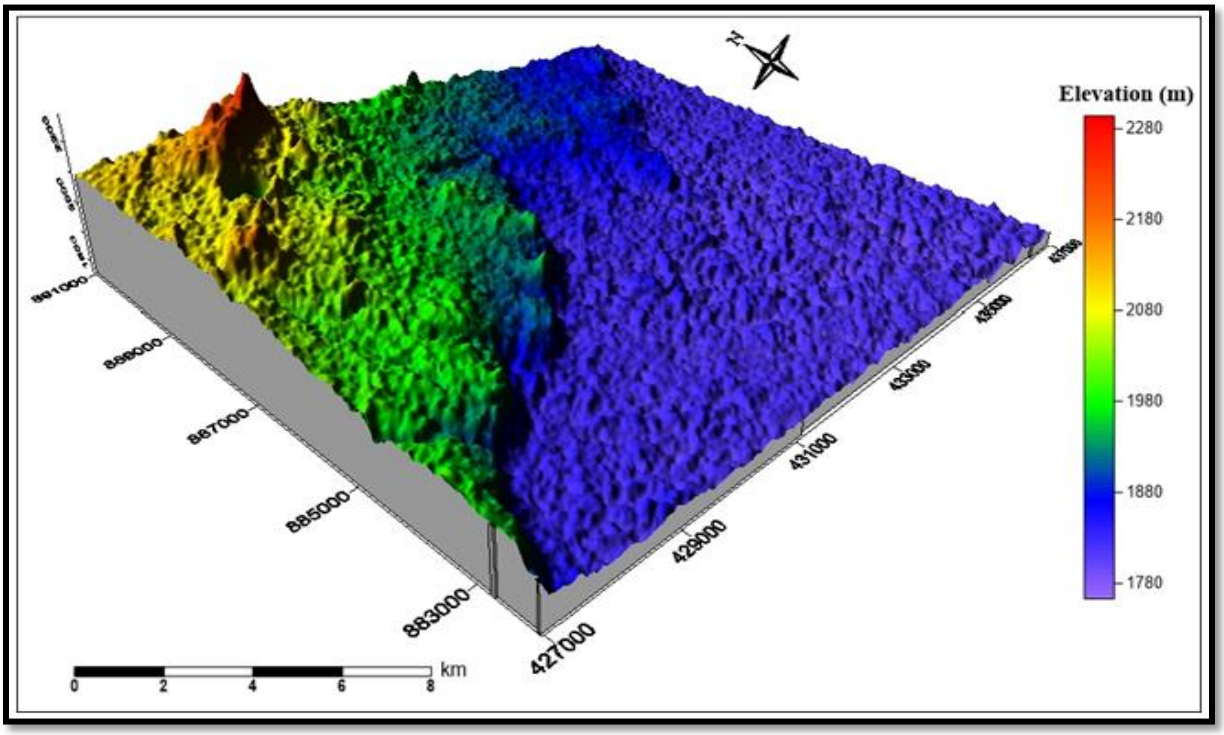

Figure1.4. Physiography of the study area I 3D view

1.3.3 Climate condition

The MER climate is influenced by the annual shifts of the intertropical convergence zone and physiography. Since the area is located in CMER within Ziway–Shala region that is mainly characterized by alternating wet and dry seasons (Nicholson, 1996; Elisabeth Gibert et al 1998). Climate condition of the study area is classified as warm and temperate. In winter, there is much less rainfall than in summer. In this location, the highest temperature record

has in March, on average around 18.9 ^{0}C while the lowest average temperature is recorded in July around 18.9 ^{0}C and an average annual temperature of 17.4 ^{0}C. In a year, the average rainfall is 1055 mm, in which the least amount of rainfall occurs in November (11mm on average) and most precipitation falls in July, with an average of 17 mm. The variation in the precipitation between the driest and wettest months is 168 mm and the average temperatures vary during the year by 2.5 ^{0}C **(http://en.climate-data.org).**

1.3.4 Land use and land cover

In the northern part is high elevated area dominated by scoria cones that have excavated quarry sites that used as a raw material for road construction. The low land area is covered by weathered fertile soil that used for agricultural crop production like Taff, Maize (corn), Millet (Sorghum), Wheat etc. While the plain land area on the southern and eastern part is beneficial for the sugar plantation in the specific locality. Generally, the area has sparsely vegetated and relatively good vegetation is observed on fault escarpments such as Acacia, Bush, deciduous woodland, bamboo forest etc. The plain land of the eastern part of the study area is covered by different types of dry savanna grass along swampy area as well as around the top of cinder cones.

1.4 Statement of the problem

With the increase in world population, industrialization and improvement in the standard of living, there has been a continuous increase in the consumption of energy. As consequence, there has been a growing recognition for the use of renewable energy sources like geothermal energy which supplements hydroelectric and crude oil, especially in rural and remote areas. Even though most geothermal systems around the world at different geological setting have been successfully exploited for electrical production and different purposes like district heating, exploration and development of new geothermal prospect are commonly restricted by the risk of unsuccessful drilling. A basic problem is that the geothermal systems in the prospect area (Butajira-Silte) is poorly characterized in terms of favorable geological settings and tectono-stratigraphic controls.

To increase the renewable energy supply of Ethiopia extensive and intensive investigations have been conducted almost five decades within main Ethiopian rift to exploit the available geothermal resource. At present, more than 22 geothermal prospects are identified and

expected to have the capacity to generate electricity. Among these prospects, only one geothermal pilot power plant generating 7.2 MW was installed at Aluto - Langano geothermal field (Omenda & Meseret Teklemariam, 2010; JICA, 2015; Solomon Kebede, 2015). In addition, temperature gradient wells at Tendaho and temperature gradient wells at Corbetti were drilled for feasibilty studies while others prospects are at reconnaissance to prefeasibility phase of exploration (Solomon, 2013;Selamawit worku , 2015).

UNDP, (1973) report proposed further investigation in other geothermal areas namely; Butajira- Siliti area, Belbo springs, Nech Sar springs, and Lake Ziway areas. Butajira - Siliti area is the focus of the study because only limited geological and geothermal knowledge is currently available. According to Di Paola (1970), geothermal fresh water temperature with 48 c^0 emerges at the base of a small rhyolite dome, isolated completely from southern parts of a swampy plain about 10 km south-east from a phreatic explosion crater (Har-Shetan lake), near the main road about midway between Butajira and Siliti as well as many springs are found in the swamp area. Recent basalt scoria cones with steep outer flanks and shallow summit craters are associated with the western limit of the rift in Butajira – Siliti region (Di Paola, 1970; UNDP, 1973).

A geothermal phreatic eruption occurred during deep well drilling for irrigation purpose on Dec $6^{th,}$ 2014 in Siliti Wereda Buraku Kebele (Demise A., Salahadin A., and Solomon K., June 2014). According to the final report of Geological Survey of Ethiopian (GSE), a technical team concluded that the geothermal system is vapor-dominated at depth of 234 m to 255 m with a temperature of 200 ^{0}C -250 ^{0}C and reaches the surface as shown in Figure 4.11 D at chapter 4. The cold water was heated by a heat source that found beneath groundwater level. Onward this circumstance, Geological Survey of Ethiopian; geothermal energy directorate performed reconnaissance geo-scientific investigations (Magnetic, soil temperature survey and fluid geochemistry) but detail geological and geothermal investigation wasn't yet performed.

1.5 Objectives of the study

1.5.1 General Objective

The main objective of this study is to assess the existence of promising geothermal system components at the Butajira geothermal prospect through investigating the geology and surface geothermal manifestations.

1.5.2 Specific objectives

The following are the specific objectives

- Prepare a geologic map at a scale of 1: 50,000 with an appropriate cross-section.
- Prepare a geothermal map at a scale of 1: 50,000 that incorporate geothermal surface manifestations, young volcanic centers, and major tectonic structures.
- Develop a preliminary geothermal conceptual model in 2-D view in reference to the identified geothermal play type.
- Suggest promising sites for further explorations i.e. to attain deep-seated information about geothermal system components.

1.6 Research questions

Even though, the geothermal surface indicators lead to an expectation of a convenient geothermal field, the study area raises a number of scientific questions that need to be addressed.

- What kind of lithology the study area comprises that offers a clue for probable heat sources, reservoir, and capping layer?
- Where are the major tectonic structures that serve as a conduit /fluid pathway that favors fluid circulation from the surface to a reservoir and vice versa?
- Which types of surface geothermal surface manifestations are observed in the study area? Where they are found intensively?
- Where is recharge and up flow zones located in the prospect area?
- Under which geothermal play type the prospect area categorized?

- Where are the promising sites recommended for further detail studies and test well drilling?

These research problems have been identified from the review of previous works and emphasis was not given yet to answer these questions. Those problems were the motivations to conduct research work in the prospect area. Therefore some of the identified problems have been addressed, since new data incorporated with previous studies.

1.7 Significances of the study

In the study area, Butajira geothermal prospect, detail geological and geothermal investigation yet not studied and this research work will be accomplished through field observation and petrographic and XRD analysis that will have the following worth:

- The study will provide the basic geological and geothermal knowledge of the geothermal resource and system components of the prospect area.
- The study will be used as a backbone to perform further exploration phases such as detailed geochemical and geophysical studies, and test well siting.
- The study will also serve as documented information and used as guidance in a specific subject matter for the concerned body for various purposes.

1.8 Organization of the thesis

This thesis was organized into six chapters: started by introduction part and finish up with conclusion and recommendation in the last chapter.

Chapter one: familiarizes background of the study and general overview about geothermal resources, description of the study area (location physiography and drainage pattern, climate and temperature), plus problem of the statement, objectives and research questions, as well as significance and limitation of the study.

Chapter two: focused on the methodology used in the study. The summaries of methods adopted were presented in four categories: review of secondary data sources, geological fieldwork, petrographic studies and XRD analysis.

Chapter three: states about the review of previous works through investigating previous works i.e. magnetic, soil temperature, magnetotelluric (MT), and fluid geochemical data accomplished in the study area besides regional literatures.

Chapter four: investigates results of field work, petrographic and XRD analysis. This part comprehends three subdivided namely local geology, geothermal manifestations and hydrothermal alteration minerals noticed in the Butajira geothermal prospect. As a result, geological map with appropriate cross section were prepared likewise the geothermal map.

Chapter five: deals about an assessment of geothermal system components that focused on the existence of favorable geological setting in the surveyed area by relating what has been known previously with what is revealed from the results presented in chapter 4. It then discusses the characteristics of the Butajira geothermal system components i.e. heat source, reservoir, cap rock, geothermal fluids and permeable structures of the system. At the end, a preliminary conceptual model of the Butajira geothermal prospect was prepared and discussed.

Chapter six: deals about conclusion and recommendations, which concludes the final output of the thesis and provide an evaluation on characteristics of geothermal system components of the study area .It then accomplished by a recommendation through endorsing the promising geothermal site location that suggested for detail investigations need to be performed regarding the future development.

CHAPTER TWO

2. METHODOLOGY USED IN THE STUDY

In order to achieve the desired objectives of the research different tasks have been performed sequentially from office pre-field secondary data collection up to post field laboratory analysis and data interpretation to attain the desired result. Those data have been obtained from review of secondary data, geological field observations accompanied by data generated from Petrographic studies and XRD geochemical analysis. Systematic organization and interpretation of these information support to acquire the general overview of the geological and tectonic setting of the area and its favorability in geothermal system point of view. Amalgamation of those data used for the development a preliminary geothermal conceptual model for siting promising areas for next step of geothermal exploration.

2.1 Review of secondary data sources

All existing relevant secondary data that obtained from different websites, public institutions/ organizations such as geological, hydrogeological, geochemical and geophysical data were collected and reviewed. Unpublished reports prepared by Geological Survey of Ethiopia that attained within the study area were engaged to comprehend the study such as geophysical investigations reports i.e. magnetotelluric survey (MT), magnetic survey and soil temperature survey and fluid geochemical analysis. The combinations of this information were used to forecast heat source at depth, predict reservoir temperature, to trace lineaments structures in the area that controls the fluid flow path and enhances the permeability of the reservoir and impermeable cap rock. In addition, it helps for preparation of preliminary conceptual model that comprise geothermal system components.

2.2 Geological field work

Understanding the geological and tectonic setting of the area is the first most important part in geothermal resource exploration. A geothermal geological field work was performed during December - January, 2017. During the survey different lithological unit were described, identified and their contact were traced, geological structures were measured, labeled and geothermal surface manifestations were pointed out in the topographic map with precise location and appropriate measurement. A total of 60 rock samples were collected through each traverse line from various rock outcrops. Among these, 10 (ten) representative

rock samples for thin section analysis and 9 (nine) for XRD sample preparation were selected. Different geothermal surface manifestations such as hot spring, mud pool, and hot drill hole were identified and exactly marked on the map and try their relation with the observed and inferred tectonically features.

Accordingly geological and geothermal map were prepared. Then the geothermal map overlaid by soil temperature and magnetic map to assess the relationship of tectonic structures with surface geothermal manifestations. Different mapping equipment has been used for various purposes to accomplish field work activities like Global positioning system (GPS), Compass, hammer and sample bag. Moreover different software tools were relevant in the preparation of geological and geothermal map like ArcGis10.3, Sulfur 10, and Global mapper.

2.3 Petrographic studies

During surface geoscientific studies, petrological techniques are employed to identify lithology units, to recognize alteration mineral assemblages. Consequently, petrographic analysis was focused on textural description and mineral identification from selected rock samples. It involves through examination of the optical properties of minerals from thin sections using petrographic microscope taken under plane-polarized light (PPL) and cross-polarized light (XPL). The abundance of identified minerals noticed in thin section used as the basis to characterize, differentiate and confirm various rock units and also altered index minerals were identified. Ten (10) representative samples from all the lithology units encountered in the field were selected and thin sections will be prepared at Ethiopian geological survey laboratory and inspected at the AAU Earth science, petrography laboratory.

2.4 XRD analysis

It is a fingerprint technique, which the crystalline sample exposed to X-ray radiation; the sample diffracts X-rays into a pattern which is unique to each crystalline substance. Nine (9) samples were selected from major rock units and altered grounds aimed to identify alteration mineral assemblages. These samples were crushed into powder and sieved by 0.425μm for separating wanted elements from an unwanted material as well as the particle size distribution of a sample is mixed. Powder XRD was accomplished using diffractometer model DX-2700 SSC held at Mekelle University. The instrument configured with K radiation

of Cu, λ=1.54056 Å, 30 mA, and 40 kV; analysis was done in 2-theta geometry and Bragg–Brentano configuration, with a step size of 5 degrees/ min and a step time of 0,02 degrees. The diffractometer is equipped with fixed slits 1deg &1deg 2mm monochromatic. Samples were scanned from 4 to 70 degrees two theta, at 0.02 degrees per step and a count time of 1 second per step. The acquired data matched against to diffraction pattern database for compound identification by means of Match software. In this study, since the concentration of major rock-forming minerals are abundant at this sieve size the clay minerals are masked within the XRD graphs and non-clay alteration minerals are used to predict the nature of alteration.

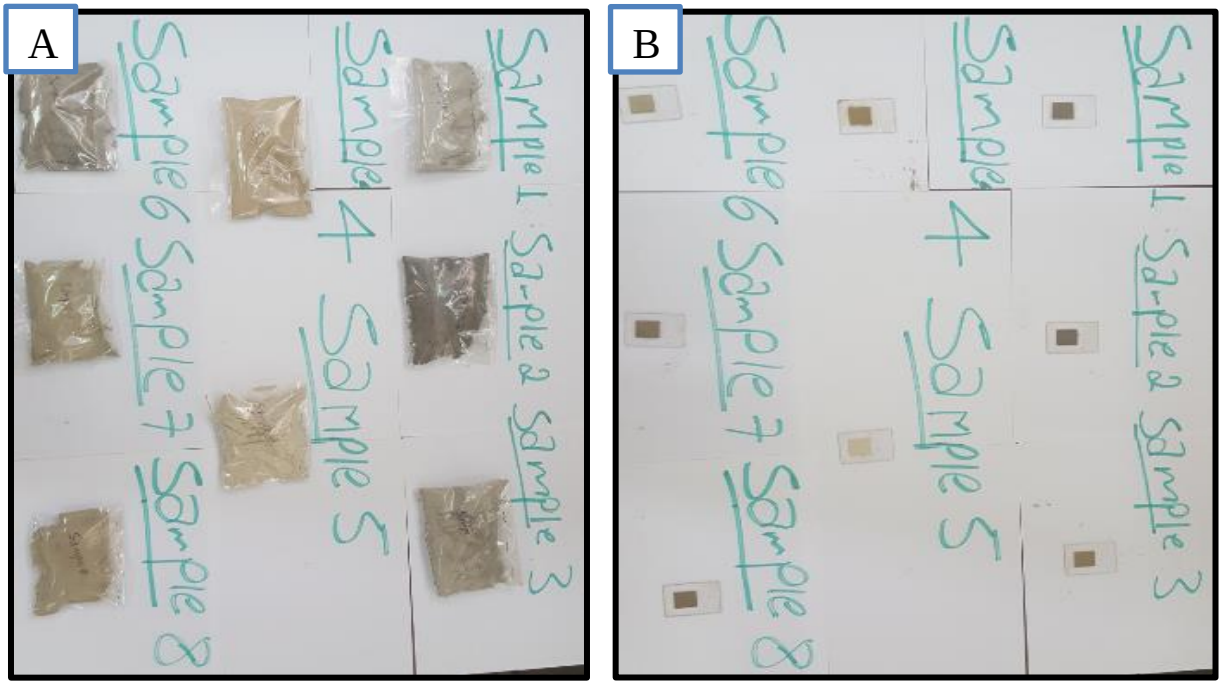

Figure 2.1. Sample preparation for XRD analysis

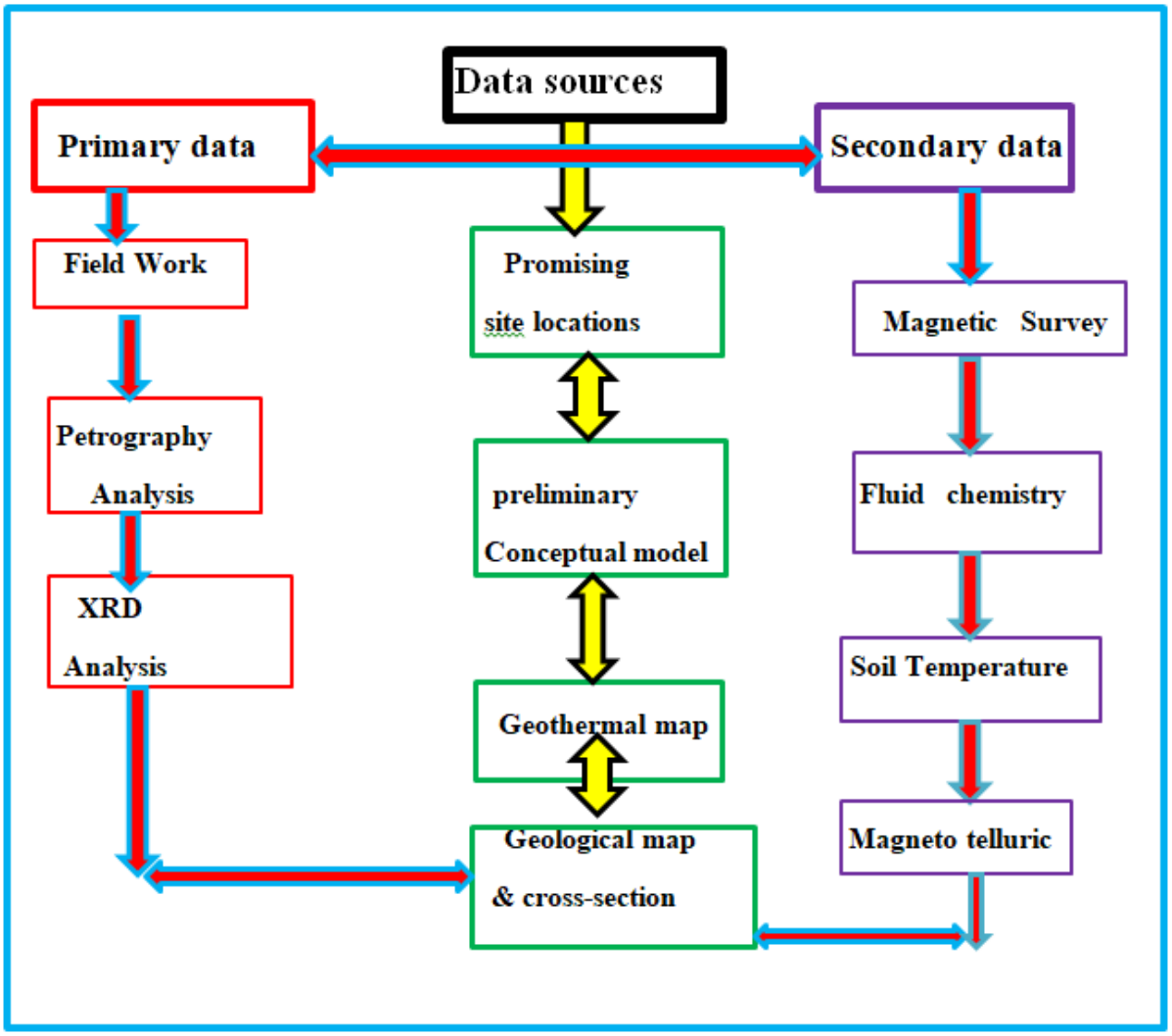

Figure2.2. Methodology flow chart

CHAPTER THREE

3. REVIEW OF PREVIOUS WORKS

3.1 Geological setting of Main Ethiopian Rift (MER)

The Ethiopian rift system is an active continental rift, formed by up-doming followed by volcanism and rifting that outspreads about 1000 km in a direction of NE–SW from the Afar depression southwards up to the Turkana depression through main Ethiopian rift valley (MERV). The MER is a complex system that rift propagation preceded both from the south Ethiopia Rift (SER) and northern Ethiopia Rift (Afar Rifts) towards the CMER (Bonnini et al., 2005, Corti et al., 2013). Rifting in the MER did not start until about 8 Ma (Abebe et al., 2010), possibly due to the presence of transversal structures of GBL and YTVL to the south and to the north of MER, respectively, that stopped propagation of rifting for a long geological period. During the early stages of the MER, several central volcanoes erupted forming very thick pyroclastic deposits, thought to have been partially produced from fissures. These volcanic products have about 5 Ma and are known as the Nazret group (Kazmin and Berhe, 1978; WoldeGabriel et al., 1999; Boccaletti et al., 1999; Chernet et al., 1998; Abebe et al., 2005). MER is subdivided into three segments that reflect different stages of the continental extension and characterized by different fault architecture, the timing of volcanism and deformation, crustal and lithospheric structure (Boccaletti et al., 1998; Corti G., 2009).

In the NMER, the boundary faults are oriented ~N40°E started to develop at around 11 Ma. This sector is marked by Arboye and Sire faults characterized by a right-stepping en-echelon pattern which dip towards the NNW down to the rift depression and the major western Ankober border fault system which in turn characterized by the structurally complex ‘corner’ between the NE-trending MER and the N–S trending Red Sea rift (Wolfenden et al., 2004). The central part of this rift sector form asymmetric rift basin which tilted to the southeast toward the large-offset Arboye normal faults indicates E–W extension direction (MacKenzie et al., 2005). While, the SMER sector have trend from N0°E to ~N20°E located within the major fault escarpments of Chencha which is marked by a curvilinear boundary fault having an orientation between N–S and N40°E and Agere Selam eastern margin have linear fault system and is characterized by NNE–SSW trend (Boccaletti et al., 1998; Bonini et al., 2005).

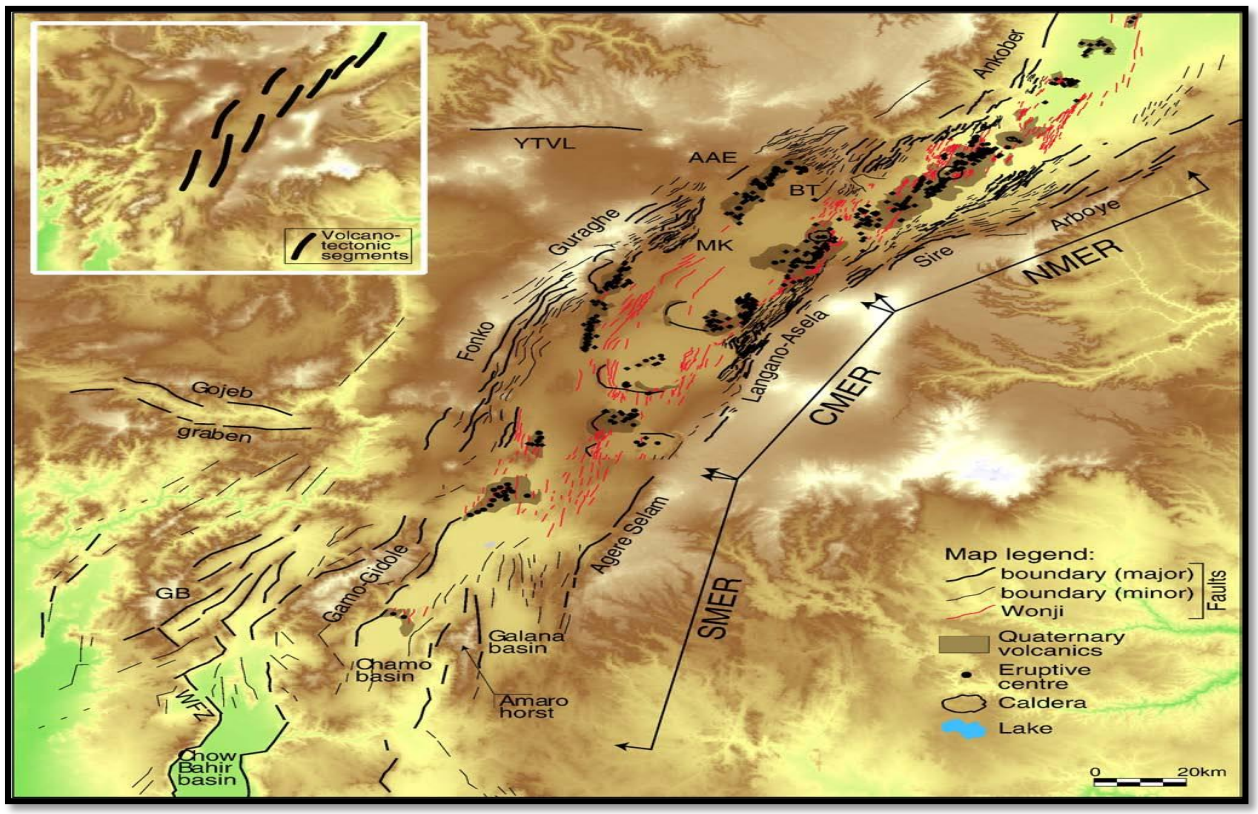

Figure 3.0.1. Tectonic sketch map of the MER adopted from (Giacomo Corti 2009; modified from Boccaletti et al., 1998).Inset shows the en-echelon, right-stepping arrangement of the volcano-tectonic segments of the Wonji Fault Belt. AAE: Addis Ababa Embayment; BT: Boru

3.2 Geological setting of CMER

Formation of the rift margins of the Central MER took place about 8 Ma ago when the Munesa and Guraghe escarpments were formed (WoldeGabriel et al., 1999). The CMER fault systems give rise to a roughly symmetric rift valley oriented between N25°E and N45°E characterized by an extension direction of roughly ESE–WNW, with local variations between E–W and NW–SE that formed in the late Miocene–Pliocene (post ~6 Ma) (Bonini et al. 2005). The western margin of this segment is well expressed by the N25°E–N35°E-trending and ESE-dipping Guraghe and Fonko faults, whereas the eastern margin is well represented by the N30°E-trending and WNW-dipping Asela–Langano fault system. Both systems are characterized by high-dip angle (› 60°) normal faults, with a large cumulative vertical throw. The border faults are normally segmented and characterized by the presence of minor transversal structures and local complex geometries. These two intersecting trends result in the typical S- or Z-shaped pattern of Fault System e.g. Langano (Haroresa) (Mohr, 1987;

Boccaletti et al., 1998; Bonini et al., 2005; Pizzi et al., 2006). This gives rise to a sinistral component oblique-slip on the NE–SW-trending fault planes, as supported by local structural features as pull apart, en-echelon tensional fissures and the en-echelon right-stepping arrangements of the boundary fault segments accommodated by the internal Wonji faults belt (Boccaletti et al., 1998; Corti,G., 2009; Bonini et al, 2005).

In the CMER, voluminous eruption of rhyolitic ignimbrites and the collapse of very large calderas occurred in Early Pliocene (Di Paola, 1972; Woldegabriel et al., 1990). The western escarpment shows 1000 m thick of basaltic lava flows, with inter-bedded ignimbrite horizons, overlain by massive rhyolites, tuffs, and basalts (Di Paola, 1972; Woldegabriel et al., 1990). The active marginal graben called SDZFS contains lacustrine sediments and welded tuff on which are interspersed coalescing nested scoria cone aligned parallel to Guraghe escarpment. The active marginal graben called SDZFS contains lacustrine sediments and welded tuff on which are interspersed coalescing nested scoria cone aligned parallel to Guraghe escarpment. While the eastern plateau is characterized by shield volcanoes of Pliocene to early Pleistocene (4.6−1.6 Ma) consisting of main trachyte with subordinate basalts and phonolites (Di Paola, 1972).

From period to the present, tectonic and volcanic activity was concentrated along the Wonji Fault Belt (WFB) to the east, and along the Silti Debre Zeit Fault Zone (SDZFZ) to the west (Di Paola, 1972). Volcanism in WFB started about 0.83Ma and shifted from the median towards the marginal zone as indicated by a pattern of decreasing the age of volcanic rocks towards the margin of the rift (WoldeGabriel et al., 1990). Unlike the Siliti Debre Zeit Fault Zone (SDZFZ), WFB has peralkaline silicic centers along it rather than Calc-alkaline (William Hutchison et al., (2016). Pre-Tertiary crystalline basement and Mesozoic sedimentary rocks that are unconformably overlain by Oligocene to Pliocene basalt flows and silicic tephra are also exposed in the western margin of the central main Ethiopian rift at the Gurage at Kella typical locality (Woldegabriel et al., 1990).

At the western margin of CMER around the Guraghe escarpment at Kella typical locality, a crystalline basement is exposed with altered Biotite Gneiss intruded by swarms of North-West trending quartzo-feldsphtic pegmatites(Woldegabriel et al., 1990). Mesozoic sedimentary formation unconformable overlies this rock unit, which has about 200m, i.e. 150

early Jurassic Adigrat Sand Stone, 20 m of variegated shale, 30m of Jurassic Antalo limestone (Weldegebriel etal, 2009). Above these formations, a thin about 40-60m, fine-grained Oligocene basaltic flows (32 Ma), and overlying thin fluvial strata (2m-10m) is exposed along fault scarp. All of them overlain by a thick sequence of Pliocene Basalt flows (4.2-2.5Ma) and particularly crystal-rich welded Tuff which have a thickness about 150m-200m and 200m-250m respectively. A number of thin ash fall tuffs (2m-10m) that cover the individual step up faulted blocks in front of Guraghe escarpment are Pliocene (2.72Ma-2.59Ma) in age and thicken against the rift wall (Di Paola, 1972; Woldegabriel et al 1990, Abebe et al, 2010). According to Woldegabriel et al 1990 the CMER set chronostratigraphic units and classified with regional stratigraphic framework age wise as follow.

A. Kella Basalt (26-32Ma)

They are the oldest volcanic rock found in Agere Selam, Ambo and Kella, dominantly contains fine grained Oligocene basalt with localized rhyolite and sedimentary strata. This thick basaltic lava flow (40m-60m) is exposed along fault controlled stream cut traverses to the rift margin that overlain by thin (2m-10m) fluvial strata.

B. Shebele trachyte (12Ma-17 Ma)

This group of mid Miocene age exposed in deep river canyon of Omo and Wabi Shebele and Mount Chike is the shoulder volcano that is made upon. It is chiefly consists of basalt, trachyte, phonolite, rhyolite, and intercalated pyroclastic strata.

C. Guraghe Basalt (8.3Ma- 10.6Ma)

This group was formed during Late Miocene that composed basalt and subordinate silicic flows and exposed in Omo River Canyon basalt (10.6Ma) overlies mid Miocene age (15-16.9Ma) Shebele group rhyolite and Trachyte.South along the strike of the pre Tertiary rocks, the rift escarpment is off set sharply to the west at the arcuate Guraghe escarpment .there are at least 14 thick ,generally aphyric ,basalt flows and intercalated vitric ash are exposed ; these yielded ages of 10.6 and 9.1Ma for the basal and top flows of the section respectively. Along the foot hills of the main Guraghe scarp, a geologically significant glassy and perlitic welded tuff abuts and thickens against the rift wall with consistent date 8.3 Ma, and provides the

minimal age of the boundary fault.The top of the section at Guraghe is capped by 20 m thick Pliocene welded tuff (3.85Ma).

D. Butajira Ignimbrite (3Ma-4.2Ma)

This group of rocks is formed in early-middle Pliocene epoch, characterized by voluminous eruption of silicic pyroclastic material and subordinate basaltic flow. This Butajira Ignimbrite is distinguished from Quaternary Wenji group as being calcalkaline or mildly peralkaline rather than peralkaline.

E. Chilalo trachyte (1.6Ma-3.5Ma)

This middle to upper Pliocene stratigraphic unit includes trachyte, silicic rocks, and basalt that overlie either the Shebele trachyte or the Butajira Ignimbrite units. The pre Tertiary rock, Oligocene basalt, and the fluvial strata unconformable overlain by thick sequences of Pliocene basalt flow (4.2-2.5Ma) and particularly crystal reach welded Tuff (15-40 % crystals, 3.5Ma), that together exceed a total thickness of 400m.

F. Wenji Group (<1.6Ma)

This group consist various Quaternary lava, pyroclastic rocks, volcanoclastic strata younger than 1.6Ma confined to Wenji Fault Belt and Siliti Debre Zeit Fault Zone (Kazmin, 1979; Woldegabriel et al 1990). A number of thin Ash fall tuffs (2-10 m) that cover the individual step –faulted blocks in front of main Guraghe scarp are late Pliocene, having age range from 2.72 Ma to 2.59Ma. Adjacent to the Guraghe escarpment, the western marginal graben, here called Siliti –Debre Zeit fault zone, contain lacustrine sediment and welded tuff on which are interspersed coalescing nested scoria cones aligned to the Guraghe escarpment. Basaltic flows erupted along the axis of this graben for more than 60Km along strike.an age of 0.13Ma was obtained on one of the aphyric flow which is younger than the 0.24 Ma reported from this general area (Mohr et al, 1980) faulting and stream erosion along the Meki river along the Dugda expose a stratigraphic section more than 100m thick. This step scarp fault forms the eastern wall of the western marginal graben.the bulk of this section (60m thick) consists of reworked pyroclastic rocks separated by a thin (30cm) spherulite obsidian flow

that yielded an age of 1.58Ma. The top of the section is blanketed by bedded ash falls erupted from Quaternary silicic centers of the rift axis.

3.3 Previous investigations in the study area

3.3.1 Hydrogeology of the area

Ministry of Water Resources (MoWS, 2008), report categorized the area into two based on observable topographic feature having their own hydrogeological characteristics within the aquifers. These are Cinder cones and basaltic flow areas, and Kuntane – Inseno-Kela Plain, which is bounded by Butajira Crescent and Tora – Koshe – Dugda Ridge in the western and eastern direction respectively.

Basaltic cinder cones region is located East of Butajira crescent on topographic upland area dominantly composed of scoria cones and associated vesicular basalts. The thickness of the basaltic lava flow is highly variable over 100m where the volcanic vents are situated and becomes thinner away from the volcanic centers. Other Quaternary volcanic rocks like ignimbrite and unwelded tuff lie beneath the scoria cones and associated vesicular basalts besides Tertiary volcanic rock and Mesozoic Sedimentary formations are expected at depth under these formations (MoWS, 2008).

The existing borehole data indicates the aquifers in the area are composed of scoria and vesicular basalt and at some places outside the study area at Shereshera sand and gravel deposit underlying thin layer of flows contribute to the aquifer. Groundwater monitored at reasonably deeper level with respect to surface topography as compared with Butajira crescent and Kontane-Inseno-kela plain. The main recharge source of the aquifers is from subsurface groundwater inflow from the Butajira Crescent to east ward to the area and direct recharge from rainfall put minute contribution. A Crater Lake, Har-Shetan, is connected to the groundwater in the area having low transmissivity. The aquifer varies from unconfined to semi confined within the basaltic formation and in alluvial sediment respectively.

Kontane -Inseno -Kela plain is plain trough is bounded by scoria cones and associated vesicular basalts and to the east by Tora-Koshe Dugda ridge (horst). This region is covered by pyroclastic fall and reworked water lain pyroclastic deposits, lacustrine, alluvial, debris flow deposits. These sediments shows thickness variations from few meters in the west to

several meters and becomes thicker that exceed 260 meters in the central part the area and along Woja River. Quaternary and Tertiary volcanic rock formations and Mesozoic Sedimentary strata are expected to occur in deeper parts underneath. The surface runoff from Butajira and Kibet areas during raining seasons drains to Kontane Marsh and Slight to Lake Abaya. Abundant groundwater is generally found at shallower depth confirmed from hand dug and shallow wells. The aquifer in this area is basically unconfined; however, since the aquifer materials are variable it is possible that some confined or semi confined layers may be happened at various depths. Moreover, thermal springs are observed in two localities of Kontane marsh, groundwater heated up probably related to the development of the young volcanism of the cinder cones and associated basaltic eruption.

3.3.2 Fluid chemical analysis

Fluid geochemical sampling and analysis from 6 different hot springs and cold spring, and lake have been performed by GSE starting from February, 8 – 24, 2017. As a result, the discharge temperature has been noticed in a range from 23°C - 91.06°C and pH values near neutral to slightly alkaline in nature (7.0 - 8.92) immature, peripheral waters types (Figure 3.4 A). Molecular ratios of anions were used to show origin (source rock) of water samples. According to Ternary diagram plot result (Figure3.4C), the chemical composition of the sampled waters is classified as peripheral waters (water with a high percentage composition of HCO 3). In piper diagram (Figure 3.4B), the clustering nature of samples has seen between sample labeled as 0.06 and 0.02(cold water samples), while the other is between samples labeled as 0.01, 0.03 and 0.05(hot springs). According to Giggenbach diagram (Figure 3.4A), most of collected water samples from the study area falls on the zone of immature waters except the one which is labeled as sample code 0.04 (Butajira hot pool) that fall above the partial equilibrium line.

The Na-K is higher than the silica geothermometer that have an estimated temperature of 170.9 ^{0}C-274.7 ^{0}C and 117.59°C-158.86°C. The difference in the results between various geothermometers may indicate shallow conditions of mixing with groundwater. Results of those geoththermometers indicate that some hot springs and hot pools have sufficient heat-generating capabilities and warrant further exploration work to assess their suitability for energy generation. Regional heat flow anomalies exist within the rift due to an upper mantle

intrusion beneath the very thin crust layer. The variation in temperature between samples may confirm the presence of local intrusion of the magma chamber that induces heat flow anomalies.

During the exploration phase, water or solute geothermometer is used to estimate subsurface temperatures, i.e., temperatures expected to be encountered by drilling, using the chemical and isotopic composition of the hot spring and fumarole discharges (Cyrus W. Karingithi, 2010). The Na-K geothermometers as shown in appendix VI have extremely high-temperature (897 ^{0}C) for the sample feature labeled as sample code 0.02(at Har Shetan).This might not be acceptable /reasonable temperature values for such cold surface water bodies (Crater Lake). The reason for such anomalously high-temperature values is because of the low concentration of Na+ (sodium ion) and relatively high concentration of K+ (potassium ion)(GSE,2017|). From the silica geothermometers, it is observed that the hottest spring is Ashute hot spring-1 (sample code 0.03) with a subsurface temperature of about 158.86 ^{0}C, followed by Ashute hot spring-1(sample code 0.01) with a subsurface temperature of about 151.8 ^{0}C. Based on Silica and molecular ratio geothermometers applied in the study; Butajira geothermal prospect area may be considered as a geothermal field with intermediate to high enthalpy resources (GSE, 2017).

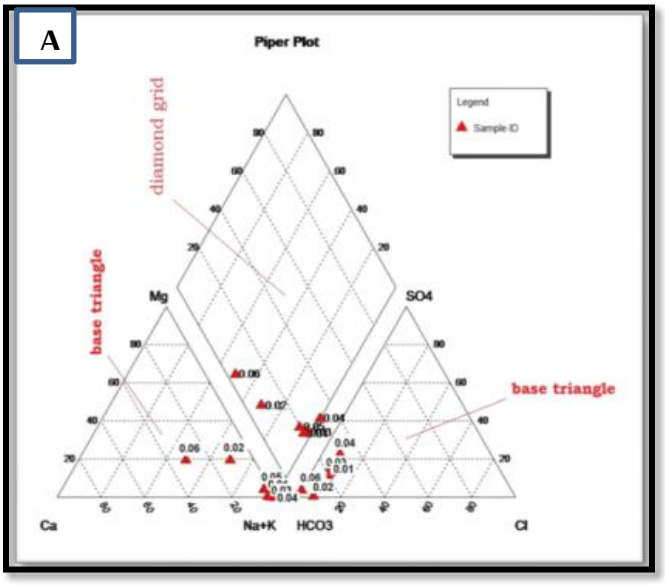

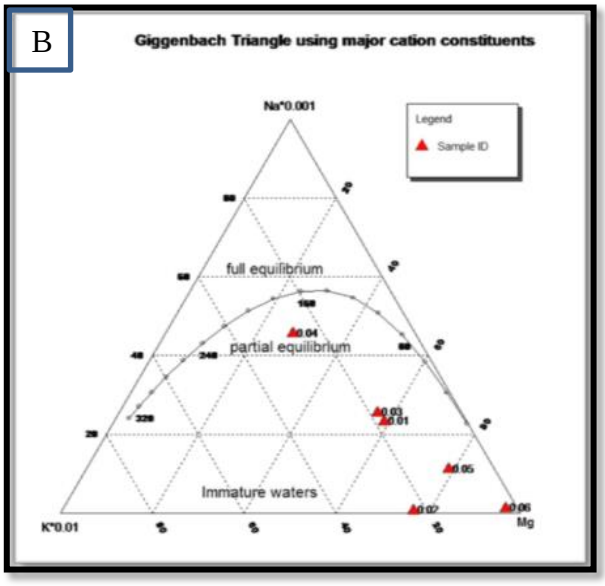

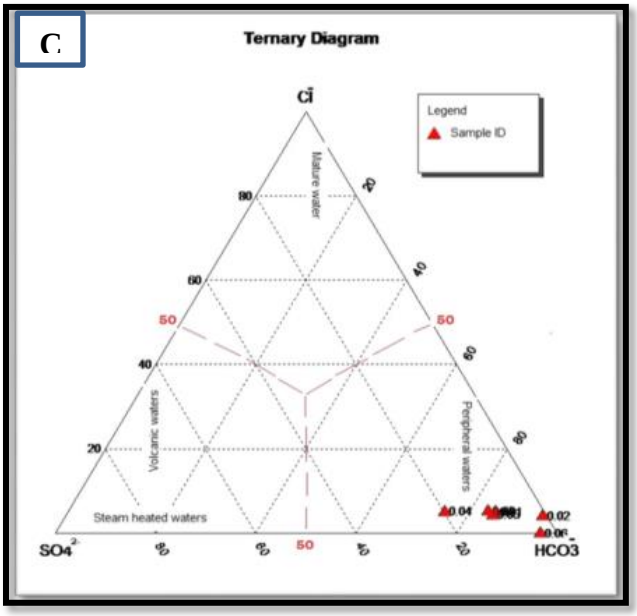

Figure 3.2. A) Piper diagram B) Giggenbach C) Ternary diagram plot adopted from GSE, 2017.

3.3.3 Magnetic survey

The magnetic surveys were conducted by GSE over Ashute area, covering an area of 5 Km^2.. The analytical signal map reveals high magnetic anomalies in the western and northeast, associated with presence occurrences of recent basaltic lava flow and scoria cones, revealed roughly by circular high values in NE-SW extension direction. The low magnetic anomaly is observed in the southern and southeastern part characterized by areas pyroclastic ash fall, alluvial deposits and associated with lineaments, whereas ignimbrite rocks are mapped by medium magnetic values. Tilt angle derivative map shows structures with a general alignment of NE-SW; but there are structures oriented to the NE-SW, NNE-SSW and N-S directions. The striking direction coincides with the direction of the main Ethiopian rift margin, associated graben and different local faults. The alignment of the geothermal manifestations is also in line with the lineaments outlined from the magnetic anomaly. This implies the presence of hidden normal faults or fractures parallel with the general NE-SW direction of the MER along the flat plain Ashute area.

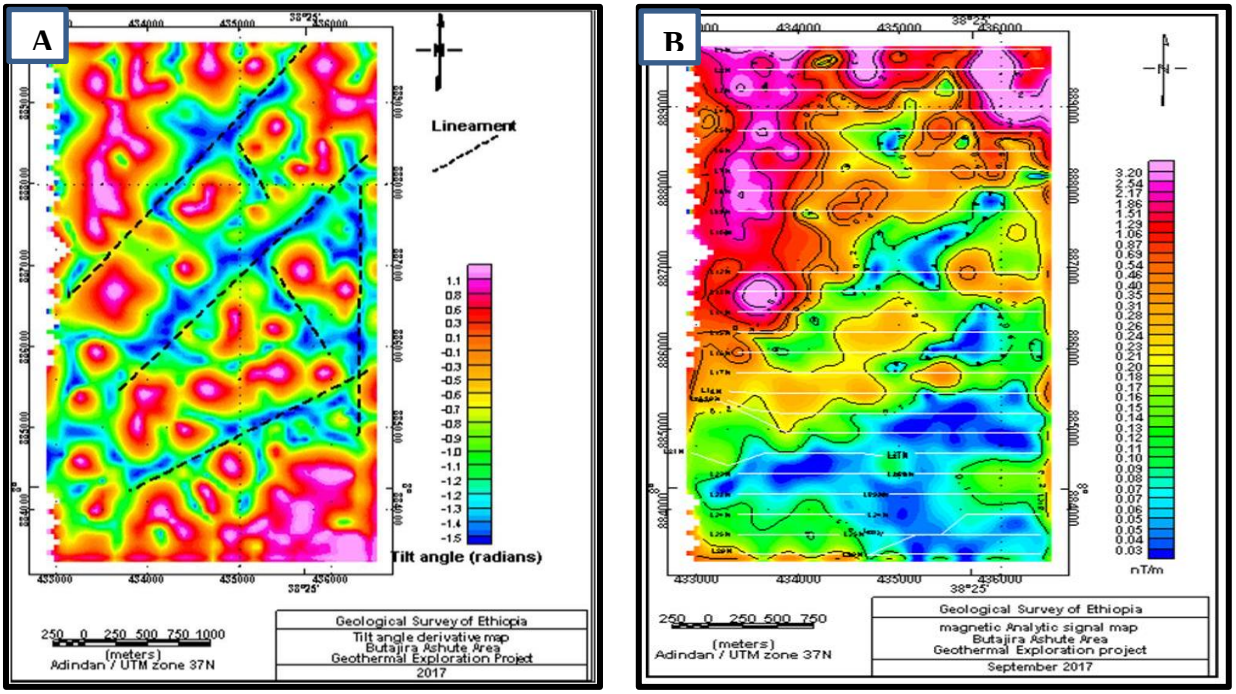

Figure3.3. Magnetic map A) Tilt angle derivative B) analytical signal map adopted from GSE, 2017)

3.3.4 Soil temperature survey

Near-surface soil temperature measurement increase the efficiency of geothermal exploration program by locating thermal anomaly zones in an early stage of exploration, mapping thermal aquifers and by reducing the number of gradient wells needed thereby reduce costs (Sladek. et al., 2007). One meter depth temperature survey was carried out on and around surface manifestation of the study area by GSE in 2017. The survey covered 188 measurement points, distributed along a 2.3x3.5 km grid with an interval of 200 m. Results found from the measured 1 m temperature record ranges from 20.04 to 101.3 °C and high-temperature anomaly is concentrated on two zones of the area; identified as area A and area B. Structural lineaments are outlined from the temperature anomaly oriented in NNE-SSW, NE-SW, and NW-SE directions. This implies the presence of a hidden fault and fractures associated with the general NE-SW direction of the main Ethiopian rift along the flat (Fig 3. Ashute area. On the soil temperature map below(Fig 3.4), dotted line '2' and '3' show respective NE and NNE trending lineaments corresponding to the general direction of the rift margin including Guraghe fault escarpment. Both liniments are also along the lines of the local faults called Dobo-Sabola Fault zone and Ajira faults (MOWR, 2008). They are also

parallel to the youngest geological feature of the area, a series of cones representing the active part of the area. The other lineament, line '1' aligned on N-S direction might follow the regional structures that are located to the south and northeast of Mt. Guraghe that are characterized by N-S orientation (Boccalleti et al., 1998).

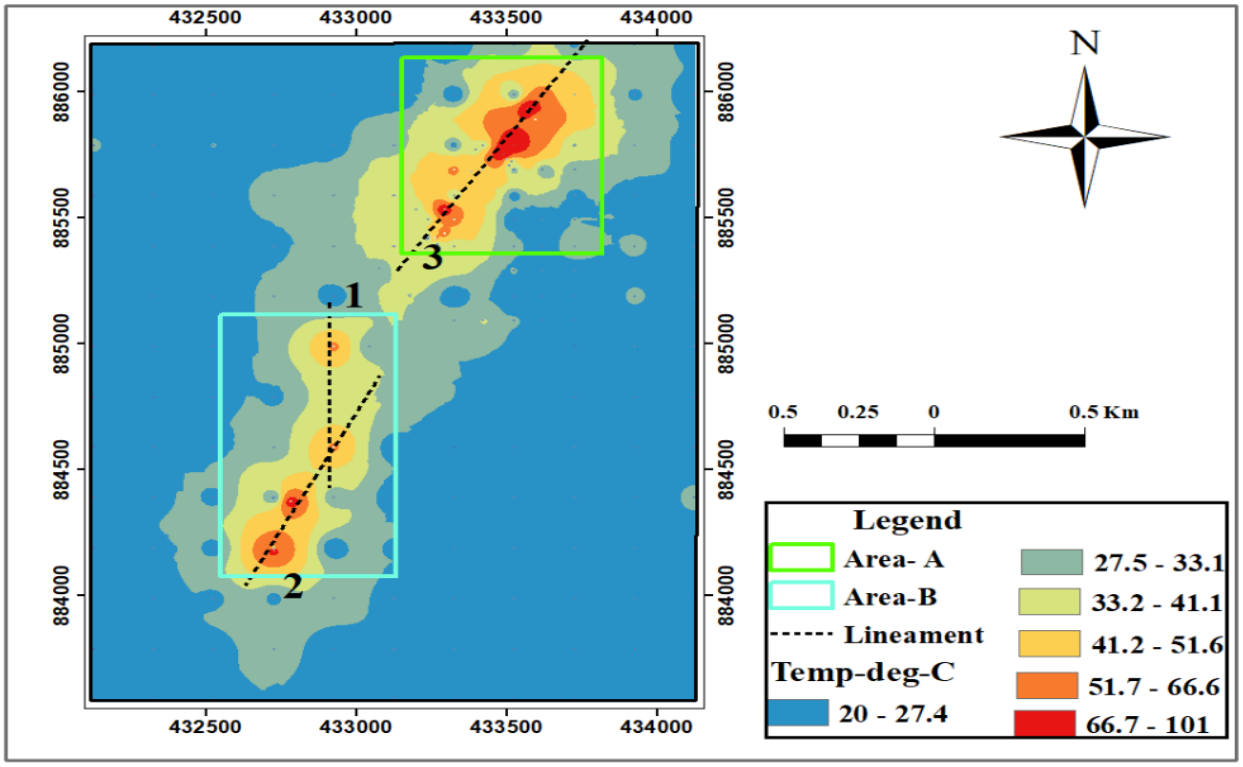

Figure 3.4. 1- m depth Soil temperature map modified from GSE,2017

3.3.5 Magneto-telluric methods

The 1D and 2D inversions were carried out by GSE in 2017. The sounding locations were assigned to four profiles oriented almost N-S, namely P1, P2, P3, and P4. The result (Fig3.5) depicts that three main resistivity layers were observed. The first one is a low resistive surface layer (< 10 Ωm) of up to about1.5 km depth; this can be correlated with alteration zones caused by geothermal activity or with lacustrine sediments or with a hydrothermally altered clay cap. Below this low resistive layer resistivity increasing up to (10-60 Ωm) is observed. This indicates the advancement to a possible reservoir at the depth below about 1 km with a thickness of up to 1.5km. Lastly the third one is beneath the thick high resistivity layer; here a deep conductor is revealed that could be associated with a heat source (Yohannes Lemma, 2007). Faults have been discovered on the profiles 1, 2 and 3.

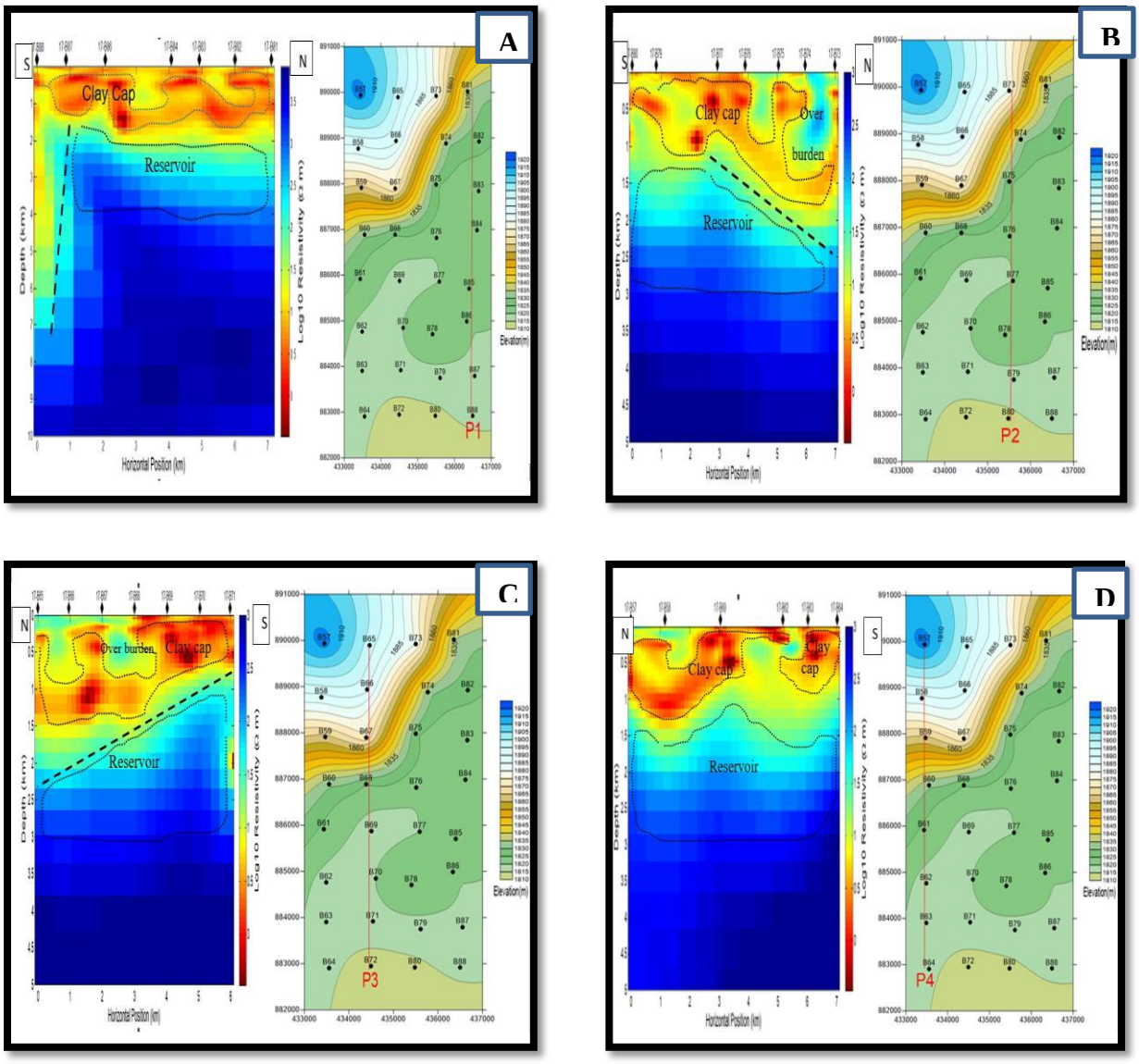

Figure3.0.5. 2D Occam model along Profile A) P1, B) P2, C) P3and D) P4 adopted (GSE.2017).

CHAPTER FOUR

4. RESULTS OF FIELD WORK, PETROGRAPHIC AND XRD ANALYSIS

The study area is located in central main Ethiopian rift nearby Western escarpment associated with SDZFZ that is dominantly covered by both quaternary basaltic rock and pyroclastic deposits and pronounced with the presence of numerous geological structures and surface geothermal manifestations. Results obtained from geological field observation, petrographic description, and geothermal surface mapping as well as XRD analysis have been played a vital role in the preparation of geological and geothermal mapping and selecting promising area besides preliminary conceptual model preparation. This chapter covers two major parts i.e. local geology and surface geothermal manifestations. In a local geology portion more emphasis has been given to characterize and mapping of lithologic units of the study area by means of field observations and petrographic analysis as well as to recognize different geological structures. In geothermal surface manifestations, various surface manifestations like hot spring, mud pool, altered ground and abandoned well sites were described and their distribution was drawn besides volcanic vents in the geothermal map. Moreover, secondary alteration minerals were identified and characterized from petrographic as well as XRD analysis.

4.1 Local geology

4.1.1 Lithology and their petrographic description

The recent findings from geological field work and petrographic thin section analysis revealed that the study area is dominantly covered by five (5) major lithological units namely; alluvial and reworked pyroclastic deposits, Basaltic Scoria, Basalt lava flow, Welded Ignimbrite, unwelded tuff and Phreatomagmatic deposits that comprise rock fragments of trachyte and Diorite around Har-Shetan Lake. Compositionally these rock units varied from basaltic up to felsic igneous rock and recent sediments intercalated with miscellaneous reworked volcanic fragments. These rock units are shown in different landscape from a relatively low-lying flat area up to highly rugged topography features. The study area was affected by tectonic activity triggering different secondary structures, like fault, joints and quartz veins. All lithologic units encountered in the study area were described and detailed petrographic optical property explanations are outlined in appendix IV for each rock sample.

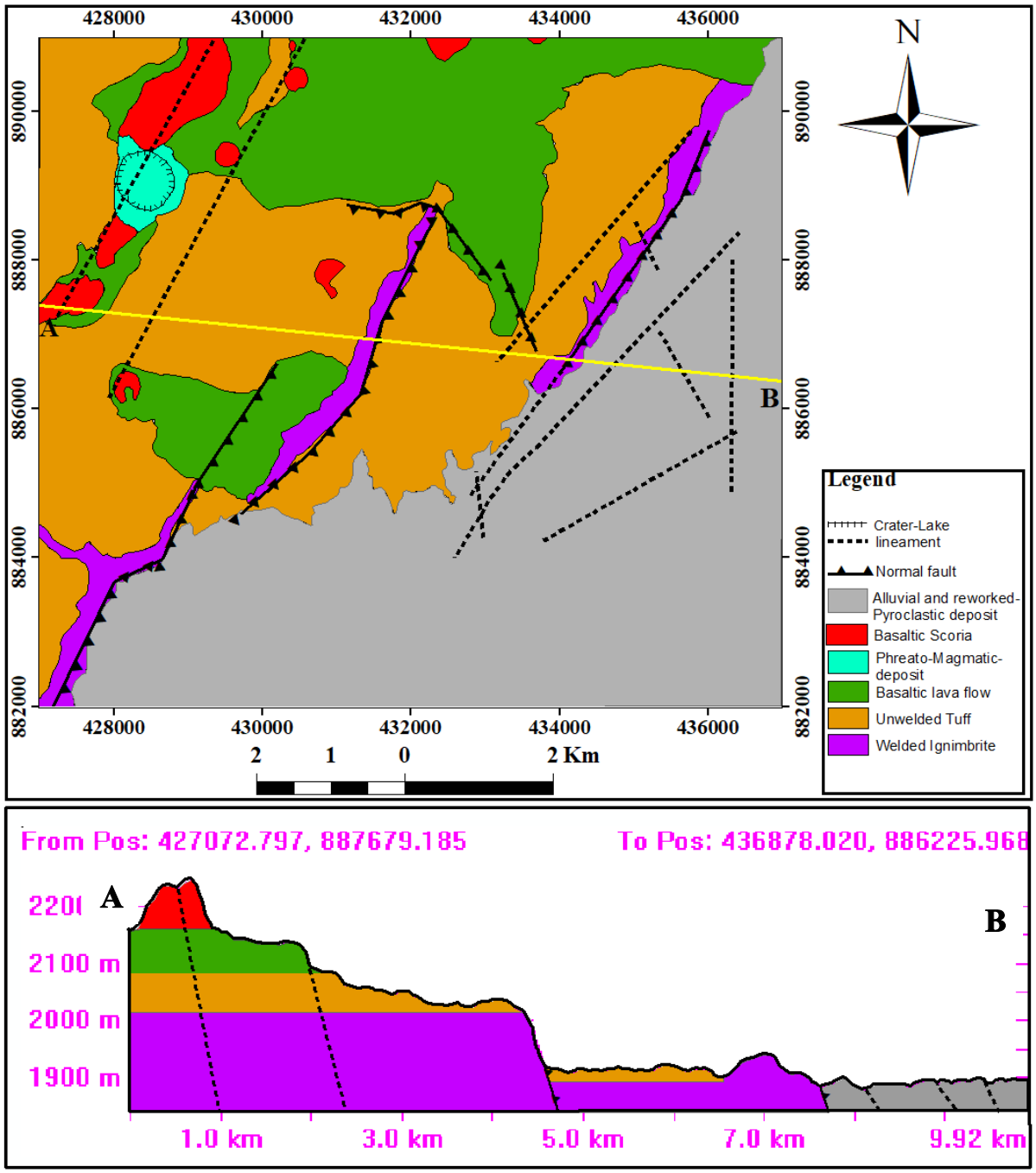

Figure 4.1 Geological map and cross section of the study area

4.1.1.1 Basaltic Scoria

Most of the scoria fall to the ground near the volcanic vent to build up a cone-shaped hill called a "cinder cone". They are generally small volcanoes produced by short-lived eruptions with a total vertical relief of less than a few hundred meters. Scoria cones are dominated in the northern and northwestern parts of the mapped area aligned in NE –SW direction

analogous to the orientation of Selti - Debre Zeit fault zone (SDZFZ). These fault controlled fissural eruptions of scoria cones and associated basaltic lava flows are the youngest product in the study area (Weldegebriel et al, 1990). They are numerous and continue up to Debre-Zeit to the north beyond the study area following the axis, whereas in the SW of Lake Abaya they follow different orientation in WNW – ESE direction (GSE, 2017). Cones in the area are characterized by steep flank with the maximum height of 120 m and < 800 m diameter. This rock unit has red- dark brown in color and shows vesicular texture with larger void space without filling material in hand specimen view.

Petrographic observation of this rock unit from the prepared thin section (TS-2) shows glomeroporphyritic texture; is a variety of porphyritic texture which has clusters of clinopyroxene and plagioclase phenocryst in fine-grained plagioclase laths, pyroxene and a minor amount of opaque minerals as groundmass (Fig.4.1). Modal percentage of mineral assemblages embraces 2% olivine, 11% pyroxene, 14% plagioclase feldspar, and 21% ground mass holding plagioclase, pyroxene, and opaque minerals and the rest 52% portion is covered by of void space. The measured maximum length for pyroxene, plagioclase and olivine phenocryst is 8.2mm, 6mm and 0.4mm respectively. The olivine and pyroxene phenocrysts show alteration around the edges / rim of minerals grains into fine-grained biotite and opaque mineral. Vesicles in this rock show spherical in shape some of them are occupied with some amygdule (inclusions of secondary materials) in concentric layering within a void space. From the modal percentage and distribution of the minerals and overall texture and amount of void spaces we can conclude that the rock is basaltic scoria.

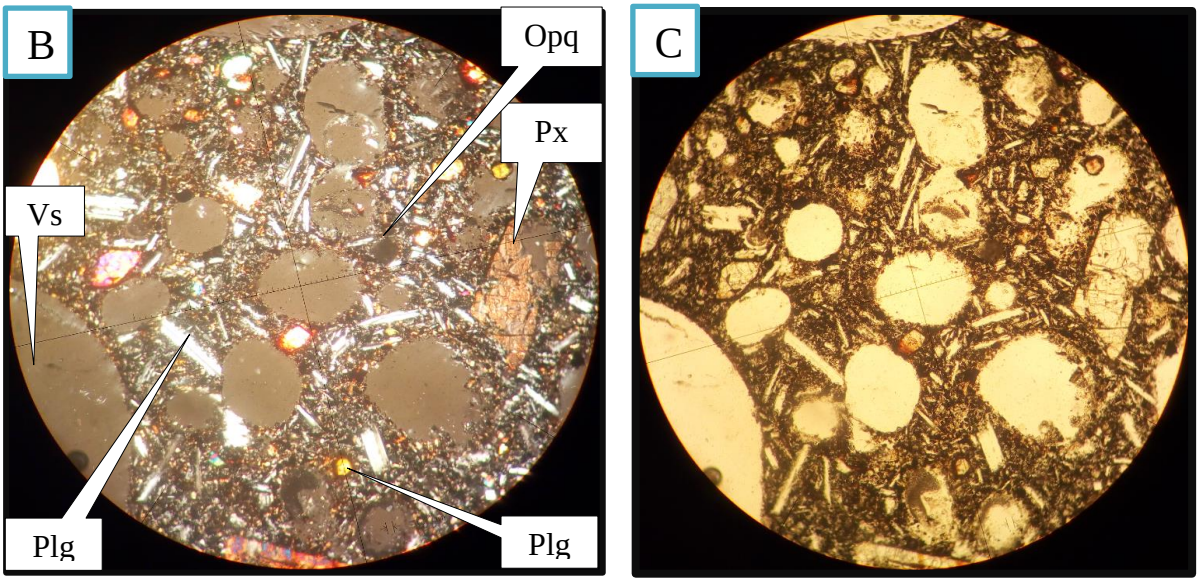

Figure 4.2. (A) Basaltic Scoria field exposure; (B) & (C) petrographic view of sample (TS-2) under XPL and PPL respectively. The labels stand for: Ol-Olivine; Plg - Plagioclase feldspar; Px – pyroxene; Gm-ground mass; Vs-void space.

4.1.1.2 Phreato-magmatic Deposit

Geological field observation and mapping reveals that Phreato-magmatic deposit is largely found in North West part of the study area and covers about 2km^2 with gentle outer flank circular tuff ring with central Crater Lake, named as Har-Shetan. The internal diameter of the crater rim measures about 750m and forms upright wall around the inside of the Lake. This upright wall comprises well stratified welded Ignimbrite as well as laminated lapilli sized Scoracious Basalt. Blocks of Trachyte and Diorite rock fragments lay over the pyroclastic deposit around the envelope of the Har-Shetan Crater Lake. This phreatomagmatic product interconnected to the base of the scoria cone as shown in figure 4.2B. These different sized blocks become dismantled and ejected from underlying country rock shown rock fragments layered also leave them disseminated around the Lake.

Petrographic thin section analysis from phreatomagmatic deposit (TS-3) exhibit trachytic texture i.e. a texture wherein plagioclase grains show a preferred orientation due to flowage, and the interstices between plagioclase grains are occupied by the glass or cryptocrystalline material. As shown in photograph below (Fig 4.2 C& D) minerals are aligned into preferred orientation and established in layer form. The abundance of minerals in modal percentage comprises 86% plagioclase feldspar; 7% potassium feldspar phenocrysts, 5% volcanic glass

and 2% volcanic glass. Alkali feldspar mineral grains are encountered in various sizes from fine-grained microlite up to relatively larger grain in the form of phenocrysts. Beside phenocrysts of mineral grains, rock fragments that were enclosed by dark brown, layered, glassy material and shows sieve texture (Moth eaten texture) wherein individual minerals grains show an abundance of glassy inclusions with a few opaque and alteration minerals. Among those alteration minerals Biotite, Chlorite, and Actinolite are noticed. The measured maximum lengths of plagioclase, orthoclase phenocryst, and rock fragment are 0.6mm, 5.6mm, and 7.2mm respectively. Considering the type and modal percentage of minerals and overall texture this rock is Trachyte.

Petrographic observation from the other rock fragment attained from phreatomagmatic deposits, sample (TS-6) shows both intergranular and ophitic texture which have coarser mineral grains with abundant opaque minerals. As notice at lower photography (Fig 4.2 E&F) ophitic texture is revealed phenocrysts plagioclase laths are oriented in precise path and encloses a coarse-grained matrix of pyroxene crystals. Moreover, it shows intergranular texture, thus the angular interstices are occupied by grains of ferromagnesium minerals such as olivine, pyroxene, or opaque iron-titanium oxides. The modal percentage of mineral composition of the rock unit is 3% opaque minerals, 3% olivine, 29% pyroxene, and 65% plagioclase feldspar. The maximum lengths of grains size of opaque, olivine, plagioclase feldspar, and pyroxene is 2.2mm, 2.4mm, 4.6mm, and 5.8mm respectively. Accordingly, the presence of a number of minerals, their modal percentage and texture make a distinction to identify the rock unit as Diorite.

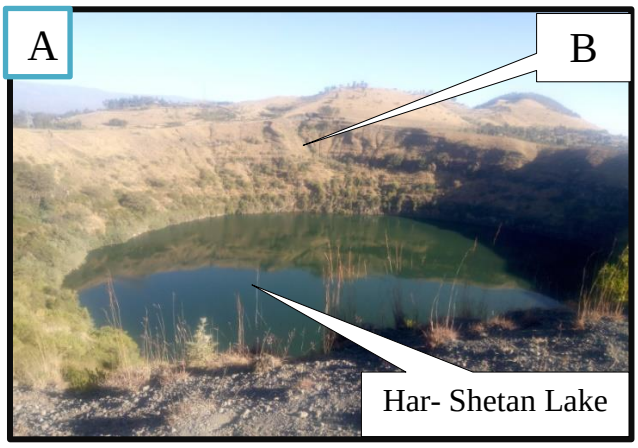

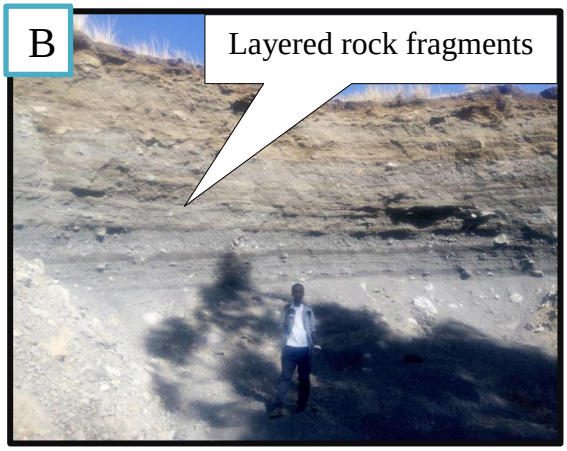

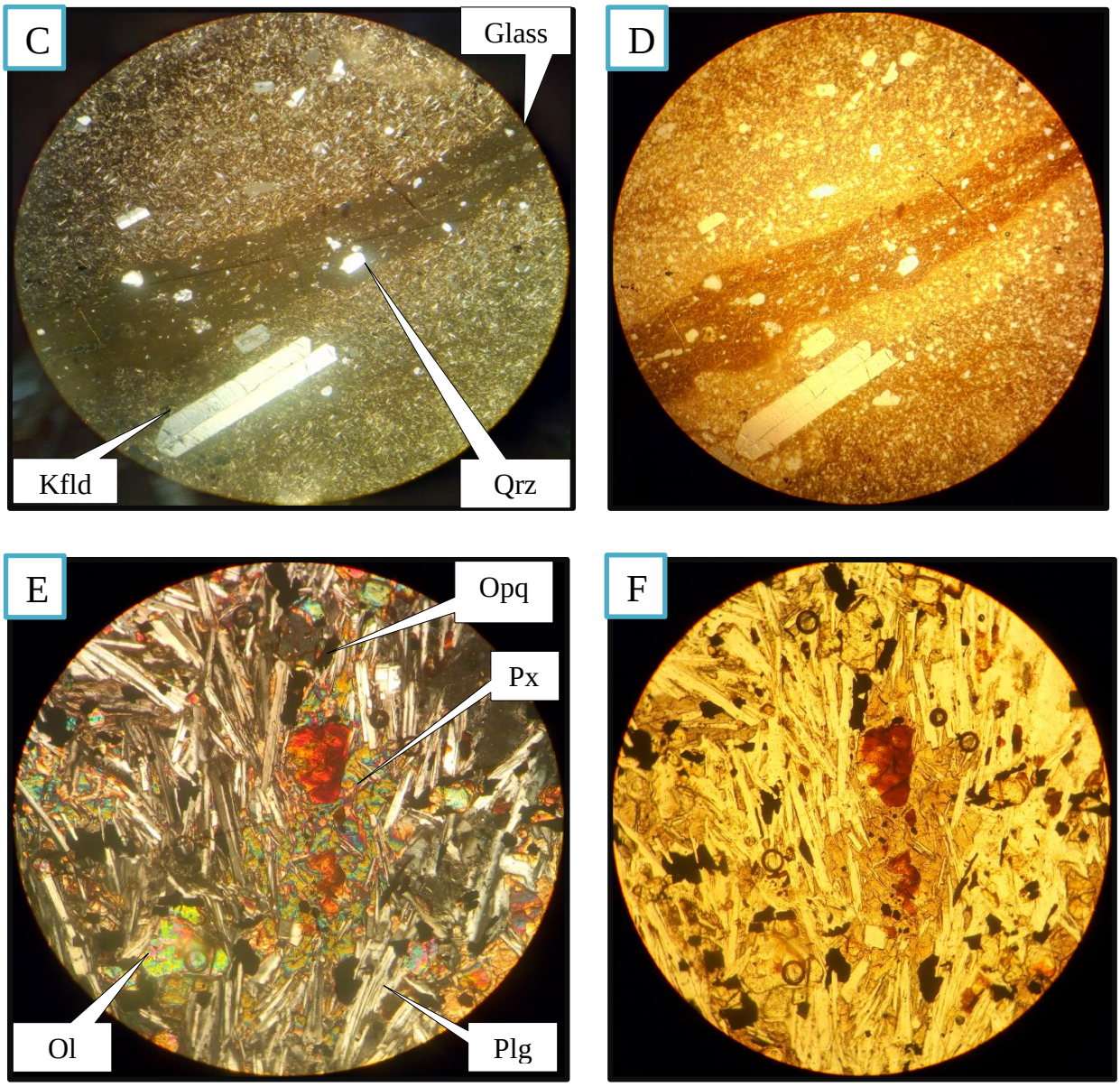

Figure 4.3 Phreatomagmatic deposits: A & B Har-Shetan Lake and field exposure; C & D petrographic view of sample (TS-3) and E & F (TS-6) under XPL and PPL respectively. The labels stand for: Ol-Olivine; Plg - Plagioclase feldspar; px -pyroxene; Op- opaque

4.1.1.3 Basaltic lava flow

Basaltic lava flows in the study area are associated with the eruption of basaltic scoria cones. This rock unit is dominant in northern and north western parts of the study area at the base the of cinder cone resulted from the out flow of lava resulted during collapse of highest part of the cones. The formation of this rock unit was associated with later stage of eruptions from the scoria cones. Stratigraphically, the basalt lavas lies on top of tuff and ignimbrite units in most area whereas in some localities , at Lebu River bottom around Senena village, Tuff

deposit having greater than 20 m in thickness overlies the basaltic lava. Texturally, both porphyritic and vesicular textures are existed. The vesicular texture is especially dominated on the top of the flow around the cones flanks.

Two thin sections (TS-4 & TS-5) for petrographic analysis were selected from vesicular and porphyritic basalt to characterize the rock unit. Consequently both samples show similar minerals assemblages but differ in rock texture and a modal percentage of the phenocrysts. In both thin sections olivine, pyroxene, plagioclase and opaque minerals as ground mass are present in various proportions. The modal percentages of those minerals observed in TS-4 are 2% olivine, 23% pyroxene, 37% plagioclase feldspar and the rest of this portion is covered by of ground mass. In this sample Coronas / reaction rims, Moth eaten texture (sieve texture) and Oscillatory zoning were observed in plagioclase feldspar and olivine and pyroxene minerals altered into volcanic glass and opaque minerals. Crystal shapes of olivine and pyroxene grains are dominantly anhedral and alkali feldspar show euhedral prismatic laths. Phenocryst of olivine, plagioclase, and pyroxene has a maximum length of 1.2mm, 3.4mm, and 4.2mm respectively. While, sample (TS-5) displays more void spaces and little alteration have been observed. The modal percentages are 1% olivine, 22% pyroxene, 34% plagioclase feldspar, 36% of ground mass and the rest of this portion is void space. Crystal shapes of olivine and pyroxene grains are dominantly anhedral and alkali feldspar shows euhedral prismatic laths. The phenocrysts of olivine, pyroxene, and plagioclase have a maximum length of 0.4mm, 3.2mm and 3.6mm respectively. Generally this rock unit shows glomeroporphyritic texture; is a variety of porphyritic texture which has clusters of phenocryst olivine, pyroxene and plagioclase enclosed in fine grained groundmass. This sample shows different feature indifferent phenocryst like Coronas or reaction rims in olivine crystals besides Moth eaten texture (also called sieve texture) and Oscillatory zoning in plagioclase feldspar. Petrographic optical analysis of minerals and their modal percentage confirms this rock unit is vesicular basaltic.

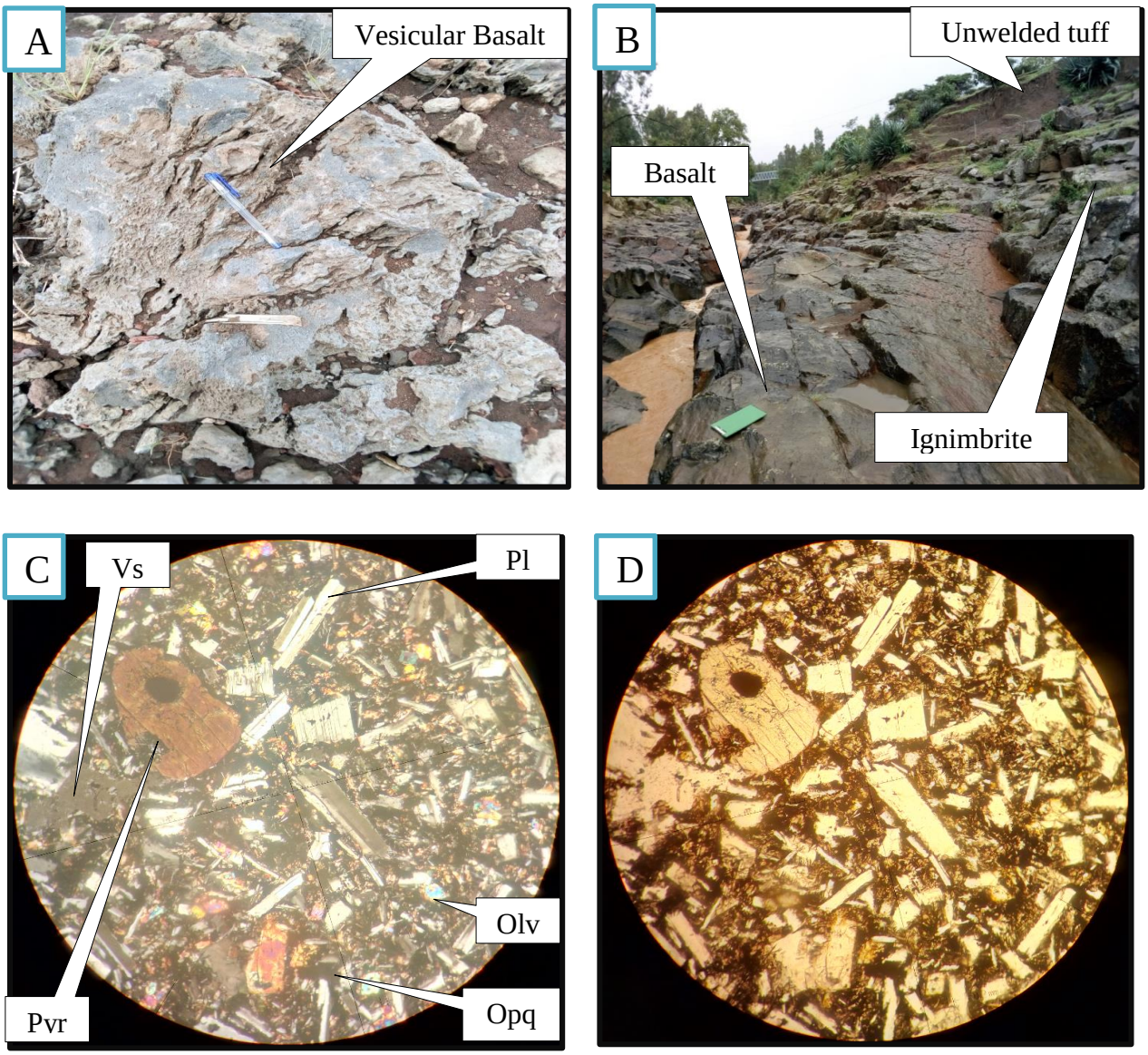
A
Vesicular Basalt
B
Unwelded tuff
Basalt
Ignimbrite
C
Vs
Pl
Olv
Pvr
Opq
D

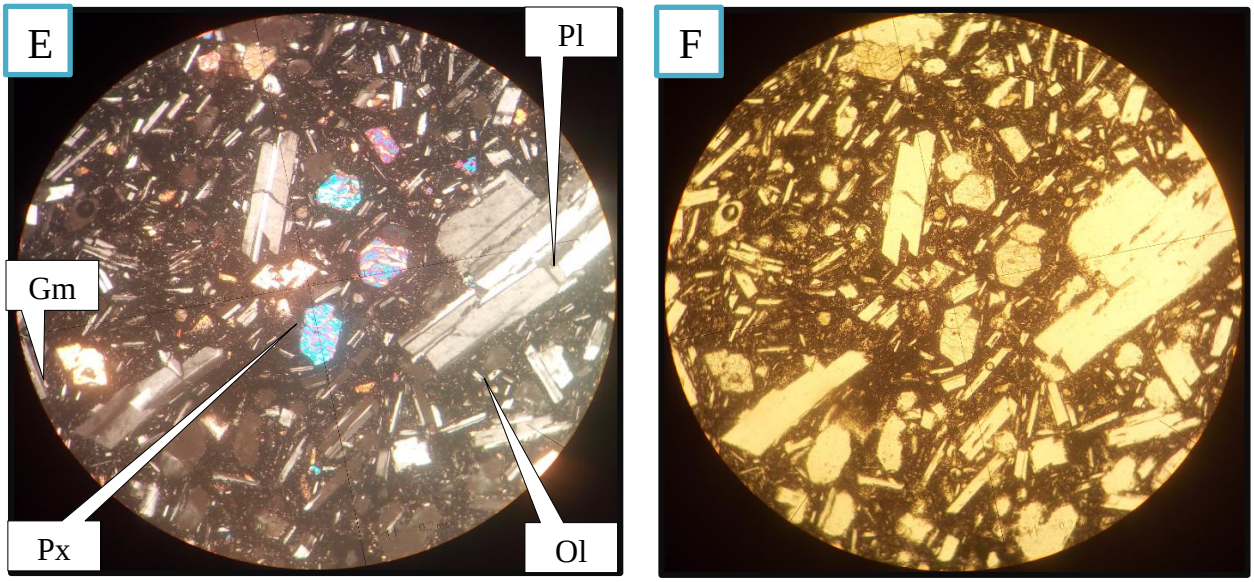

Figure 4.4. Har-Shetan Lake field exposure A & B; C & D petrographic view of sample (TS-4) and E & F (TS-5) under XPL and PPL respectively. The labels stand for: Olv-Olivine; Plg - Plagioclase feldspar; Op- opaque; Gm-ground mass.

4.1.1.4 Welded Ignimbrite

This lithological unit is located in central part of the study area exposed due to downward fault movement extends in NE direction. Consequently this rock unit covers relatively smaller area associated with fault escarpments which have thickness from 15m-45m. Texturally there are two varieties of welded pyroclastic deposit in the area. The first one is highly welded crystalline ignimbrites with crystals of quartz and K-feldspar. This ignimbrite type mostly exposed in north east margin towards the central part of the mapped area along down throw fault and also layered within rim of Lake Har-Shetan underneath phreato-magmatic deposit. The second variety of ignimbrite is mostly dominated by highly welded ash and bombs and blocks of lithic fragment (2cm-5cm). It located in south eastern side of the study area outcropped on fault zones and under riverbeds. There is also a top overlaying separate highly crystalline flow suspected from huge (>3m) transported blocks because it was not accessible. Stratigraphically the whole ignimbrite lies beneath by the surrounding unwelded tuff that covers the upland part of fault blocks.

Petrographic analysis from representative thin sections (TS-7&TS-58) reveals that quartz; plagioclase and rock fragments are available in various proportions. Moreover secondary alteration minerals like Biotite, Rutile, and Chlorite were distinguished. In sample TS-7 the modal percentage of major minerals constitutes are 3% opaque; 28% orthoclase; 30% quartz,

38% of volcanic glass. The maximum length for phenocryst is 0.68mm quartz 0.68mm plagioclase and 2mm rock fragment. The plagioclase phenocrysts and rock fragments altered in to fine grained biotite and opaque mineral around the edge of the mineral grains. Volcanic glass, fine grained alkali feldspar, quartz and opaque minerals form the groundmass. As a result the glass matrix has an apparent discontinuous lamination caused by extreme compaction and welding of original pumice fragment. This regular alignment of the flattened fragments is known as Eutaxitic texture. Crystal shapes of quartz grains are dominantly anhedral and alkali feldspar show euhedral prismatic laths.

Result from other thin section (TS-8) analysis tell the modal percentages are 2% opaque; 24% plagioclase feldspar; 33% quartz ; 41% rock fragment that consists of fine grained ground mass and opaque minerals. This sample shows Moth eaten / sieve texture in rock fragments and spherulitic texture in quartz. Crystal shapes of quartz grains are dominantly anhedral while rock fragments are elliptical in shape. The measured maximum length for phenocryst is; 0.68mm quartz, 0.68mm plagioclase, and 5mm rock fragment. Dominant alteration is observed along layering and within rock fragments. The groundmass is predominantly composed of quartz, alkali feldspar and opaque minerals. Generally these rock units show porphyritic texture which phenocryst quartz and plagioclase enclosed in fine grained groundmass of volcanic glass. The modal percentage of the constituent minerals and their texture reveal the welded ignimbrite rock unit.

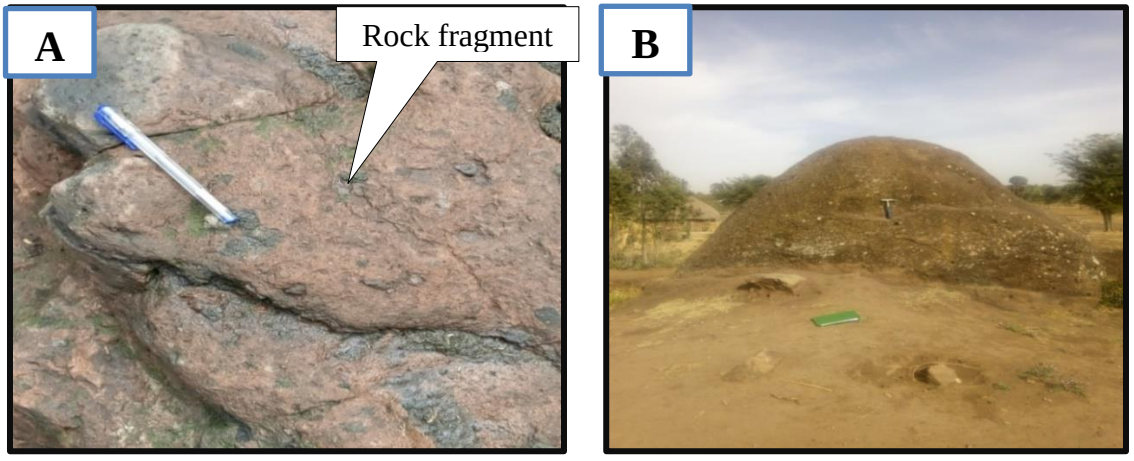

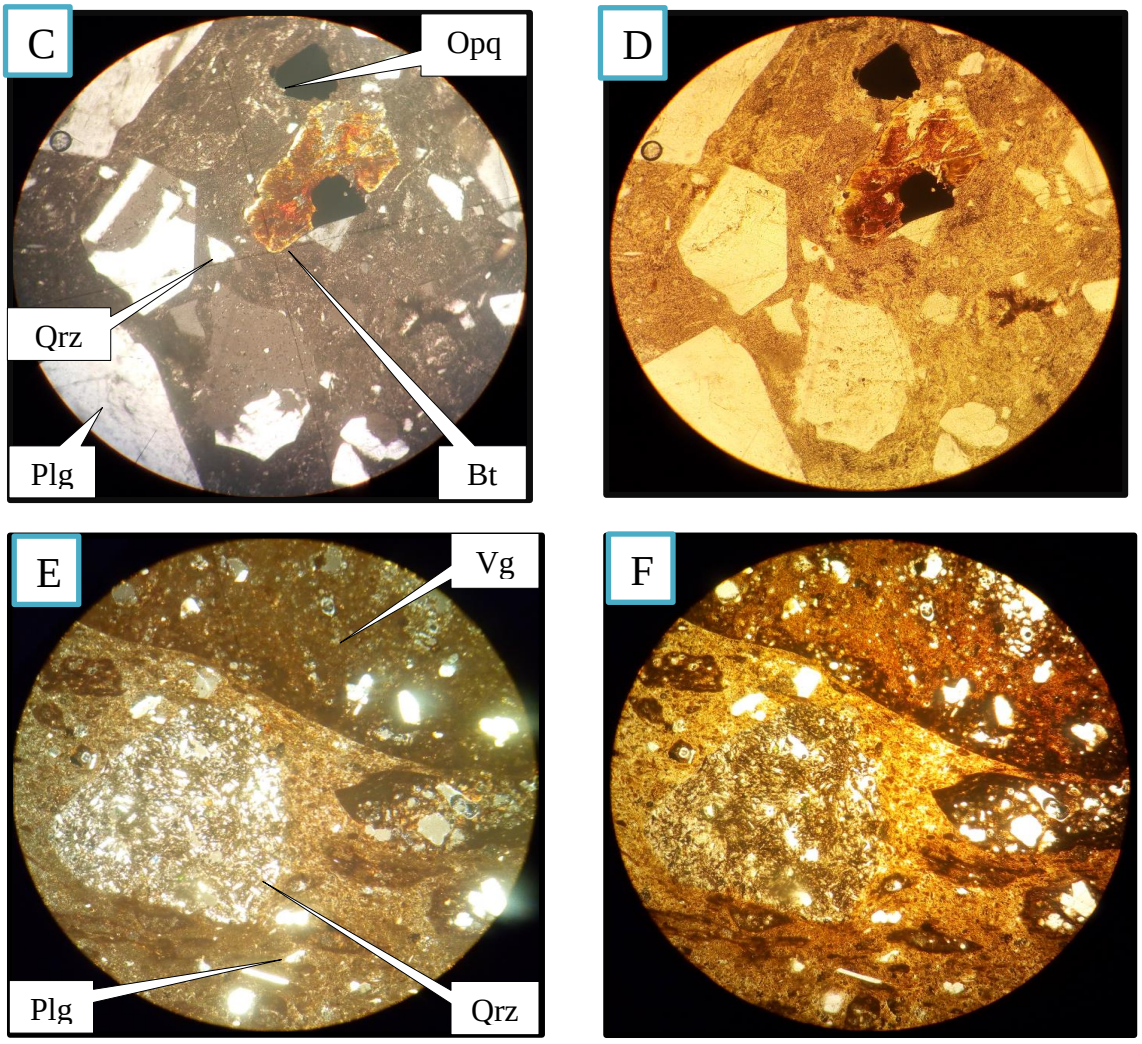

Figure 4.5 Welded ignimbrite A & B field exposure; C & D; E & F petrographic view of sample TS-7 and TS-8 under XPL and PPL respectively. The labels stand for: Qrz- quartz, plg –plagioclase, Op-opaque,Bt-Biotite ,and vg- volcanic glass.

4.1.1.5 Unwelded Tuff

This lithologic unit is un-welded fine grained pyroclastic Ash flow Deposit with large area of coverage among other lithology units. Even though, this lithology exposed in various localities, 3 thick flows outcropped along river cut in south western and western parts of the study area. In eastern parts of mapped area they occur as intercalation and form thin layering between thick overlying basalt and underlying ignimbrite with a range in thickness from less than 10m to 90m. General stratigraphy of this unit overlies the welded ignimbrite and underlie with basalt. It has white to yellow brownish color and predominantly consists of volcanic ash with minor amount of crystals and rock fragments occur in two types; the glassy

and the fragmental tuff. The glassy (vitric) tuff is wholly glassy whereas the fragmental tuff is made up of lithic fragments with subordinate quartz and feldspars.

Petrographic analysis of sample (TS-10) exhibits a glassy texture with few phenocrysts of quartz and Orthoclase. The modal percentage of mineral constitutes are potassium feldspar (~2%); quartz (2%); opaque minerals (1%) and rest enclosed by glassy material. The crystal shape of quartz grains show dominantly anhedral and alkali feldspar show euhedral to subhedral with maximum length 1.84mm and 0.68mm for the largest grains of each phenocrysts respectively. The groundmass is composed microcrystalline of volcanic glass, quartz and potassium feldspar. They and the crystals of quartz and feldspar were embedded by in fine grained glassy particles (ash). Some of glassy fragments are slightly flattened even if not well welded to one another. Based on the modal proportion and grain size distribution of the phenocrysts, texture and nature of ground mass this rock is unwelded Tuff. Quartz grains relative to the other phenocrysts doesn't show any preferred orientation and also they are not welded to each other.

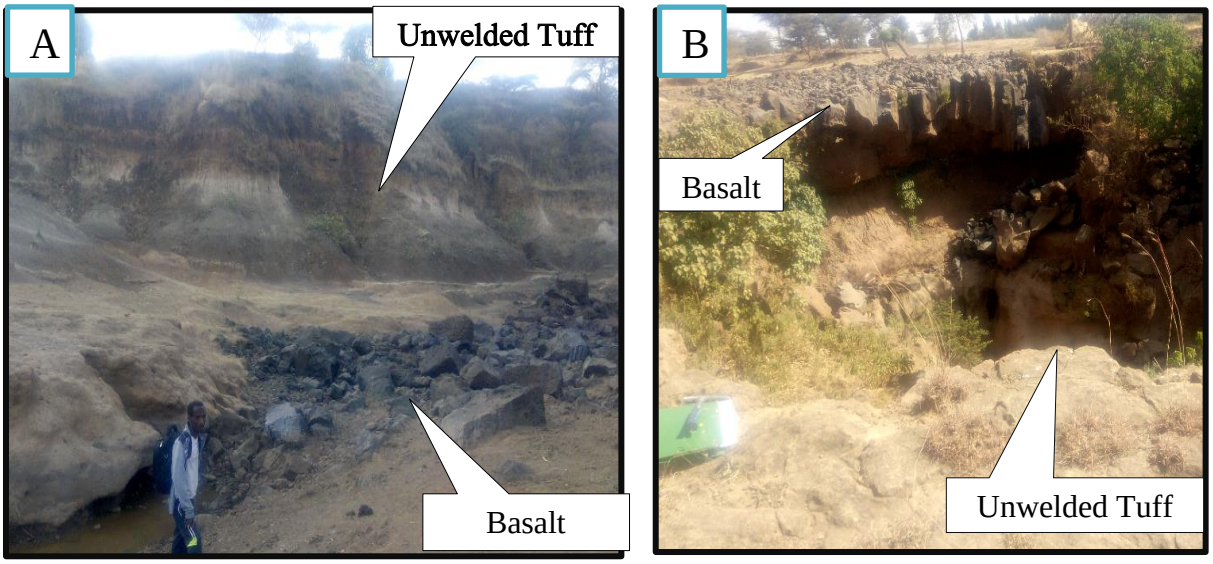

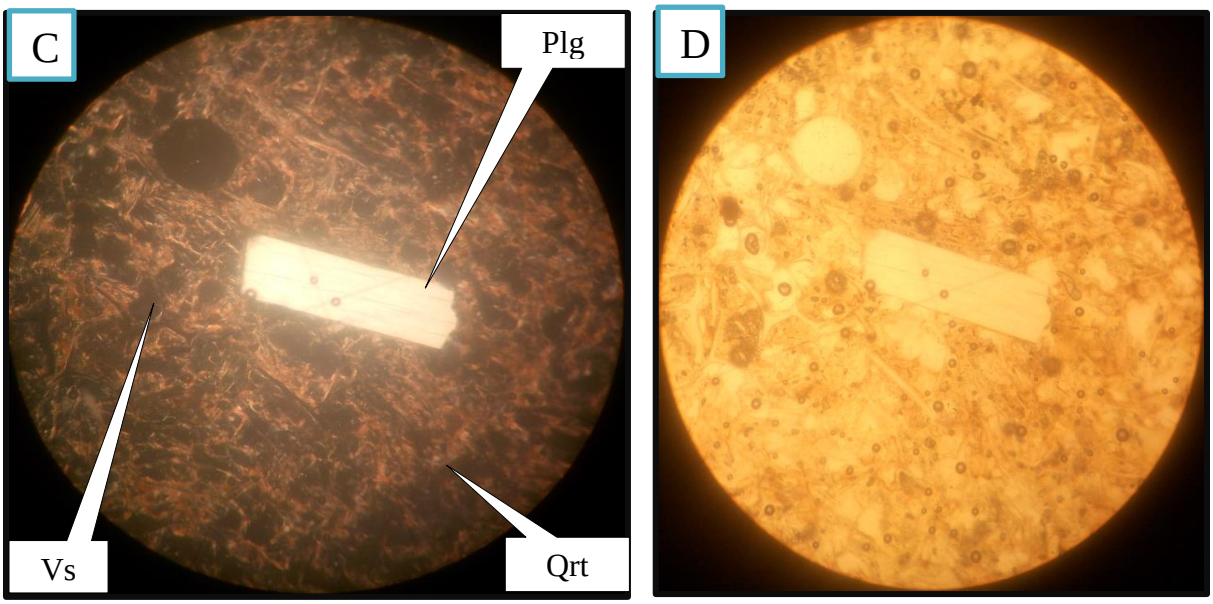

Figure 4.6 Unwelded Tuff field exposure field exposure A & B; C & D petrographic view of sample TS-10 under XPL and PPL respectively. The labels stand for: Plg - Plagioclase feldspar; Qrt –quartz; Vs-void space.

4.1.1.6 Alluvial and reworked pyroclastic deposits

This lithology unit found in the southern and south eastern part of the study area which forms flat-lying topography within Kontane Marsh along with plain land of Ashute and Gerbi Ber villages. Both pyroclastic and sediments are intermixed and stratigraphically they are set together one on another in undefined pattern. Since the area of this unit fully covered by water and grass the exact thickness is not known. But evidences confirmed by drilling in nearby area thickness exceed 70m (GSE, 2008). The rock unit is less indurated and consists of lithic fragments derived from northern part of high lands and fault scarps. This unit consists of graded sediment deposited from ash to gravel size. It is dominantly a product of reworked pyroclastic ash flow deposit and water laid turbid debris. The matrix is dominated by ash size particles of glass, quartz, obsidian and pumice.

Figure 4.7 Alluvial and reworked pyroclastic deposit

4.1.2 Geological structures

The CMER is characterizing by border faults and active fault system in the rift floor. It is mainly clustered on two major fault systems namely; Selti - Debre Zeyit fault and Wonji fault belt with associated Quaternary volcanic rocks. This rift zone strike in NNE–SSW and characterized by a serious of normal faults that obliquely cutting the rift floor in the MER. The rift floor is strongly affected by dense fault swarms with right stepping arrangement strike ~0^0-20^o exhibits small throw relative to the trend of regional rift margin (Woldegabriel et al., 1990). Butajira geothermal field situated in the western margin of CMER characterized by faults and associated aligned cinder cones and lava apron. Thus the structural features identified from aerial photograph interpretation and actual field observation display a narrow half graben. These aligned step up faults have general orientation of N25^0- 40^0E and dip 30^0 - 65^0 SE directions. In the south western flank of the area fault with vertical displaced about 70m along NE extension similar to the trend of border fault system. Another small scale transverse fault with bearing N35^0 W, 38^0 SW is found following the river flow direction. These faults are found in the east central parts of the study area and forms escarpments between ignimbrite and basalt rock units.

Lineaments were noticed in various orientations that buried under recent basaltic lava flow and alluvial deposits. They aligned in a linear to curvilinear features observed in the mapped

area and approved from magnetic and geophysical survey. They have various trend; NW-SE, NE-SW, N-S and E-W. Moreover, joints were observed within unwelded Tuff, ignimbrite and within sinter units provide awareness to the past stress. In particular, sinter-hosted joints could be recently generated and therefore they provide a measure of currently active movements and stresses. Field observations in the area indicates joints are mostly develop in a direction of NE-SW, N-S and E-W, and to some extent NW-SE. E-W and N-S sets or corresponding NE-SW and NW-SE striking presumably indicate a fault-related stress-regime. The aperture of joints is filed by secondary minerals of quartz and the surrounding rocks are highly altered suggesting circulation of hot fluids. Mineral precipitations from supersaturated geothermal fluids in the joints are evidence of extensional processes.

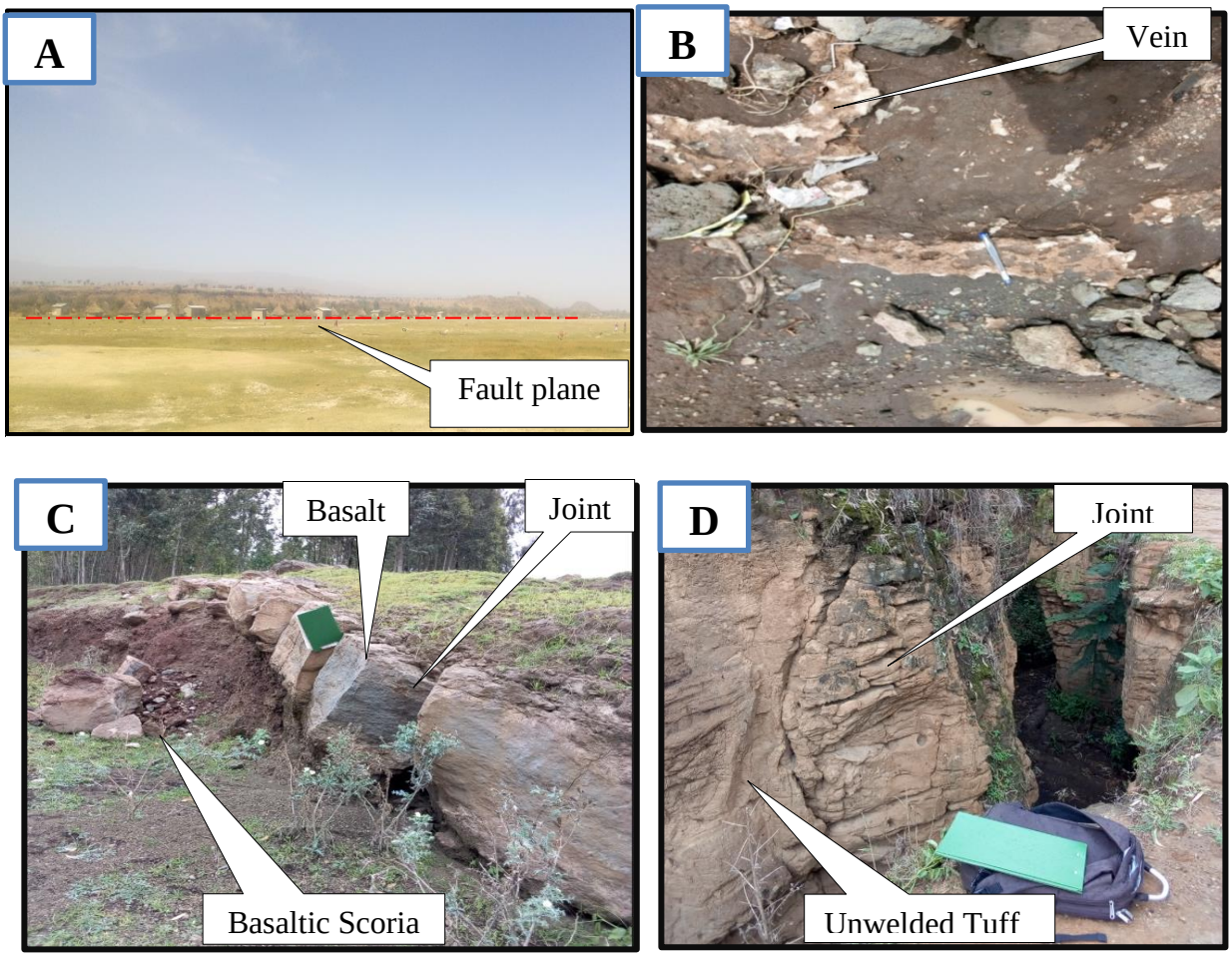

Figure 4.8 Geological structures A) fault B) Joints filled by secondary minerals C) basalt as sill in basaltic scoria D) Joint sets in Unwelded Tuff.

4.2 Surface geothermal manifestations

The geothermal map was conducted analogous to geological mapping at the same scale throughout the study area. The geothermal mapping encompasses different surface manifestations like hot springs, hot water pools, mud pool, volcanic centers, hydrothermal surface alteration, Silica sinter and sulfur deposits and Hot drill well and Abandoned well sites. In addition to these DEM used to display surface conditions as shown in figure 4.11 besides the geothermal map at a reduced scale embracing soil temperature survey having 5^0C isotherm accomplished around geothermal surface manifestations.

Geothermal surface manifestations of the study area comprises hot springs, hot water pool, mud pool, steaming ground and associated altered grounds. Temperature measurement of these surface manifestations obtained 48^0C and 101ºC in extinct thermal spring and Mud pools respectively. These manifestations are dominantly concentrated in the eastern part at Ashute and Gerbi Ber plain land of the mapped area. All these features aligned in parallel pattern associated with the trend of major fault system having a general NE strike direction. At the intersection of NE fault system with NW-SE strike fault system surface manifestations are prominent in area. Indeed, a surface manifestation may be observed fairly on the up flow zone resulted from fault structure that serves as permeability pathway for a fluid flow pattern. The presence of surface manifestation and their temperature measurement as well as the type and intensity of rock alteration indicates the south eastern part of the study area encompass better prospect to hold geothermal resource. Thus the type and distribution of geothermal manifestations of mapped area might relate to the convection of fluid through deep rooted fault zone that could be heated and rise due to the presence of shallower magma intrusions.

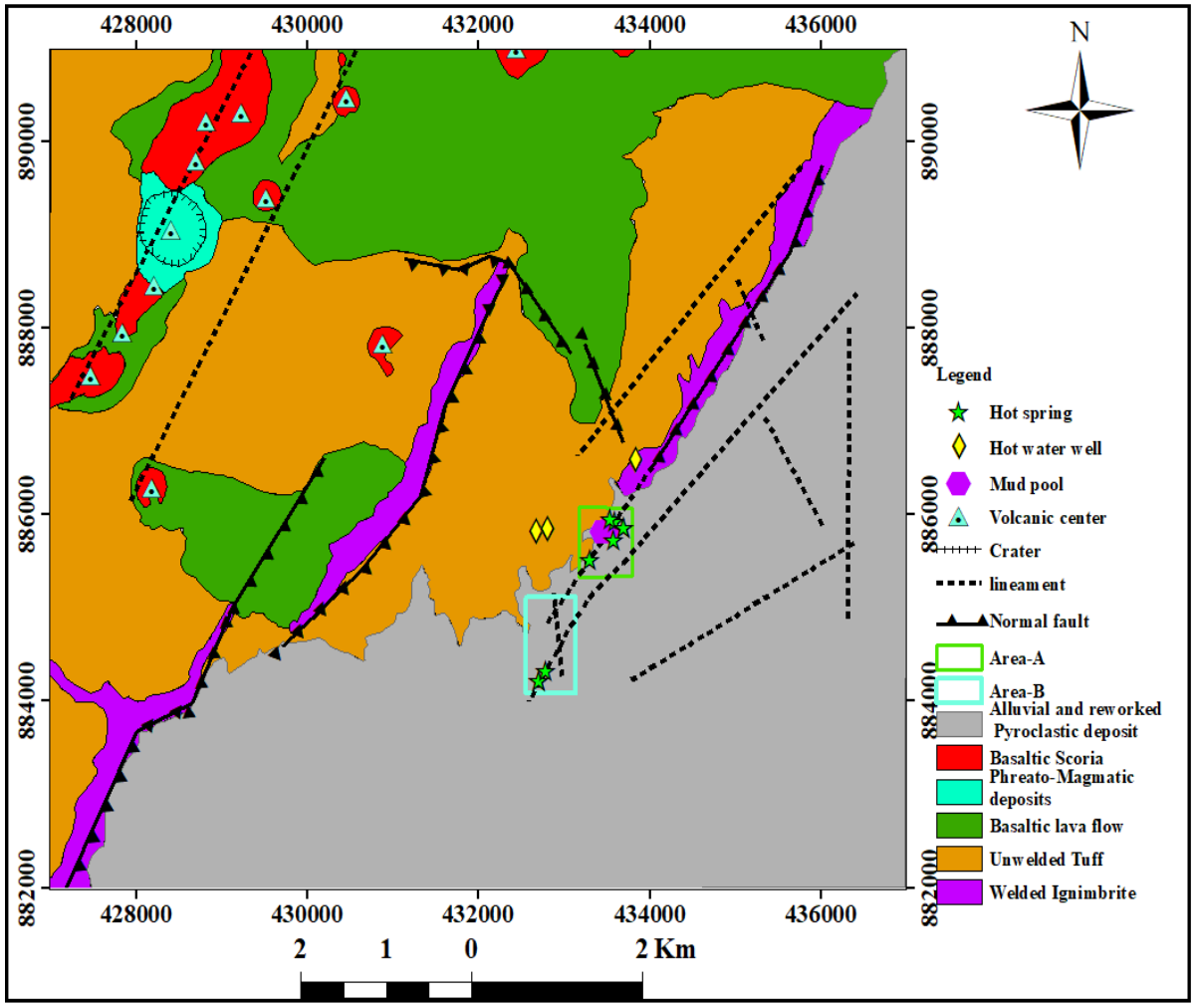
428000
430000
432000
434000
436000
890000
888000
886000
884000
882000
N
Legend
Hot spring
Hot water well
Mud pool
Volcanic center
Crater
lineament
Normal fault
Area-A
Area-B
Alluvial and reworked Pyroclastic deposit
Basaltic Scoria
Phreato-Magmatic deposits
Basaltic lava flow
Unwelded Tuff
Welded Ignimbrite
2 1 0 2 Km

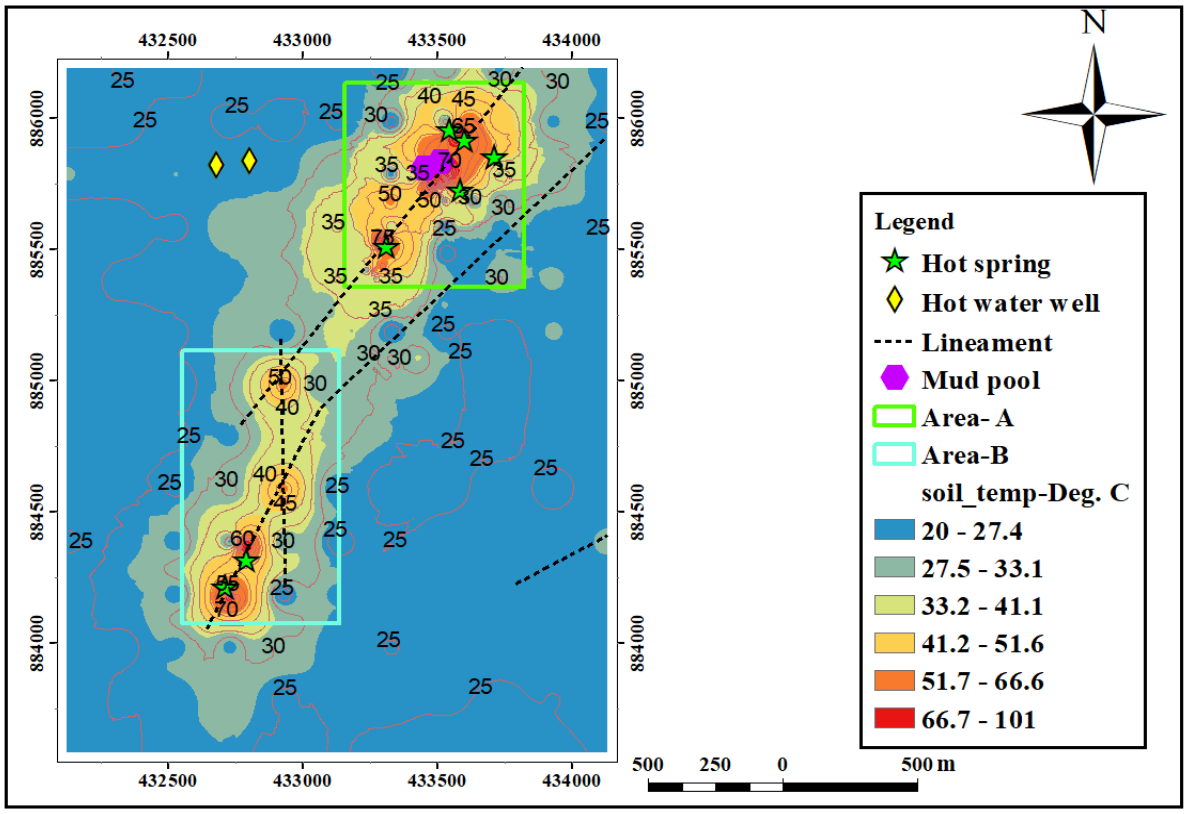

Figure 4.9 Geothermal map of the study area and proposed target areas overlap with geological map and soil temperature data

4.2.1 Hot springs

Fumaroles, Steam and muddy-water ejecting vents are concentrated in particular location, near Ashute village at 433552 E, 88592N and Gerbi Ber village at 432808 E, 884390N. They are found on big hot swampy ground covered by large grass. These surface manifestations are generally aligned and elongated along NE- SW directions. Ashute hot springs and mud pools encompass small lake with hot gas outlet. This typical high temperature surface expression indicates that of the intersection of the two fault lineaments in the area. There are numerous at least 14 small holes ejecting muddy water and steam and at most 8 hot springs are found around the mapped area. These Ashute and Gerbi Ber hot springs are used for bath and spa purpose in the local community.

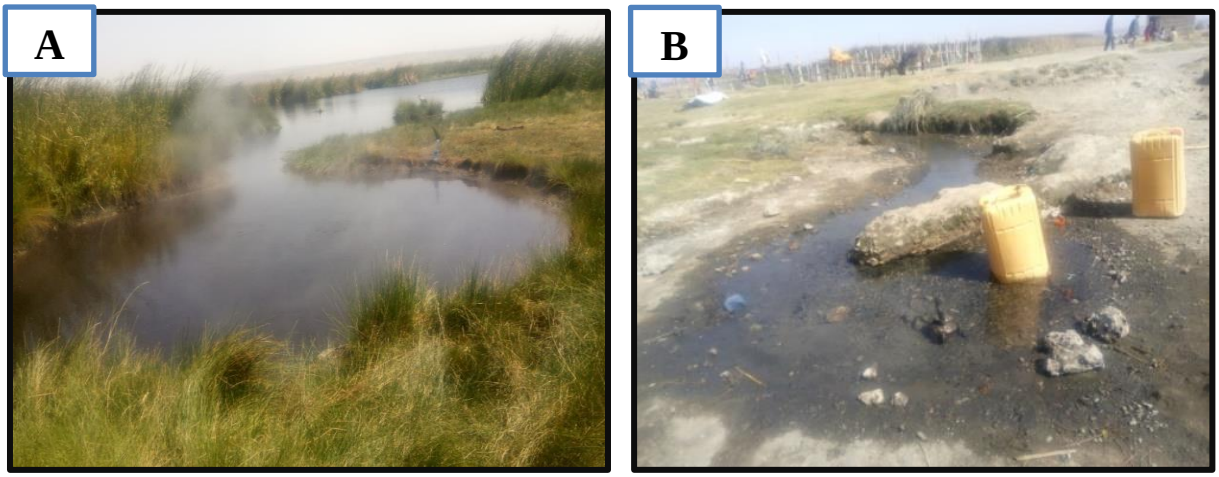

Figure 4.10 Hot water pools with gas outlet and Spa

4.2.2 Mud pools

It is a type of hot springs or fumaroles formed under limited water supply that typically forms a pool of bubbling mud. This surface manifestation situated in south eastern part of the study area at plain land adjoining other surface manifestations such as hot springs and small hot water pool area along NE-SW trend extension. They are characterized by ejecting mud and fumarolic activities enclosing more than 60 mud-ejecting eyes inside.The mud pool having an area coverage about 250m in SW and 85m in SE direction from 433157E,885150N.The hot mud pool has a maximum temperature of 101ºC mud ejected bubbles (GSE,2014). It is black in color associated with yellow colored very thin sulfur deposits that enclosed by relatively light gray grass.

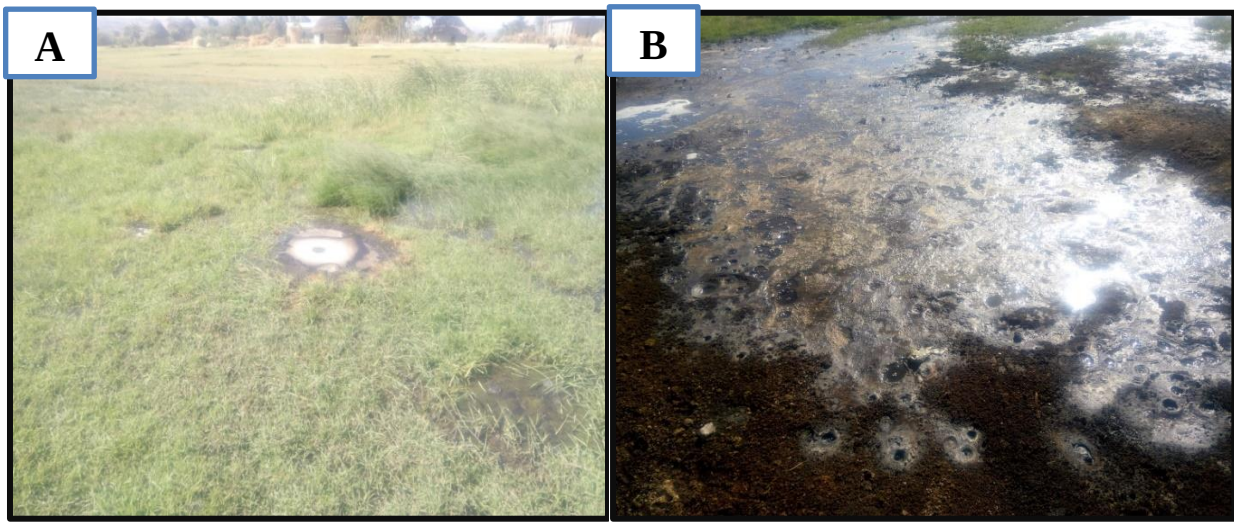

Figure 4.11 Mud pool

4.2.3 Silica sinter and sulfur deposits

Hydrothermal alteration is change in mineralogy, texture and chemistry of rocks facilitated as a result of rock interaction with geothermal fluids (hot water and gas). The intensity of alterations in geothermal area are dependent on change in prevailing conditions of temperature and composition of geothermal fluid and host rock , type of rock and its permeability, as well as duration of rock- fluid interactions (Reyes, 2000). Hydrothermal fluids cause alteration of rocks by passing through the rocks leaching out the nearby rocks and changing their composition by adding or removing or redistributing the dissolved ions.

The degree of alteration is more dominant in south eastern part of the plain area along fault zones while slightly alteration has been observed in northern and north western parts of the mapped area. Basaltic lava flow and Basaltic scoria cones how slight alterations i.e. primary rock texture and minerals are recognizable through thin section analysis. While high degree of alteration, when the principal primary minerals and rock textures are replaced by new mineral and rock texture, were detected at ignimbrites and Unwelded Tuff.

In highly altered areas silica sinters and sulfur with halite deposits are the dominant features observed in the field resulted from hydrothermal activity. Silica sinter dominantly found near hot spring and hot water pools filled in altered ignimbrite rock unit. It forms spongy like aggregate of secondary quartz mineral dominantly found adjoining hot spring and hot water pool following the NE – SW direction. It has white to dull gray color with radial growth. During field observation hydrothermal native sulfur mineral deposited around hot spring and mud poolin association with halite and clay minerals. It is identifed by yellowish color and rotten egg smell. These deposits has thin layer less than 2cm and cover large extent in NE-SW trend following other surface manifestations. Observation from field and thin section analysis reveals the degree of alteration in the study area controlled by geological structures and topography rather than lithological variations.

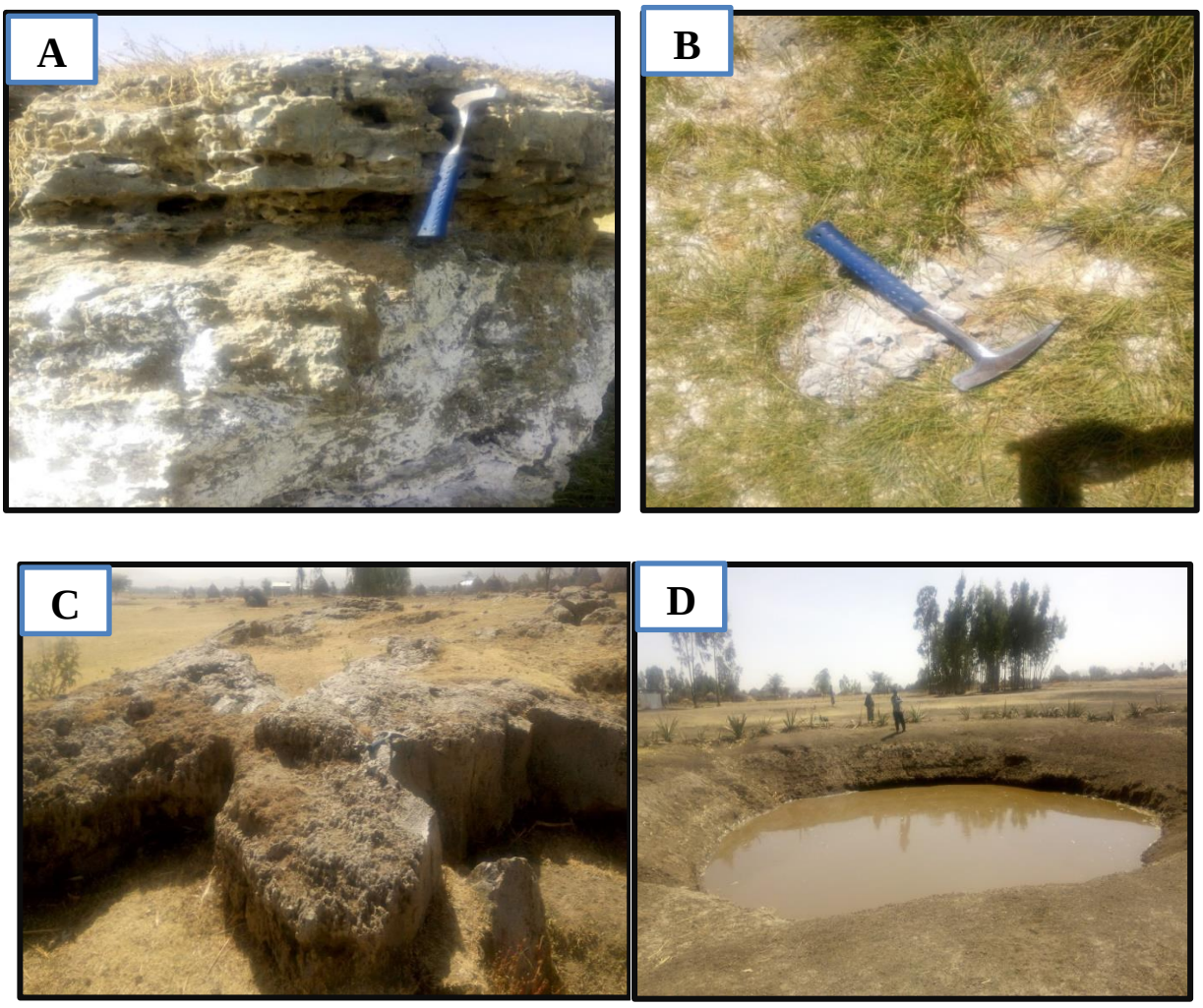

Figure 4.12 Altered ground and Sulfur deposits (A-C), borehole drilled for irrigation purpose (D)

4.2.4 Hot drill well and Abandoned well sites

There are a number of drilled well that provides hot water for domestic purpose alongside south-east of Ajira –Afuno fault. Among these wells at 4333858E, 86559N with a temperature of roughly 40 ^{0} C and well out of use due to corrosion at 432691E, 885766N are noticed. At the location of 432842E, 886073N deep water well up to 255m depth drilled for irrigation purpose in 2014. During drilling different rock unit are encountered and loss of circulation and blow out occurred on 234 and 255m respectively. Initially hot water and steam ejected explosively up to 30m from the wellhead and it forms small pit with temperature reaches up to 90°C (Solomon et al., 2014). Even though there is no thermal activity nowadays, it becomes active at summer as confirmed from local people.

4.3 Hydrothermal alteration minerals

The distribution and characteristic of alteration mineral in terms of composition, texture and the distribution of coexisting mineral assemblages documents the historical formation of the rock and provide a first order assessment for its environment formation and commonly used as geothermometer, and used to reveal the nature of the geothermal system to provide information on reservoir fluid characteristic and evolution of geothermal system whether it is heating or cooling (Giovanni Gianelli et al.,1998; Reyes, 1990*;* Thompson et al., 2001).

In the Butajira geothermal field, study area, qualitative mineral identification has been performed during field work investigation besides petrographic studies and XRD analysis performed from representative samples obtained from different parts of the study area. Alteration minerals that occurred under various circumstances are contemporaneous with neutral pH alteration and structurally-controlled and forms sharp boundary alteration zone. Those minerals are resulted by means of vesicle filling along joints besides replacement of the primary minerals. Generally, investigation confirms that the distribution and magnitude of alteration in the surveyed area mainly controlled by lithology and geological structures. Various hydrothermal alteration minerals were identified with the aid of petrographic observation and XRD analysis and described below.

- **Actinolite:** it is pale green, green and sometimes dark green in colour and occurs as fibrous, radial crystals and massive to granular aggregates in the groundmass. In thin sections it shows moderate relief with weak pleochroism of pale yellow, deep green blue and pale green colors. It is observed as filling in vesicles and is sometimes seen in veins. The mineral is formed as a replacement of pyroxenes. This mineral indicates formation temperatures of above 280^0C (Lagat, 2007; Gylfadóttir et al., 2011). In active geothermal systems hosted by intermediate to mafic igneous rocks, it is present at temperature greater than 280 ^{0}C up to 300 ^{0}C and is characteristic of alteration proximal to intrusive body.
- **Adularia:** it is detected from altered crystal rich ignimbrite (Ts-5) taken along fault scarps. It occurs as replacement of plagioclase or primary K- feldspars and is occasionally deposited in veins as well as forming incrustations in fissured rocks. In XRD graph it shows strong peaks at 21 Å, 23.5 Å and 27 Å.

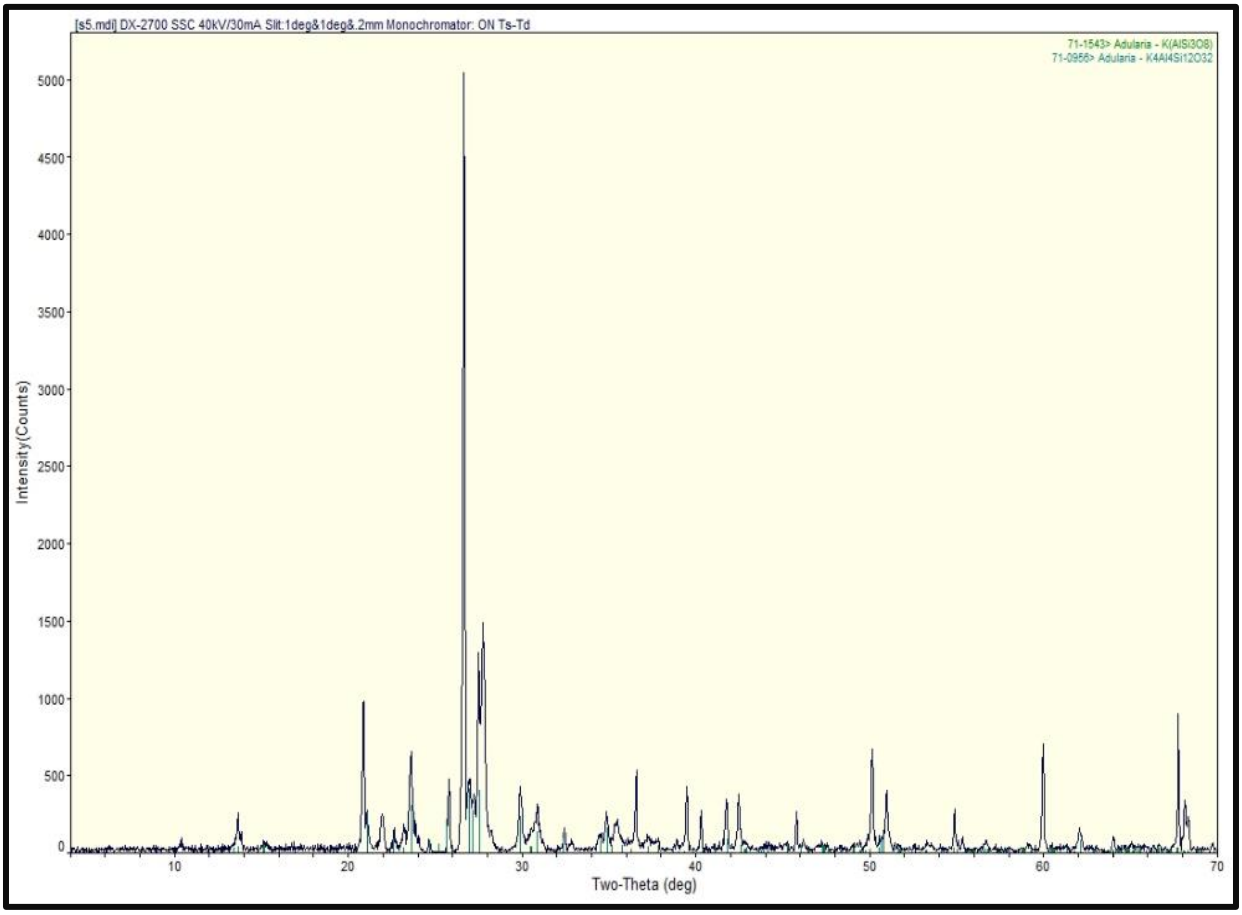

Figure 4.13. XRD graph of Adularia

- **Albite:** It is as an alteration product of Ca-rich plagioclase (Labradorite) and distinguished from primary plagioclase by their lower refractive index and extinction angle. Compositional variation (zoning) within a single mineral may be expressed changes of "natural" color from one zone to an adjoining one; or by changes in birefringence; or by changes in extinction orientation. These changes may be abrupt or gradational, and commonly occur as a sequence from the core of a mineral grain (the early-formed part) to its edge (the last-formed).

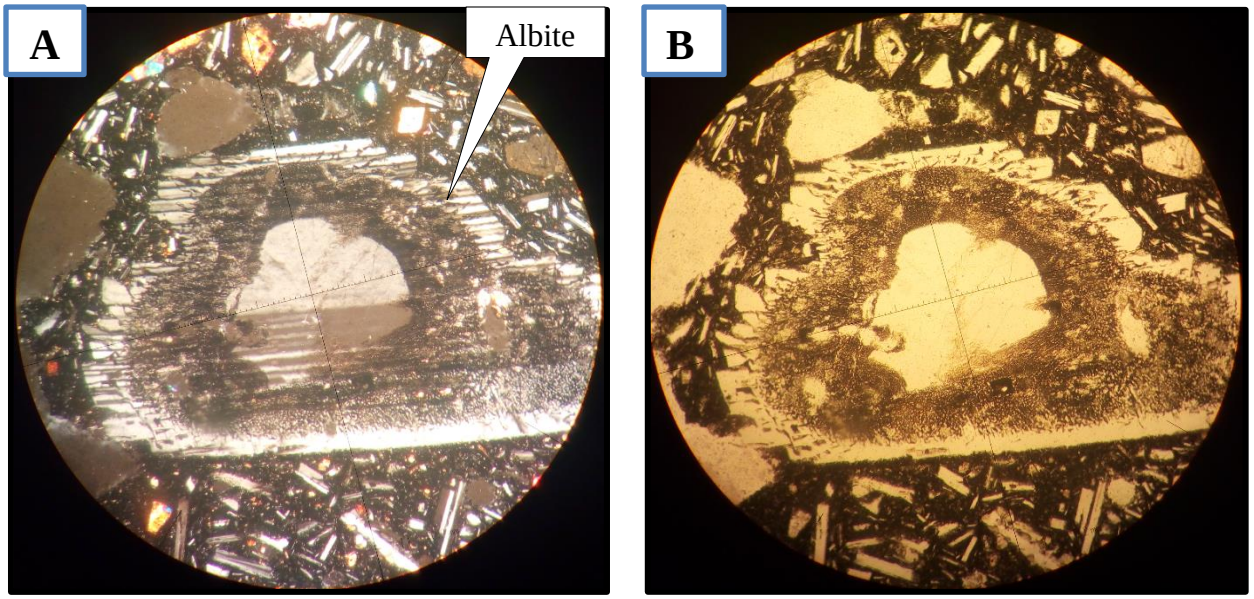

Figure 4.14 Altered Albite minerals;A-PPL and B-XPL view.

- **Biotite:** It is an alteration product of pyroxene in association with opaque minerals having brown color, cleavage and yellowish pleochroism. It formation ranges from more than 250 ^{0}C (Reyes, 2000).

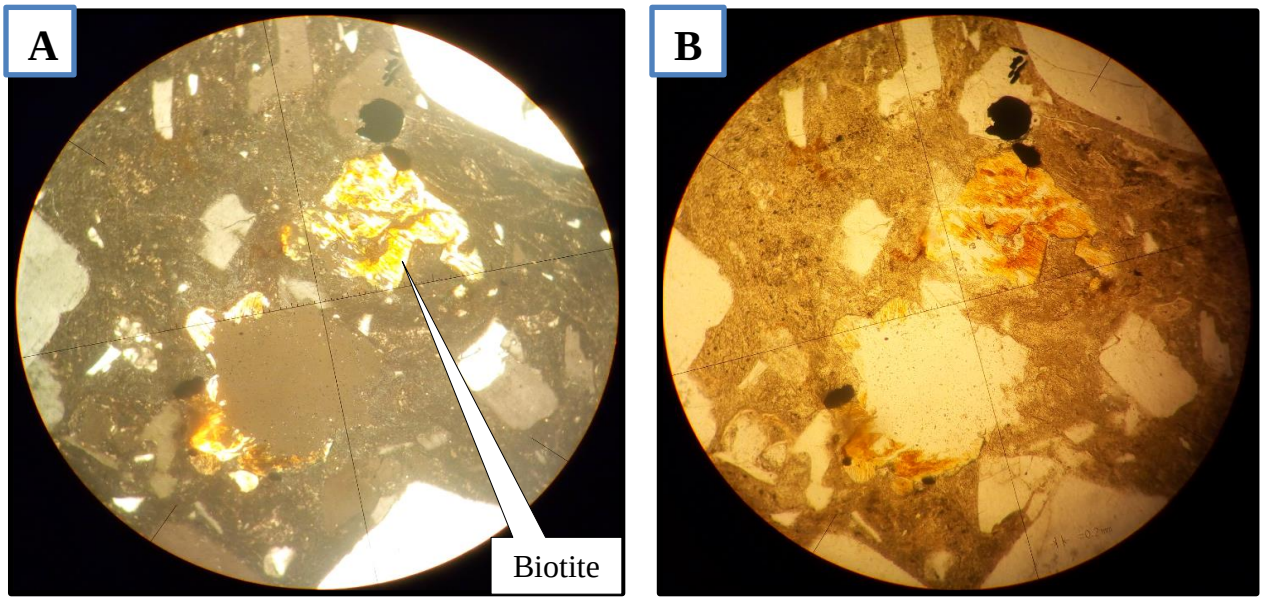

Figure 4.15. *Biotite Altered mineral; A-PPL and B-XPL view.*

- **Calcite**: It is identified through is detected from altered rock sample (Ts-7) taken around hot springs. It occurs as replacement of plagioclase or primary K- feldspars and is occasionally deposited in veins as well as forming deposits in fissured rocks. In XRD graph it shows strong peaks at 23 Å, 26 Å, 29.5 Å and 40 Å.

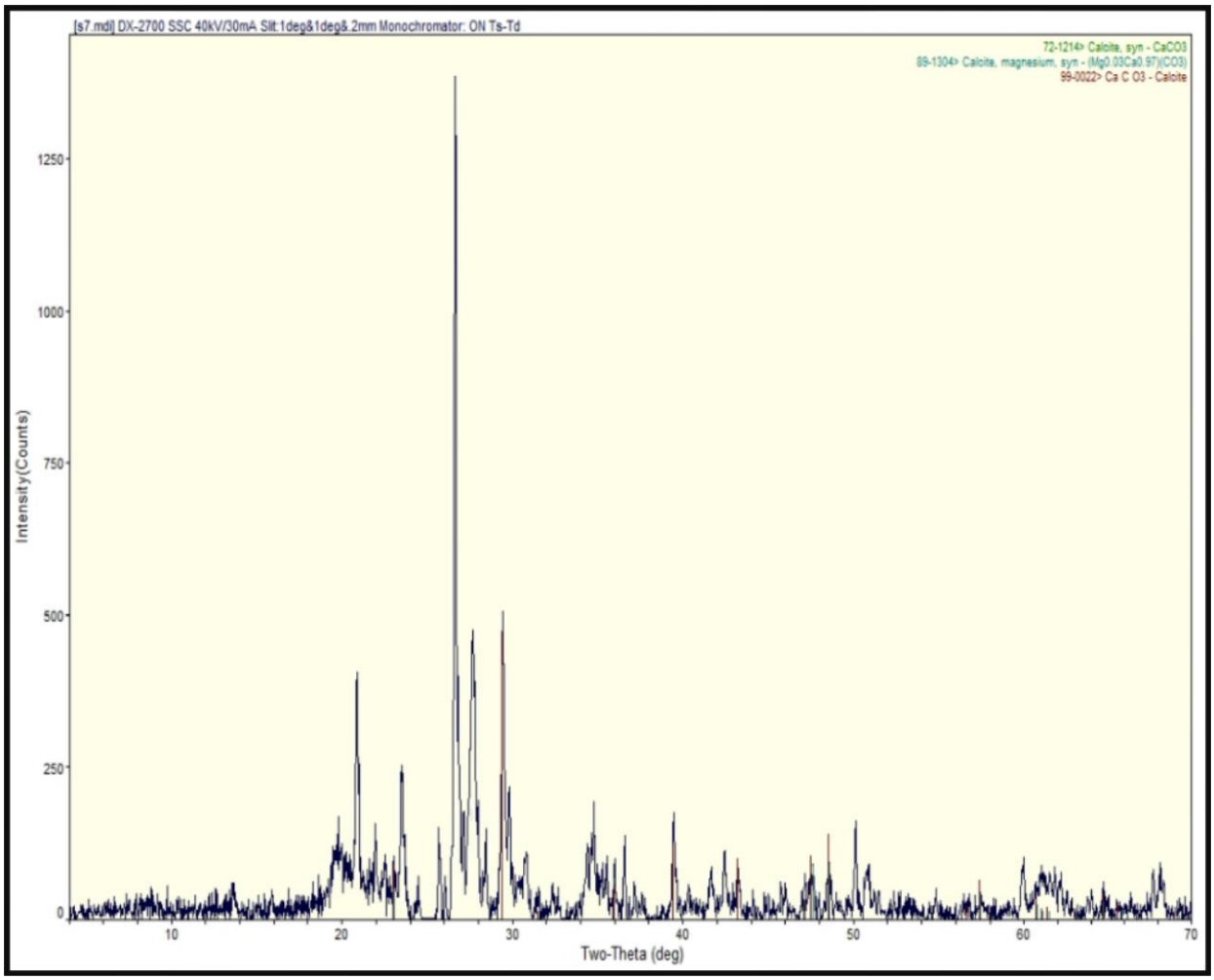

Figure 4.16. XRD graph of Calcite.

- **Chlorite:** it is usually light to medium green in thin section and pleochroic, expressed in shades of colorless, pale green, yellowish green, green, or brownish green. In thin-section it is coarse-grained and light green colored in plane polarized light in the pores, grey-blue in cross polarized light, shows tiny green needles texture and sometimes radial forms. In thin-section it was recognized inTS-3 as inclusions.
- **Cristobalite:** it is distinguished by its main common peak at 22 Å, 38.5 Å and 36 Å Adetected from altered crystal rich ignimbrite taken along fault scarps. It occurs as

replacement of plagioclase or primary K- feldspars and is occasionally deposited in veins as well as forming incrustations in fissured rocks. In XRD graph it shows strong peaks at 27 Å and 21 Å. Crystobalite crystals rarely get larger than 1mm. This is a typical example of an occurrence in small cavities of a vuggy, silica-rich volcanic rock. Numerous small, white crystals have grown in these little cavities that apparently are outlined by tiny sanidine feldspar crystals.

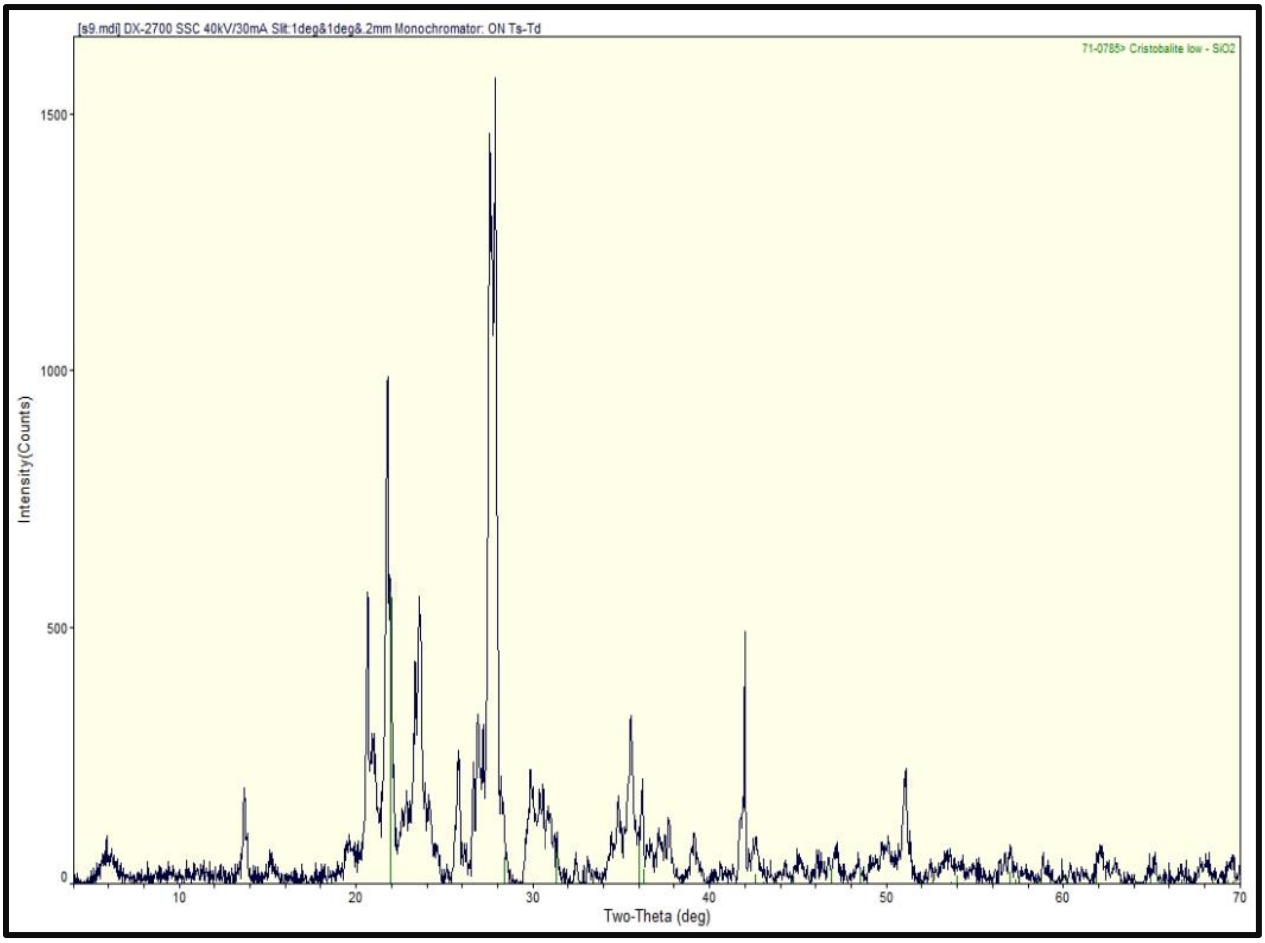

Figure 4. 17. XRD graph of Cristobalite.

- **Rutile:** Hydrothermal alteration rutile occurs as rugged aggregates of anhedral grains as small crystal. It exhibits high relief, red brown, and yellow brown color. It enclosed by Sieved texture interconnected, box shaped glass inclusions, giving the crystals spongy or porous appearance.

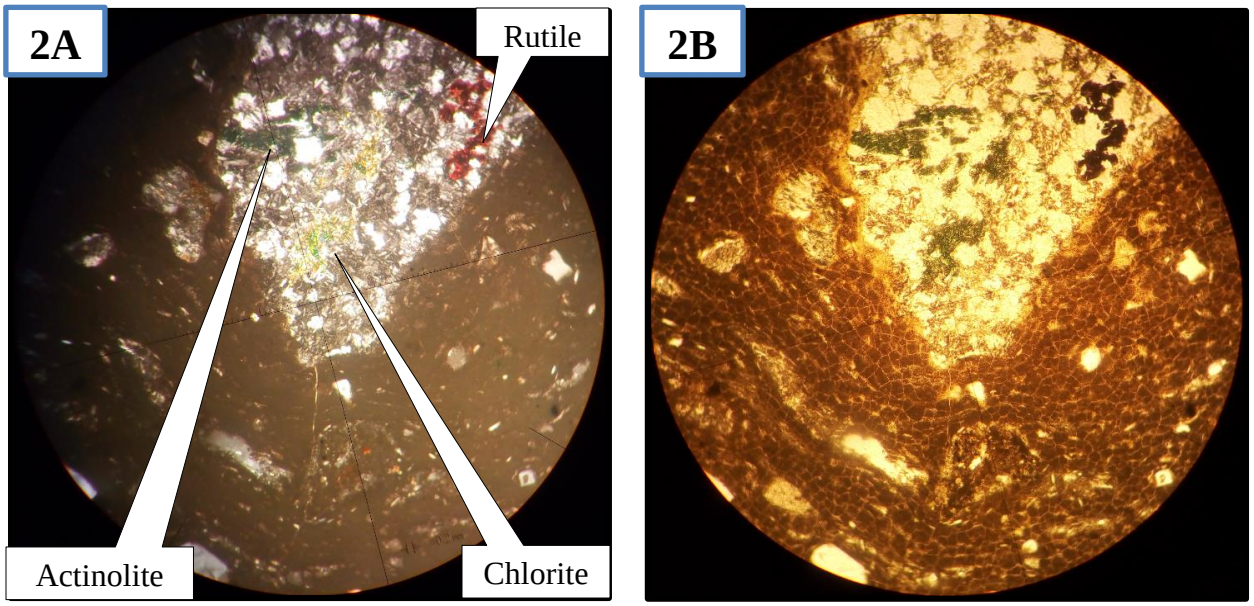

Figure 4.18 Alteration minerals chlorite, rutile and Actinolite ; A-PPL and B-XPL view.

- **Stishovite** is detected from altered crystal rich ignimbrite taken along fault scarps. It occurs during an extremely violent volcanic eruption and characterized by ultrahigh pressure conditions and low temperature. In XRD graph it shows strong peaks at 31Å and 40 Å.

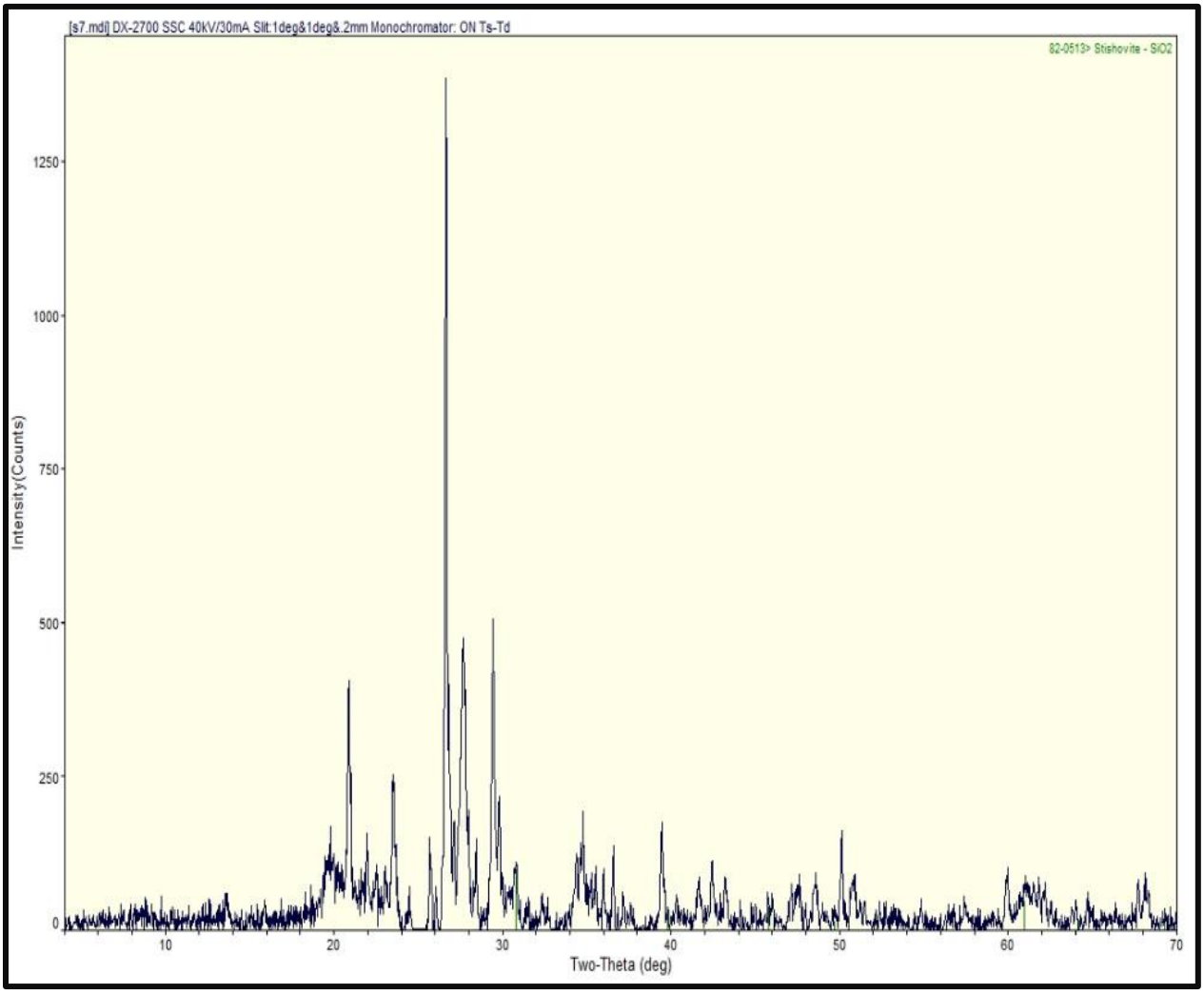

Figure 4.19 XRD graph of Stishovite.

- **Titanite:** it is occurred as an accessary mineral formed during the hydrothermal alteration of titanium bearing phases such as biotite, augite, hornblende and ilmenite. (Reyes, 1990). It identified in XRD analysis and it also recognized in petrographic microscope, where it is seen as red-brown and somewhat cloudy colored crystals. It is seen at highly altered sample (Ts-1) and (Ts-8) associated with biotite, kyanite, quartz, hornblende and glass. Titanite forms over a large temperature range of 200^0C-400^0C in various hydrothermal environments, including intrusive and skarn systems and the deeper parts of geothermal systems.

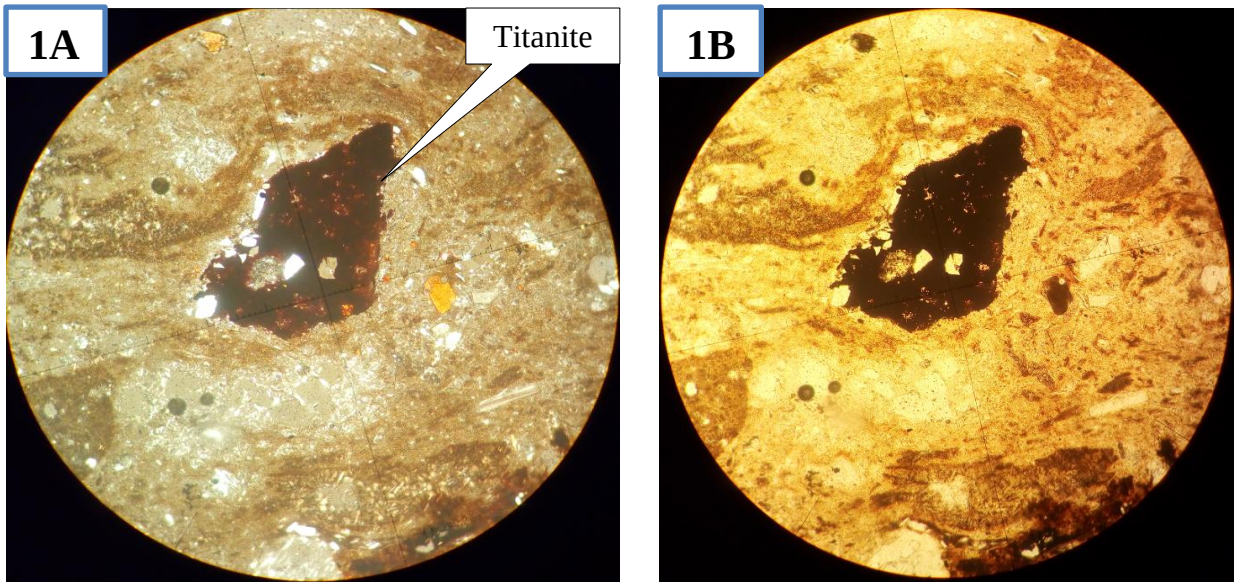

Figure 4.20. A-PPL and B-XPL view of Titanite mineral.

- **Triydmite:** It is silica polymorphs that are found principally in siliceous volcanic rocks. It is detected from altered crystal rich ignimbrite taken along fault scarps. It occurs as replacement of plagioclase or primary K- feldspars and is occasionally deposited in veins as well as forming deposits in fissured rocks. In XRD graph it shows strong peaks at 27 Å and 21 Å.

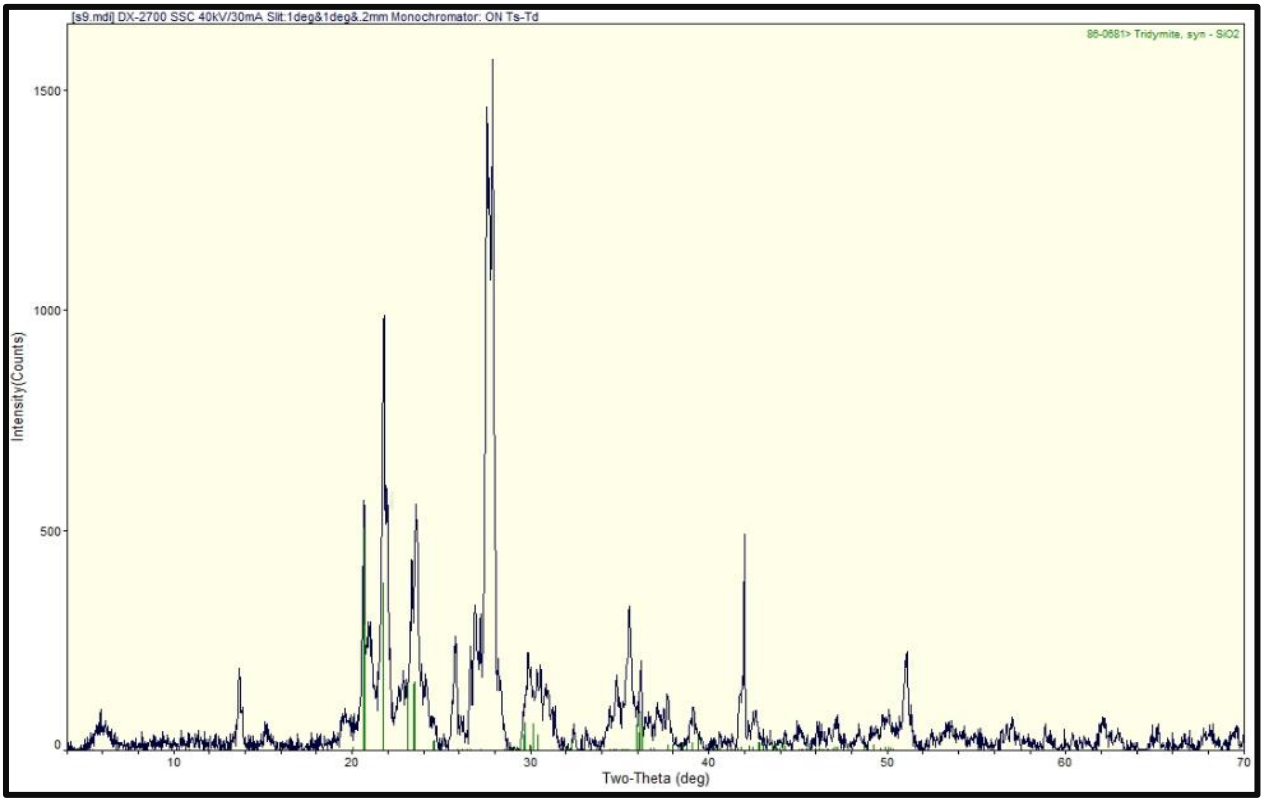

Figure 4.21. XRD graph of Triydmite.

Table 4.1. temperature of formation of Alteration minerals adopted from (Reyes, 2000)

Alteration minerals	**Temperature range (^{0}C)** 50 100 150 200 250 300
Actinolite	270-340
Adularia	165-320
Albite	175-320
Biotite	265-350
Calcite	50-320
Chlorite	120-340
Cristobalite	100-160
Quartz	180-340
Stishovite	
Titanite	200-340
Triydmite	140-200
Rutile	180-340

CHAPTER FIVE

5. ASSESSMENT ON GEOTHERMAL SYSTEM COMPONENTS OF BUTAJIRA GEOTHERMAL PROSPECT

5.1 Geothermal system components

The present geological and geothermal investigations were integrated with secondary geophysical and geochemical data that offer optimistic information for geothermal system components. As noted above the nature and source of heat, reservoir characteristics, and the presence of confining rocks above the aquifers are essential in addition to the requirement of sufficient water and recharge mechanism. Thus the following discussion and interpretations were organized based on results obtained from surface geological and geothermal field work, petrographic and XRD analysis in order to evaluate the existence of favorable geothermal system components by considering the data sets.

5.1.1 Heat source

Ethiopia rift system has undoubtedly a region of positive thermal anomaly attendant to volcanic and tectonic activity within which local anomalies are associated directly with volcanism and /or hydrothermal systems due to heat flow from shallow magma, impressively illustrated by the close association of surface geothermal manifestaions. The manifestations are more pronounced and vigorous within the axis of the rifts than on the flanks due to the favorable hydrology and relatively shallow heat sources.

The presence of Basaltic eruptions of recent age with structural controlled unidirectional fissure swarm along NE-SW alignment and explosion craters and ejecta of voluminous pyroclastic deposits in the area infers the presence of sufficient heat anomaly beneath that locality. The most encouraging features indicative of the presence of promising heat source beneath the study area for development of adequate geothermal resource are surface manifestations like hot spring, mud pools, altered ground, and hot drilled wells. In addition the incident of high-temperature blow out arisen during drilling for irrigation purpose at depth of 256m clearly confirms the presence of worthy potential heat source beneath. The occurrences of aligned Pliocene age cinder cones and Har-Shetan Crater revealing recent volcanic activity and heat will be remain lively. Accordingly, geothermal resources in the

area associated with syn-rift volcanism, rifting along Siliti Debre Zeit fault zone (SDZFZ) of the cinder cone and associated basaltic flow (Rooney, 2011). There is also the possibility to have potential heat source derived from shallow silicic magma chamber indicated by evidenced of a single thermal spring on the contact of small rhyolite lava dome located 6 Km south-west of dominant thermal manifestations (Dipola, 1970, UNDP, 1972).

Dikes and sills as intrusion could be emplaced as a heat source at shallow depth voiced and reinforced laterally in northeast-southwest structural control with strong geothermal surface manifestations. The geothermal system at Butajira is still active and this can be attributed to tectonic leading to increased activity in the area as evident by the recent fissural eruption dated even younger than 0.13 Ma (Woldgebrieal et al., 1990). Generally, two possible scenarios could be put forward regarding the local heat source anomaly that expressed by numerous surface manifestations are related to the intrusive body. The first one is a series of mantle-derived basaltic dyke intrusions emplaced at shallow depths. The second one is a series of elongate and interconnected basaltic sills or magma chambers related to dyke intrusions emplaced beneath the young basaltic scoria cones and lava flows.

5.1.2 Reservoir /permeable formations

A strong lateral distribution of geothermal surface manifestations commonly controlled by superficial faults and lineament in NE-SW direction indicating the presence of permeable formation connected to younger fault system thus faults and fissures might possess good quality of secondary permeability in the underlying rock formations. Phreatic explosion blow out during drilling also deduces sufficient aquifer could be existed. Meanwhile much of the ground water is deep beneath surface, limits the usefulness of estimating the extent underground reservoirs from an appraisal of its surface expression, because the density of parallel faults may not provide an accurate indication of vertical permeability. One more useful indication of the presence of high temperature aquifers underground is the presence Crater Lake. Hydrothermal explosions which derive explosive energy by faulting of high temperature and high pressure water stored in a hydrothermal system can be triggered by several mehanism (Lloyd,1959;1962). The Har-Shetan Crater Lake, about 700m in diameter, resulted from phreatomagmatic explosion. It formed associated with scoria cones when the uprising magma interacts with shallow ground water. Thus indicates the presence of huge amount of water in permeable rock formation underneath the vicinity.

Moreover, there are several alteration secondary minerals indicative of good permeability in prospect area such as Quartz, Adularia, and Calcite. The alteration minerals attained from XRD analysis such as adularia, calcite, and Quartz (Elizabeth T., 2007). The estimated reservoir temperatures obtained from alteration minerals and silica and Na-K geothermometer have medium temperature with range of 158 ^{0}C and 206 ^{0}C (GSE, 2014) also confirmed temperature estimated from alteration mineral geothermometer. Even though, the presence of high intensity alteration of dressy minerals associated abundant veins are predominant in sheared rock and indicative of possible aquifers, it is difficult to speculate suitable permeable formations for reservior storage at depth without deep geological sections. Data gathered from magnetotelluric investigation reveals that a depth of geothermal reservoir is located from 1500m to 3,000m, from 10-70 Ωm and characterized presence of normal faults and lineaments and forms fault compartments.Below this conductive layer, a high resistivity zone has been noticed that can be correlated to the back ground resistivity of basalts or epidote alteration zone (GSE, 2017).

5.1.3 Impermeable Cap rock

The lateral extent of surface geothermal surface manifestations and hydrothermal alteration along geological structure i.e. faults and lineament indicating that there is impermeable cap rock in the area that block the upward movement of steam and water. In addition, the occurrence of explosive phreatic eruption at depth of 252m during deep well drilling indicates a confined aquifer with thick impermeable cover. This layer could be associated with recent and sub-recent basaltic flow or due to volcanic over burden in the high land and alluvial sediments and clay alteration in lowland area.

5.1.4 Geothermal Fluid and recharge mechanism

Undulating topographic feature from high elevation of cinder cone in the western and northwestern parts and low plain land elevation in the south and south eastern parts of the area have variances about 400 m. This may be affect the hydrology of the system such as the depth of the water table , phase separation within the reservoir, the distribution and type of thermal manifestations. Fluid chemical analysis from hot springs conducted by GSE, 2017 shows that water in the Butajira geothermal system is derived from rainfall and meteoric in nature recognized by various geothermal manifestations. These geothermal fluids are alkali-

chloride-bicarbonate type, immature and display geochemical evidence for interaction with shallow ground level.

Our observations of hydrothermal features in the prospect area confirm that the recharge zones located in high elevated cinder cones and from Abaya Lake towards the low land discharge area through major geological structures that serve as a key pathway for the inflow and up flow of geothermal fluids. Lineaments detected by magnetic and soil temperature survey found on reworked pyroclastic deposits located in south east of the study area will provide enormous geothermal fluid to the reservoir in summer time, in addition to fluids percolated from high land area through normal fault zones. Moreover, high degree of alteration is more vigorous around fault and become structurally-controlled having a sharp boundary and alteration minerals formed in the area are contemporaneous with neutral pH alteration. The situation in which surface geothermal manifestations aligned and occurrence periodic phreatic eruption in the area infers hydrothermal fluids passed through fault structures that serves as fluid circulation path way. As a result fractures might play two different roles in this geothermal system i.e. contribution for the onset of natural convection in geothermal systems to form geothermal resources at depth and serve as a key fluid pathway to connect the cooler inflow and hot outflow of geothermal fluids from the geothermal reservoir.

5.2 Preliminary conceptual geothermal model of the Prospect area

A good conceptual model should encapsulate the geological framework, heat source, fluid migration pathways, reservoir characteristics, sealing cap layer, up flow and outflow zones, as well as recharge and discharge zones and surface geothermal features (Cumming, 2009; Corti, 2011). Preliminary geothermal conceptual model developed for Butajira geothermal prospect that was developed with limited geological, geochemical, and geophysical data. At this early stage the model was illustrated with 2-D cross section view in simple drawing relating to MT investigation tried to indicate the essential geothermal system components and identify the geothermal play type. In order to envisage the underground conditions of the researched area, a hydrothermal model was drawn corresponding with geological cross section profile (A-B). The model agreed to take the main source of recharge is meteoric water and recharge area are from high topographic areas of cinder cones and from Abaya

Lake that percolates to the reservoir through tectonic structures like fault, lineaments and joints. It shows schematically the role of fault serves as geothermal conduits from reservoir to surface expressed in the form of geothermal manifestations. Regard to the heat source of the field a shallow cooling intrusive complex is believed to be the principal heat source of the geothermal system interconnected to major geological structures.

It also assumes a boiling geothermal reservoir at depth ascending steam and gas, boiled off from the hot reservoir at depth; flows upwards along fractures and guide the geothermal fluids upwards. Surface temperature isotherms and forecasted reservior temperature from geothermometer confirm that Ashute and Gerbi Ber areas are the hottest part of the field where maximum surface and expected reservoir temperatures were documented and soil temperature survey. Thus the up flow zone of the system is located in the plain land of Ashute and Gerbi Ber villages resulting lineament intersections and outlined by strong surface manifestations. Evidences from the above discussion specify the prospect area is consistence with CV1b: Magmatic Play Type, Extinct Magmatic Intrusion, controlled by late Cenozoic to Quaternary plutons or batholiths with associated volcanism. This intrusion provide heat source to the system and is capable to generate high temperature geothermal fluids that manifested through outlets.

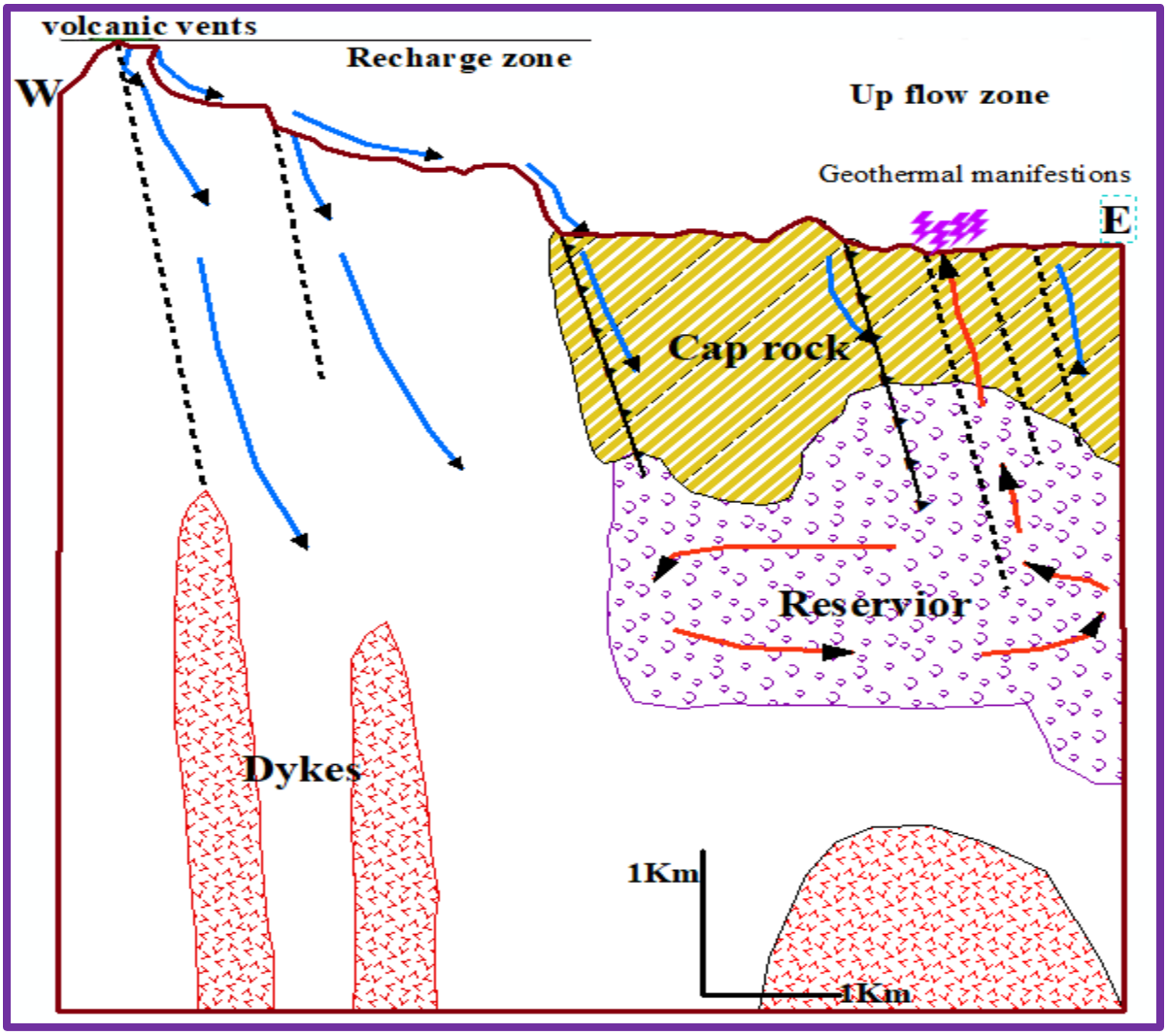

Figure 5.1. Preliminary conceptual model of Butajira geothermal prospect.

5.3 Proposed target areas for further exploration

The abundance of surface geothermal manifestations and the distribution of intense geological structures indicate nearness to an up flow zone and data combined secondary source aid to select and prioritize the target sites. Based on the current investigations two promising localities in Ashute village (area A) and Gerbi Beri village (area B) were selected as priority target areas for future geothermal exploration to gathering better information and become more confident about geothermal system components. The inferred presence of a conductive fracture zone or fault with hydrothermal fluid and shallow heat source magma intrusion makes the Ashute and Gerbi Ber areas are seemly a promising prospect for the development of convectional hydrothermal geothermal energy.

CHAPTER SIX

6. CONCLUSION AND RECOMMENDATION

6.1 Conclusion

Geothermal fields are found in areas of active tectonism associated with young volcanism or enormous intrusions, where heat source localized at shallow crustal depths, adequate permeable formation and hydrothermal fluids occurred. The current study has been conducted in Butajira geothermal area where higher geothermal gradient were expected beneath at shallower depth. As an output of the thesis work the following findings are worth mentioned ideas stated and put as conclusion:

- The study area is dominantly covered by five lithology unit i.e. volcanic products of basaltic scoria and associated basaltic lava flows, welded ignimbrite, unwelded tuff, phreatomagmatic deposits comprising trachyte and diorite as well as alluvial and reworked pyroclastic deposits.
- The major structural features in the study area are faults, lineaments and joints. The orientation of faults is expressed by NE-SW dipping towards 30^0-65^0 SE and lineaments are aligned in NE –SW, N-S and NW-SE directions. Cinder cones are aligned into NEE-SWW direction and controlled by SDZF.
- The geothermal manifestations are hot springs, warm water pools, mud pools, altered ground and sulfur laid deposits and hot drilled wells. They are intensively distributed along structural trends and seem to be fissure controlled at low-lying plain area
- The alteration mineral assemblages recognized in the area are quartz, stishovite, calcite, cristobalite, trydmite, rutile, titanite, adularia suggesting neutral PH alteration.
- Slight alteration perceived in high elevation area in welded ignimbrite along NE-SW fault plane while strong alteration is realized around hot spring along lineaments.
- Results obtained from hydrothermal alteration minerals the reservoir temperature has exceed 150 ^{0}C that is analogous to result gained from fluid chemical geothermometer.
- Presence of ample Sulphur in the geothermal manifestation relationship with the location of eruptive fissures shows increasing geothermal activity in the reservoir.

- Fractures and faults will increase permeability of geothermal reservoir in addition to primary porosity of the rock units. They also serve as the pathway for convection geothermal fluids from surface to reservoir and vice versa.
- The cap rock could be rocks formed from hydrothermal alterations of rocks and thick overburden of alluvial and reworked pyroclastic deposits in the lowland area.
- An anomalously high geothermal gradient expected there as a result of shallow intrusion that upraised to shallow depth associated with nearby cinder cones or and heat source derived from shallow silicic magma associated rhyolitic lava domes.
- The geothermal prospect is analogous to convection dominated V1b: Magmatic Play Type, Extinct Magmatic Intrusion, which controlled by late Cenozoic to Quaternary plutons or batholiths with associated volcanism which comprising promising geothermal system component.
- Two promising geothermal sites were identified and anticipated for further exploration around Ashute and Gerbi Ber villages found possible at up flow zone.

6.2 Recommendation

The main contribution of the study was to understand the nature of geothermal components through investigating surface geology and geothermal manifestation that provide insights for its certainty. Even though, investigating the distributions of different rock units and surface manifestation with in the geothermal field is crucial for site selection and smart drilling strategies, it is worth revealing and endorses the following points

- Detailed fluid inclusion studies and clay mineral analysis should be carried out especially in the up flow zone to supplement information about alteration process and understand the evolution of the geothermal system whether it is cooling or heating.
- Trace element isotope analysis is required to distinguish the type of magma sources and to be familiar on magma evolution processes that provides heat source of the resource.
- Based on the present geological and geothermal knowledge, and ease of access, it is recommended to undertake follow-up test well drilling giving priority in positive anomalous areas demarcated as area A and area B.
- A more comprehensive conceptual model is necessary achieved through further incorporation of detailed well data that allow detail information to an estimate of reservoir depth, temperature, and geometry with sufficient confidence. This will help in the preparation of numerical modelling.
- 3D MT survey and Gravity survey are to delineate the geological structure and extension of all geothermal system components.
- In the area there are indications of accidental phreatic eruptions around thermal manifestation especially near to Asute village, and the concerned body should aware the local peoples to prevent them from hazard.

References

Abebe, T., Pasqua ,C., & Kebede,S. 2016: 'Aluto-Langano geothermal field (Ethiopia), proposal of a new geo-volcanological model by combining the existing data with modern studies'. **In**: *Proceedings, 6th African Rift Geothermal Conference,* Geological Survey of Ethiopia, Addis Ababa, Ethiopia. 2nd – 4th November 2016.

Abebe, B., Acocella, V., Korme, T & Ayalew, D. (2007).Quaternary faulting and volcanism in the Main Ethiopian Rift, *Journal of African Earth Sciences*.**48**:115-124.

Arturo Quezada Muño 2015: 'Geological field mapping for geothermal exploration', Paper presented at "Short Course VII on Surface Exploration for Geothermal Resources",organized by UNU-GTP and LaGeo, in Santa Tecla and Ahuachapán, El Salvador, March 14 - 22.

Barton, C.A., Zoback, M.D., and Moos, D.(1995). Fluid flow along potentially active faults in crystalline rock. *Geology*, Vol. 23, No. 8, pp. 683-686.

Bronto, S., Sianipar, J. Y., & Pratopo,A. K., 2016: Volcanostratigraphy for supporting geothermal exploration. **In**: *Proceedings of the 5th ITB International Geothermal Workshop (IIGW2016).* IOP Conf. Series: Earth and Environmental Science.

Benvenuti etal.,(2002): The Ziway–Shala lake basin (main Ethiopian rift, Ethiopia): a revision of basin evolution with special reference to the Late Quaternary, *Journal of African Earth Sciences.* **35** :247–269.

Bertani, G., Casinin, M., Gianelli, G., and Pandelli, E. (2006): Geological Structure of a long-living geothermal system, Larderello, Italy. *Terra Nova*, **18**:163-169.

Ian Bogie & Jim Lawless 2010, 'application of mineral deposit concepts to geothermal exploration'.**In:** *Proceedings World Geothermal Congress 2000:* Kyushu - Tohoku, Japan, May 28 - June 10.

P.R.L.Browne, 2017: Hydrothermal alteration in active geothermal fields. New Zealand Geological Survey. Annu. Rev. Earth Planet.. Sci. 1978.6:229-248.

Caroline Le Turdua, Jean-Jacques Tiercelin, Elisabeth Gibert, (1998). The Ziway–Shala lake basin system, Main Ethiopian Rift: Influence of volcanism, tectonics, and climatic forcing on basin formation and sedimentation, *Paleogeography, Paleoclimatology, Paleoecology*, **150:** 135–177

Charles Wanjie, 2012. 'Overview of geothermal surface exploration methods': Presented at Short Course VII on Exploration for Geothermal Resources, organized by UNU-GTP, GDC and KenGen, at Lake Bogoria and Lake Naivasha, Kenya, Geothermal Development Company, Kenya. Oct 27-Nov 18.

Corti, G., Bonini, M., Conticelli, S., Innocenti, F., Manetti, P., Sokoutis, D., (2003). Analogue modelling of continental extension: a review focused on the relations between the patterns of deformation and the presence of magma. Earth Science Reviews

Cumming, W.2009. 'Geothermal resource conceptual models using surface exploration data'. **In:** *Proceedings, 34th workshop on Geothermal Reservoir Engineering*, Stanford University, Stanford, SGP-TR-187 CA, Feb 9-11.

Demse Alamerew, Saladin Ali, and Solomon Kebede (June 2014). Technical team report about Siliti hot water explosion: Unpublished paper, Minster of Mine and Energy, Addis Ababa, Ethiopia.

Di Paola (1970). Geological-geothermal report on the central part of the Ethiopian rift valley: Unpublished paper. Minister of Mines, Addis Ababa, Ethiopia.

Ebinger, C.J., Yemane, T., WoldeGabriel, G., Aronson, J.L., Walter, R.C., (1993). Late Eocene- Recent volcanism and faulting in the southern main Ethiopian rift, *Journal of the Geological Society of London* .**150**: 99–108.

Endeshaw A., (1988). Current status (1987) of geothermal exploration in Ethiopia. *Geothermic*, **17:** pp.477-488.

Engdawork Admassu & Selamawit Worku, 2015. 'Characterization of Quaternary Extensional Structures: Tulu-Moye Geothermal Prospect, Ethiopia'. *GRC Transactions*, Vol. 39, pp.225-232.

Faulds M., 2010: 'Characterizing structural controls of geothermal reservoirs in the Basin and Range, USA, and western Turkey: Developing successful exploration strategies in extended terranes'.**In:***Proceedings WGC 2010,* Bali, Indonesia,April 25-30.

Geological Survey of Ethiopia (GSE) (2017). A Report on Geophysical investigation magnetic Surveys Report on Ashute, Butajira. Unpublished report, (GSE), Addis Ababa, Ethiopia. 22pp.

Geological Survey of Ethiopia (GSE) (2017). A Report on result on 1 –meter temperature survey conducted at Butajira geothermal prospect, southern Ethiopia. Unpublished report, (GSE), Addis Ababa, Ethiopia. 20 pp.

Geological Survey of Ethiopia (GSE) (2017). A Report on Geothermal Geochemistry of Butajira prospect area, Central Main Ethiopian: Implication for potential areas to Geothermal Energy in Ethiopia. Unpublished report, (GSE), Addis Ababa, Ethiopia.43pp.

Geological Survey of Ethiopia (GSE) (2017). A Report on 1D and 2D inversions of magnetotelluric data from Butajira geothermal field, Southern Ethiopia. Unpublished report, (GSE), Addis Ababa, Ethiopia. 30 pp.

Corti, G. (2009). Continental rift evolution: From rift initiation to incipient break-up in the Main Ethiopian Rift, East Africa, *Earth-Science Reviews*.**96** : 1–53

Corti, G. (2011). Fault architecture in the Main Ethiopian Rift and comparison with experimental models: Implications for rift evolution and Nubia–Somalia kinematics, *Earth and Planetary Science Letters.* **301**: 479–492.

Grant and Bixley (2011).*Geothermal Reservoir Engineering*, 2nd ed., British Library Cataloguing in Publication Data. ISBN 978-0-12-383880-3.

Hickman et al., (2004).Tectonics and stratigraphic evolution of the Sarulla graben geothermal area, North Sumatra, Indonesia. *Journal of Asian Earth Sciences*. **23**: pp.435-448.

Gianelli,G., Alessandro Chersicla, Paolo Garofalo , Giovanni Ruggieri, Mirco Manganelli, Zewde Gebregziabher(1998).Water–rock interaction and hydrothermal mineral equilibria in the Tendaho geothermal system: *Journal of Volcanology and Geothermal Research.* **86** : pp.253–276.

Negussie Mekuria, Stefano Battaglia , Axelsson, G. 2013, 'conceptual models of geothermal systems –introduction', Paper presented at "Short Course V on Conceptual Modelling of Geothermal Systems", organized by UNU-GTP and LaGeo, in Santa Tecla, El Salvador, February 24 - March 2.

Axelsson, G. 2013, 'Dynamic modelling of geothermal systems', Presented at "Short Course V on Conceptual Modelling of Geothermal Systems", organized by UNU-GTP and LaGeo, in Santa Tecla, El Salvador, February 24 - March 2.

Gutema Megersa and Endalkachew Getaneh, (2006). A report on Geological, Surface Hydrothermal Alteration and Geothermal Mapping of Dubti-Semera area, Tendaho Geothermal Field. Geological survey of Ethiopia ,GSE, Addis Abeba Ethiopia.

http://en.climate-data.org accessed on 14.06.2018.

International Geothermal Association (IGA) (2014). *Best practices guide for geothermal Exploration* (Colin Harvey, Ed.) Bochum University of Applied Sciences Bochum, Germany, pp196.

Japan International Cooperation Agency (JICA), (2015) .The project for formulating master plan on development of geothermal energy in Ethiopia. Unpublished report of geological Survey of Ethiopia, Addis Ababa, Ethiopia.

John Lagat 2007: 'Hydrothermal alteration mineralogy in geothermal fields with case examples from Olkaria domes geothermal field, Kenya'. ***In:*** *Presented at Short Course II on Surface Exploration for Geothermal Resources*, organized by UNU-GTP and KenGen, at Lake Naivasha, Kenya, November 2-17.

Kristján S. 2009. 'Geothermal systems in global perspective'. **In:** *Presented at Short Course IV on Exploration for Geothermal Resources*, organized by UNU-GTP, KenGen and GDC, at Lake Naivasha, Kenya, November 1-22.

Keranen, K., & Klemperer, S.L. (2007). Discontinuous and diachronous evolution of the Main Ethiopian Rift: Implications for development of continental rifts. *Earth and Planetary Science Letters*, **265:** pp.96–111.

Mackenzie, G.H., Thybo, G.H., & Maguire, P., (2005). Crustal velocity structure across the Main Ethiopian Rift: results from 2-dimenional wide-angle seismic modeling. *Geophysical International Journal*, **162**:pp.994–1006.

Pürschel, M., Gloaguen, R. and Stadler, S. (2013). 'Geothermal activities in the Main Ethiopian Rift: Hydrogeochemical characterization of geothermal waters and geothermometry applications (Dofan-Fantale, Gergede-Sodere, Aluto-Langano)', *Geothermics*, **47**: pp.1– 12.

Meseret Teklemariam, Stefano Batfaglia, Giovanni Gianelli and Giovanni Ruggieri 1996, 'Hydrothermal alteration in the aluto-langano geothermal field, Ethiopia'. *Geothermics,* Vol. 25, No. 6, pp. 679-702.

Meseret Teklemariam and Kibret B. 2005: 'Geothermal Exploration and Development in Ethiopia'. **In:** *Proceedings World Geothermal Congress 2005,* Antalya, Turkey, 24-29 April 2005, Geological Survey of Ethiopia

Meseret Teklemariam. 2008:'Strategic plan for geothermal exploration and development in Ethiopia'. **In:** *Presented at Short Course III on Exploration for Geothermal Resources*, organized by UNU-GTP and KenGen, at Lake Naivasha, Kenya, October24 – November 17.

Meseret Teklemariam. 2012: 'overview of geothermal resource utilization and potential in the east african rift system' **In:** *Presented at Short Course III on Exploration for Geothermal Resources*, organized by UNU-GTP and KenGen, at Lake Naivasha, Kenya, Octo.24 – Nov.17.

Mineyuki H., 2000: 'Two different roles of fractures in geothermal development'. **In**: *Proceedings World Geothermal Congress 2000* , Kyushu - Tohoku, Japan, May 28 - June10.

Minissale, A. , Corti, G., Tassi, F. , Darrah, T.H., Vaselli, O., Montanari, D., Montegrossi, G., Yirgu, G., Selmo, E. & Teclu , A. (2017) : Geothermal potential and origin of natural thermal fluids in the northern Lake Abaya area, Main Ethiopian Rift, East Africa. *Journal of Volcanology and Geothermal Research* ,**336** : 1–18.

Moeck, 2013, 'Classification of geothermal plays according to geological habitats'. University of Alberta, Canada. IGA, Vol. 1.

Moeck, (2014): Catalog of geothermal play types based on geologic controls. *Renewable and Sustainable Energy Reviews,* **37**: pp.867-882.

Ministry of Water Resources Ethiopian Water Technology Centre (MoWS) 2008: Butajira – Ziway areas development study hydrogeology and groundwater modeling: Unpublished technical report, (MoWS), Addis Ababa, Ethiopia.

Ministry of Water Resources Ethiopian Water Technology Centre (MOWS) (2008). Geology of Butajira – Ziway areas development study GEOLOGY. Unpublished technical report, (MoWS), Addis Ababa, Ethiopia.

Nukman and Moeck (2013): Structural controls on a geothermal system in the Tarutung Basin, north central Sumatra. *Journal of Asian Earth Sciences*, Vol.74, Pp.86-96.

Omenda, P.A. and Meseret Teklemariam 2010: 'overview of geothermal resource utilization in the east African rift system'. **In**: *Presented at Short Course V on Exploration for Geothermal Resources,* organized by UNU-GTP, GDC and KenGen, at Lake Bogoria and Lake Naivasha, Kenya, Oct. 29 – Nov. 19.

Omenda,P.A. 2007: 'The geothermal activity of the east African rift' **In:** *Presented at Short Course II on Surface Exploration for Geothermal Resources*, organized by UNU-GTP and KenGen, at Lake Naivasha, Kenya, November 2-17.

Reyes, (2000). *Petrology and mineral alteration in hydrothermal systems: From diagenesis to volcanic catastrophes*. Institute of Geological and Nuclear Science. Lower Hutt, New Zealand. ISBN - 9979-68-048-2.

Selamawit Worku. (2015): Sub-surface geology, hydrothermal alteration and 3D modeling of wells LA-9D and LA-10D in the Aluto Langano Geothermal field, Ethiopia. Unpublished MSc Thesis,University of Iceland, Iceland.

Solomon Kebede, 2015: 'country update on geothermal exploration and development in Ethiopia'. **In:** *Presented at Short Course IX on Exploration for Geothermal Resources*, organized by UNU-GTP, GDC and KenGen, at Lake Bogoria and Lake Naivasha, Kenya, Nov. 9 - Dec.1.

Solomon Kebede, 2016: 'Country update on geothermal exploration and development in Ethiopia'. **In:** *Proceedings, 6th African Rift Geothermal Conference Addis Ababa, Ethiopia,* Geological Survey of Ethiopia ,Addis Ababa ,Ethiopia, November 2nd – 4th .

Suryantini, 2015: 'Volcanological Approach for Evaluation of Geothermal Potential in Volcanic Associated Hydrothermal System at the Early Stage of Exploration'. **In:** *Proceedings World Geothermal Congress,* Melbourne, Australia, 19-25.

Tadiwos Chernet , (2011): Geology and hydrothermal resources in the northern Lake Abaya area (Ethiopia), *Journal of African Earth Sciences*. **61:**pp.129–141.

Tamiru A. Abiye & Tigistu Haile 2008. 'Geophysical exploration of the Boku geothermal area, Central Ethiopian Rift'. *Geothermic*. Vol. 37, PP. 586-596.

Tsegaye Abebe, 2000: 'Geological limitations of a geothermal system in a continental rift zone: example the Ethiopian rift valley'. **In:** *Proceedings World Geothermal Congress*, Kyushu - Tohoku, Japan, May 28 - June 10.

Tsegaye Abebe, Maria Laura Balestrieri and Giulio Bigazzi (2010): The Central Main Ethiopian Rift is younger than 8 Ma: confirmation through apatite fission-track thermochronology. *Terra Nova*. **22**: 470–476.

Rooney,T.O. (2011): Insights into extensional processes during magma assisted rifting: Evidence from aligned scoria cones. *Journal of Volcanology and Geothermal Research.* **201:** 83–96.

United Nation Development Program (UNDP) (1973). Investigation of geothermal resources for power development: Geology, geochemistry and hydrology of hot springs of the East Africa rift system within Ethiopia. Unpublished technical report, (UNDP), United Nations, New York, 146pp.

Wolde Gabriel, et al (1990). Geology, Geochronology, and Rift basin Development in the Central Sector of the MER. The Geological Society of America Bulletin, V102, pp.439-458.

Wolde Gabriel and Grant Heiken, 2000: Volcanism, tectonism, sedimentation, and the paleoanthropological record in the Ethiopian Rift System, Geological Society of America, Special Paper 345.

Hutchison,W., David M .Pyle ,Tamsin A. Mather , Gezahegn Yirgu, Juliet Biggs , Benjamin E. Cohen , Dan N. Barfod, & Elias Lewi (2016): The eruptive history and magmatic evolution of Aluto volcano: new insights into silicic peralkaline volcanism in the Ethiopian rift. *Journal of Volcanology and Geothermal Research*, **328**: 9–33.

Wolfenden, E., Ebinger, C., Yirgu, G., Deino, A., Ayale, D., (2004). Evolution of the northern Main Ethiopian rift: birth of a triple junction. Earth and Planetary Science, Letters 224, 213–228.

Yiheyis Amdeberhan, 1998: a conceptual reservoir model and production capacity estimate for the Tendaho geothermal field, Ethiopia. Ethiopian Institute of Geological Surveys, Addis Ababa, Ethiopia, pp.43.

Yohannes Lemma, 2007: Magneto telluric and transient electromagnetic methods in geothermal exploration, with an example from Tendaho geothermal field, Ethiopia, Geological Survey of Ethiopia, Addis Ababa, Ethiopia, pp.47.

Appendix-I: Sample locations for thin section preparation

S. No	Sample code	Location (UTM)			Sample code	Rock type
		Longitude	Latitude	Altitude		
1	St-Ts-1	433012	885539	1819	BT-TS-1	Highly altered rock
2	St-Ts-2	430568	890772	2081	BT-TS-2	Scoria
3	St-Ts-3	428526	888847	2097	BT-TS-3	Trachyte
4	St-Ts-4	431412	890556	1985	BT-TS-4	Aphanitic basalt
5	St-Ts-5	430043	889158	2022	BT-TS-5	Vesicular basalt
6	St-Ts-6	428526	888847	2097	BT-TS-6	Rhyolite
7	St-Ts-7	436409	890336	1830	BT-TS-7	Welded ignimbrite
8	St-Ts-8	428542	884181	1884	BT-TS-8	Welded ignimbrite
9	St-Ts-9	432908	884490	1816	BT-TS-9	Altered rock
10	St-Ts-10	427195	885433	1970	BT-TS-10	Unwelded tuff
11	St –Ts-11	431880	886206	1824	BT-TS-11	Unwelded Tuff

Appendix-II: Sample locations for XRD Analysis

S. No	Sample code	Location (UTM)			Rock type	Identified Alteration minerals in each sample
		Longitude	Latitude	Altitude		
1	St-XRD-1	433012	885539	1819	Highly altered	Sulfur ; titanium oxide sulfate; barium iron sulfide -$ beta
2	St-XRD-2	430568	890772	2081	Scoria	Albite -high; Calcium Aluminum Silicate
3	St-XRD-3	428542	884181	1884	Welded Ignimbrite	Lead tecto-dialuminosilicate; silicon oxide-$-alpha; quartz low
4	St-XRD-4	435053	888315	1851	Welded ignimbrite	Albite high , microcline maximum ,Sanidine
5	St-XRD-5	436409	890336	1846	crystalized ignimbrite	Quartz , Silicon oxide-$ alpha, Adularia
6	St-	432808	884390	1816	Altered	Quartz , Silicon oxide-$ alpha,

	XRD-6				vesicular rock	Iron Hydroxide Phosphate, Oxo titanium Sulfate
7	St-XRD-7	433157	885150	1818	Alluvial deposit	Silicon oxide-$ alpha, calcite; Stishovite ; Chromium Titanium Hydroxide
8	St-XRD-8	433488	885749	1817	Black soil from mud pool	Quartz , Silicon oxide-$ alpha, Lead Indium Sulfide ; Barium Sulfide; sodium Borate
9	St-XRD-9	430685	886258	1922	Un welded Tuff	Albite ; Cristobalite ; Tridymite ; Sulfide

Appendix-III: Location of Geothermal Surface manifestations

S. No	Location (UTM)			Surface manifestations	Temperature
	Longitude	Latitude	Altitude (m)		
1	432727	884183	1815	Thermal spring	91 ^{0} C
2	432785	884372	1815	Thermal spring	80 ^{0} C
3	433155	881367	1816	Extinct Thermal spring	48 ^{0} C
4	433292	885440	1825	Thermal spring	80 ^{0} C
5	433295	885530	1820	Thermal spring	71 ^{0} C
6	433488	885749	1831	Thermal spring with mud pool	101 ^{0} C
7	433493	886755	1838	Mud pool	101 ^{0} C
8	433552	885923	1821	Small hot lake	Not measured
9	433575	885934	1820	Thermal spring	52 ^{0} C
10	433602	885896		Thermal spring	61.9 ^{0} C
11	432691	885766	1853	Hot community well	Not measured
12	432842	886073	1824	Irrigation bore hole	
13	433858	886559	1826	Hot water borehole	Not measured
14	433102	885539	1819	Altered ground	115m *2Km

Appendix-IV: Petrographic analysis result

Sample code: BT-TS- 1						
Mineral composition	Modal proportion (Wt. %)	Max grain size (mm)	Crystal Shape	Diagnostic features	Rock textures	Rock name
Chlorite and Fluorite	1	0.6	Anhedral	Dark green	Spherulitic texture	Altered volcanic rock
Titanite	3	2.4	Anhedral	Reddish ,dark brown color , relief		
Sanidine	4	1.8	Euhedral	Twinning		
Quartz	5	1.2	Anhedral	Dendritic and radiate layering		
Devitrified glass	87	2.8	Anhedral	spherulite devitrification		

Sample code: BT-TS- 2						
Mineral composition	Modal proportion (Wt. %)	Max grain size (mm)	Crystal shape	Diagnostic features	Rock texture	Rock name
Olivine	2	0.4 mm	Anhedral	Altered at its rim into biotite and opaque	Vesicular Texture	Basaltic scoria
Pyroxene	11	8.2 mm	Subhedral	Inclusion of opaque minerals		
Plagioclase	14	6 mm	Euhedral	Prismatic laths , simple twinning		
Ground mass	21			Fine grained opaque minerals		
Void space	52			Spherulites amygdaloidal		

Sample code: BT-TS- 3						
Mineral composition	Modal abundance (Wt. %)	Max grain size (mm)	Crystal Shape	Diagnostic features	Rock textures	Rock name
Rock fragment	2	7.2	Anhedral	Altered into chlorite, calcite , Epidote , Rutile	Trachytic texture	Trachyte
Volcanic glass	5		Anhedral	Dark brown color, covering rock fragment		
Orthoclase	7	5.6	Euhedral	Twining		
Plagioclase	86	0.6	Euhedral	Elongated laths		
Sample code: BT-TS- 4						
Mineral composition	Modal proportion (Wt. %)	Max grain size (mm)	Crystal shape	Diagnostic features	Rock textures	Rock name
Olivine	2	1.8	Anhedral	Altered into Opx and opaque	Porphyritic texture	Aphanitic Basalt
Pyroxene	23	4.2	Subhedral	2 set of cleavage at right angle and altered into biotite		
Plagioclase	37	3.4	Subhedral	Melt inclusions and Corona texture		
Ground mass	38			Opaque, plagioclase and pyroxene		

Sample code: BT-TS- 5						
Mineral composition	Modal proportion (Wt. %)	Max grain size (mm)	Crystal shape	Diagnostic features	Rock textures	Rock name
Olivine	1	0.4	Anhedral	High interference color	porphyritic texture	Vesicular Basalt
Void space	7			Perfect circle with opaque inclusions		
Pyroxene	22	3.2	Subhedral	Melt inclusion		
Plagioclase	34	3.6	Euhedral	Compositional Zoning , exsolved opaque and fluid inclusions		
Ground mass	36			Opaque, plagioclase and pyroxene		
Sample code: BT-TS- 6						
Mineral composition	Modal proportion (Wt. %)	Max grain size (mm)	Crystal shape	Diagnostic features	Rock textures	Rock name
Opaque	3	2.2	Anhedral	High relief , dark color	Ophitic texture-intergranular	Diorite
Olivine	3	2.4	Subhedral	Alteration along fracture		
Pyroxene	29	5.8	Subhedral	Brown color altered into hornblende		
Plagioclase	65	4.6	Euhedral	Elongated laths		

Sample code: BT-TS- 7						
Mineral composition	Modal proportion (Wt. %)	Max grain size (mm)	Crystal shape	Diagnostic features	Rock textures	Rock name
Opaque	3	2	Subhedral	Graphic texture	Porphyritic texture	Crystalline ignimbrite
Orthoclase	28	7.4	Euhedral	Cleavage		
Quartz	30	6.8	Subhedral	Dendritic , spherulitic texture		
Volcanic glass	39		Anhedral	Brown dusty appearance		
Sample code: BT-TS- 8						
Mineral composition	Modal proportion (Wt. %)	Max grain size (mm)	Crystal shape	Diagnostic features	Rock texture	Rock name
Opaque ,biotite	2	1.2	Anhedral	High relief black/red color	Porphyritic texture	Welded ignimbrite
K-feldspar (Orth& Sani)	24	6	Euhedral	Two set of cleavage and alteration		
Quartz	33	8.6	Subhedral	Lack of cleavage		
Rock fragments	41			Sieve texture		

Sample code: BT-TS- 9						
Mineral composition	Modal proportion (Wt. %)	Max grain size (mm)	Crystal shape	Diagnostic features	Rock textures	Rock name
Opaque	7	0.6	Anhedral	Black color	Sieve texture	Altered felsic rock
Plagioclase	15	2.2	Subhedral	Elongated laths		
Quartz	31	1.4	Anhedral	Lack of cleavage		
Glass	47			Brown color		
Sample code: BT-TS- 10						
Mineral composition	Modal proportion (Wt. %)	Max grain size (mm)	Crystal shape	Diagnostic features	Rock textures	Rock name
Sanidine	1	2.6	Euhedral	One perfect Cleavage	Glassy texture	Unwelded Tuff
Quartz	1	0.8	Anhedral	Undulose extinction		
Opaque	1	0.4	Anhedral	Black color		
Volcanic glass	97			Fine grained Brown color		

Appendix-V: XRD analysis result

St-XRD-1

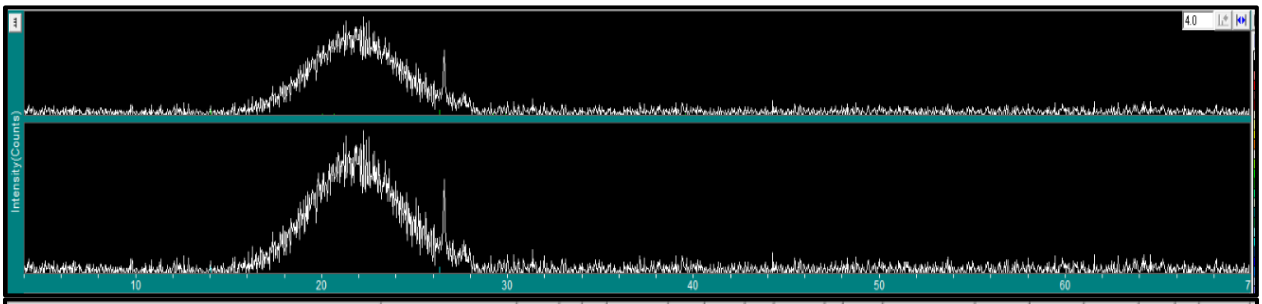

X 36 Hits Sorted on Figure-Of-Merit	Chemical Formula	FOM	J	D	PDF-#	Hits	#d/I	I%	2T(0)	RIR	Space Group	a	b	c	Z	G	CSD#
2-Methyl-1,3-cyclopentanedione	C6H8O2	7.8	+	D	43-1642	1	24	5	0.100		C2/m (12)	12.750	6.790	6.430	4		
Boron Nitride	BN	16.0	+	D	45-1171	3	6	47	-0.060		R3m (160)	2.504	2.504	10.000	3		
Barium Niobium Oxide	Ba4Nb2O9	17.2	+	X	35-1156	0	44	10	0.060			12.030	20.990	24.810			
Tetraiodine 14-fluorotriantimonate hexafluoroantimonate	(I4)(Sb3F14)(SbF6)	20.0	C	C	76-2163	2	123	75	0.120	1.55	P21/c (14)	8.425	15.980	16.804	4		37002
Quartz low, dauphinee-twinned	SiO2	20.8	C	C	89-1961	18	18	47	0.060	4.11	P6222 (180)	4.921	4.921	5.416	3		42498
4-nitrobenzenediazonium tetrafluoroborate	C6H4BF4N3O2	22.3	+	D	51-2371	0	41	75	0.120		Fdd2 (43)	22.539	31.071	5.326	16		
Copper Phosphate	CuP4O11	22.4	+	V	52-1346	0	22	62	0.020		C1 (1)	13.084	13.024	10.533	8		
2-Amino-4-p-bromophenyl-5-triazolidinyl-6-ethoxy-pyrimidine	C14H13BrN6O	22.5	+	D	47-2252	0	85	81	0.120	0.85	Pc21b (29)	17.430	9.737	17.739	8		
$GA-Glutaric acid	C5H8O4	23.2	+	D	51-1902	0	25	79	0.000		P2/c (13)	25.571	5.012	10.195	4		
1-Methyl-2-nitro-5-vinylimidazole	C6H7N3O2	23.2	+	D	30-1804	0	13	5	0.060		Pbca (61)	13.050	10.830	10.210	8		
2,2'-bipyridine	C10H8N2	23.3	+	D	37-1801	0	75	81	0.100		P21/n (14)	11.800	6.199	5.604	2		
Phosphorus Oxide Selenide	P4O6Se	23.5	+	D	51-1711	0	11	74	0.040		P21/c (14)	10.518	6.529	11.786	4		
Titanium Oxide Sulfate	TiOSO4	23.5	+	D	49-0467	0	30	63	0.060		Pnma (62)	10.938	5.150	6.416	4		
1-Methylthiolanium iodide	C5H11IS	24.2	+	D	32-1768	0	12	75	0.100		P^{nca} (69)	10.970	6.720	11.630	4		
Quartz	SiO2	24.9	C	C	85-1054	0	18	56	0.000	3.07	P3221 (154)	4.914	4.914	5.405	3		34644
Titanium Aqua Oxide Hydroxide	(H2O)Ti4O7(OH)2	25.4	+	X	38-0699	0	18	5	-0.120		C	19.880	3.735	12.090			
Quartz	SiO2	27.3	C	C	70-3755	0	18	56	0.000	2.93	P3121 (152)	4.916	4.916	5.409	3		90145
Leucoemeraldine base	(C6H5N)n	27.9	+	D	49-2499	0	29	81	-0.060			8.340	5.210	9.520	4		
$GG-Aminobutyric acid	C4H9NO2	28.4	+	D	39-1788	1	93	75	0.120		P21/a (14)	8.259	10.125	7.164	4		
Chromium Niobium Oxide	CrNb11O29	28.8	+	V	49-1553	0	5	64	-0.060			31.162	3.832	20.579			
Diaqua bis(4,5,6,7-tetrahydro-5,7-dioxo-[1,2,4]triazolo[1,5-a]py	C10H6FeN8O4I2H...	29.9	+	D	51-2005	0	13	17	-0.100		P-1 (2)	4.976	8.260	9.100	1		
Aluminum Niobium Oxide	AlNb11O29	32.8	+	V	22-0009	0	22	67	-0.120		A2/a (15)	31.140	3.813	20.550	4		
Bis-(4-chlorophenyl)carbamide	C13H10Cl2N2O	34.7	+	C	47-2340	0	78	74	0.120		C2/c (15)	27.382	4.608	10.140	4		
Petalite-1M	LiAlSi4O10	37.3	+	C	35-0463	0	51	57	-0.060		P2/a (13)	11.754	5.140	7.630	2		
Manganese phyllo-undecaoxotetraphosphate	MnP4O11	38.4	C	C	70-1804	0	114	75	0.100	0.74	P21/n (14)	8.608	8.597	12.464	4		4282
Chromium Hydrogen Sulfate Hydrate	Cr4H2(SO4)7(H2O)...	39.0	C	C	72-0981	0	135	75	0.060	0.69	P-1 (2)	12.613	13.250	7.402	1		16449
Potassium hydrogen tri-L-malate	C12H16K2O15	39.2	+	D	54-2129	2	88	85	-0.080	0.53	P212121 (19)	7.725	7.891	29.804	4		
4-[2-hydroxy-3-[(1-methylethyl)amino]propoxy]-benzeneaceta...	C14H22N2O3	40.1	+	D	52-1981	0	145	74	0.000		P-1 (2)	14.418	28.019	11.446	12		
Sodium bis[trihydroxostannate(II)] oxotetrahydroxodistannat...	Na4(Sn(OH)3)2(Sn...	41.2	C	C	76-1312	0	137	56	0.100	1.69	P21/n (14)	15.224	8.300	12.760	4		35420
Potassium pentasulfate	K2S5O16	42.4	C	C	74-0544	0	143	81	0.000	1.69	Pbcn (60)	9.190	10.891	14.522	4		26180
Chromium Hydrogen Sulfate Hydrate	CrH(SO4)2(H2O)7	42.4	C	C	70-0462	0	142	74	0.040	1.13	P21/c (14)	7.371	10.535	16.703	4		1100
Potassium niobium tungstate	K2Nb10W7O47	43.3	C	C	78-0994	0	133	79	0.100	4.86	P2/m (10)	18.882	3.957	12.378	1		62130
Sulfur	S	45.6	C	C	78-0793	0	127	75	-0.080	0.44	P21/c (14)	12.950	12.360	17.610	104		61705
Barium iron sulfide - $-beta	Ba9Fe4S15	47.4	C	C	77-0428	0	130	85	-0.040	1.55	Pnma (62)	25.212	9.594	12.575	4		41841
Sulfur Arsenic Fluoride	(S4(AsF6)2)(AsF3)	47.4	C	C	70-3693	0	150	79	0.040	1.74	P21/c (14)	7.886	9.261	19.191	4		90078
13-Fluoroantimonium(III) pentakis(hexafluoroantimonate(V)) -...	Sb6F13(SbF6)5	48.6	C	C	77-1932	0	137	70	-0.040	1.40	P21/c (14)	11.638	8.995	16.723	2		60095

St-XRD-2

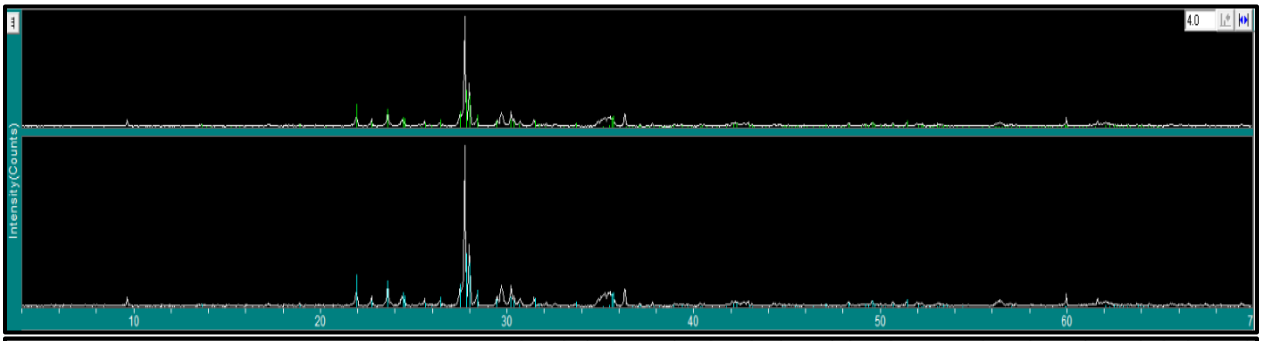

X 28 Hits Sorted on Figure-Of-Merit	Chemical Formula	FOM	J	D	PDF-#	Hits	#d/I	I%	2T(0)	RIR	Space Group	a	b	c	Z	G	CSD#
Labradorite	Ca0.65Na0.32[Al1....	5.6	C	C	83-1367	0	148	31	-0.020	0.56	C-1 (2)	8.174	12.874	7.102	4		100232
Albite, disordered	Na[Si3Al]O8	6.1	+	X	10-0393	0	42	31	-0.080		C-1 (2)	8.165	12.872	7.111	4		
Labradorite	Ca0.65Na0.35[Al1....	6.9	C	C	83-1369	0	150	31	-0.020	0.57	C-1 (2)	8.175	12.871	7.101	4		100234
Labradorite	Ca0.68Na0.30[Al1....	7.0	C	C	83-1372	0	149	31	-0.100	0.56	C-1 (2)	8.152	12.834	7.079	4		100237
Labradorite	(Ca0.64Na0.31)[Al...	7.3	C	C	83-1417	0	137	31	-0.020	0.53	C-1 (2)	8.175	12.871	14.203	8		100283
Anorthite, sodian, disordered	(Ca,Na)[Si,Al]4O8	7.8	+	D	41-1481	0	50	34	-0.060	0.73	P-1 (2)	8.181	12.874	7.097	4		
Augite	(CaMg0.74Fe0.25)...	7.9	C	C	70-3753	0	72	10	-0.100	1.11	C2/c (15)	9.750	8.901	5.274	4		90143
Unnamed	(Ca0.68Na0.32)[Al...	8.1	C	C	89-1469	0	134	31	-0.020	0.54	I-1 (2)	8.173	12.869	14.200	8		86327
Augite	(Mg,Fe,Al,Ti)(Ca,N...	8.5	C	C	88-0857	0	72	10	-0.080	1.24	C2/c (15)	9.756	8.903	5.283	4		85168
Augite	(Mg,Fe,Al,Ti,Cr)[Ca...	9.4	C	C	88-0851	0	72	10	-0.080	1.22	C2/c (15)	9.749	8.888	5.289	4		85162
Calcium Aluminum Silicate	Ca0.88[Xs0.12Al1....	9.6	+	D	52-1344	0	29	18	-0.060		C	8.165	12.871	14.171	8		
Diopside	CaMgSi2O6	10.4	C	C	72-1497	0	71	9	-0.060	1.21	C2/c (15)	9.750	8.926	5.251	4		17043
Diopside	(Ca0.959Ti0.041)[...	10.7	C	C	81-0487	0	79	10	-0.080	0.90	C2/c (15)	9.752	8.917	5.265	4		71835
Unnamed	(Ca0.72Na0.28)[Al...	10.8	C	C	89-1468	0	139	31	-0.020	0.53	I-1 (2)	8.174	12.880	14.200	8		86326
Anorthite, sodian	Ca.66Na.34Al1.66...	10.8	C	C	86-1650	0	139	31	0.020	0.54	I-1 (2)	8.175	12.871	14.230	8		201648
Unnamed annealed, mineral [NR]	(Ca0.78Na0.22)[Al...	10.9	C	C	89-1480	0	137	18	-0.040	0.55	I-1 (2)	8.174	12.870	14.184	8		86339
Augite	(Mg,Fe,Ti,Al)[Ca,N...	11.0	C	C	88-0848	0	73	10	-0.080	1.27	C2/c (15)	9.764	8.902	5.289	4		85159
Albite calcian low	(Na0.84Ca0.16)Al1...	11.0	C	C	76-0927	0	147	18	-0.100	0.61	C-1 (2)	8.155	12.821	7.140	4		34917
Andesine	Na.499Ca.491[Al1....	11.3	C	C	79-1149	0	150	75	0.000	0.56	C-1 (2)	8.179	12.880	7.112	4		66127
Diopside ferrian, syn	Ca1.007[Mg0.805F...	11.7	C	C	89-0835	0	67	10	-0.040	1.38	C2/c (15)	9.772	8.918	5.284	4		85690
Anorthite, ordered	CaAl2Si2O8	11.7	+	D	41-1486	0	69	28	0.000	0.41	P-1 (2)	8.176	12.872	14.183	8		
Diopside ferroan	(Mg0.992Fe0.008)[...	12.0	C	C	83-0100	0	74	10	-0.100	1.10	C2/c (15)	9.749	8.914	5.256	4		79184
Anorthite, sodian	Ca0.86Na0.14Al1....	12.0	C	C	76-0832	0	139	10	-0.020	0.55	I-1 (2)	8.183	12.883	14.186	8		34791
Diopside ferrian, syn	Ca1.022[Mg0.857F...	12.6	C	C	89-0834	0	73	9	-0.020	1.30	C2/c (15)	9.765	8.920	5.271	4		85689
Andesine	Na0.685Ca0.347Al...	12.7	C	C	83-1939	1	144	31	0.020	0.59	C-1 (2)	8.178	12.865	7.109	4		100868
Diopside, ferrian, syn	Ca1.022[Mg0.906F...	12.9	C	C	89-0833	0	73	9	-0.040	1.30	C2/c (15)	9.758	8.923	5.264	4		85688
Diopside ferroan	(Mg0.998Fe0.002)[...	12.9	C	C	83-0102	0	73	9	-0.060	1.17	C2/c (15)	9.750	8.916	5.259	4		79186
Albite - high	Na (Al Si3 O8)	20.8	+	C	99-0001	0	200	18	-0.100	0.32	C-1 (2)	8.149	12.880	7.106	4		1

St-XRD-3

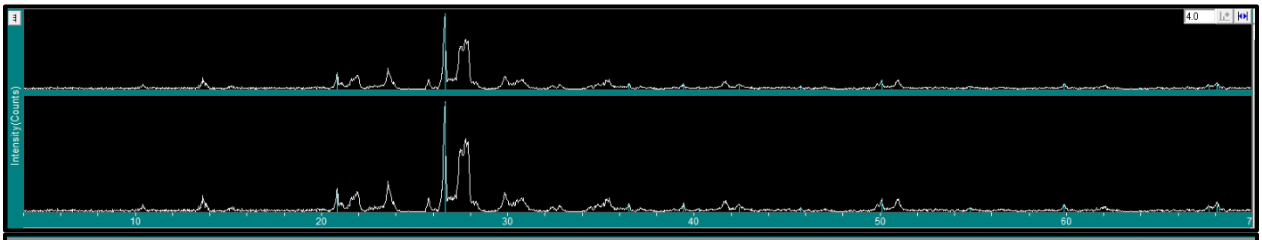

X 36 Hits Sorted on Figure-Of-Merit	Chemical Formula	FOM	J	D	PDF-#	Hits	#d/I	I%	2T(0)	RIR	Space Group	a	b	c	Z	G	CSD#
Quartz	SiO2	0.8	C	C	86-1560	1	18	93	0.020	3.03	P3221 (154)	4.916	4.916	5.405	3		100341
Quartz low, syn	SiO2	0.8	C	C	83-2465	0	18	92	0.000	3.05	P3121 (152)	4.915	4.915	5.406	3		200721
Silicon oxide - $-alpha	SiO2	0.9	C	C	77-1060	12	20	93	0.020	1.04	P1 (1)	4.916	4.917	5.407	3		39830
Quartz	Si O2	1.2	+	C	99-0088	17	18	93	0.000	2.11	P3221 (154)	4.913	4.913	5.405	3		88
Quartz low, dauphinee-twinned	SiO2	1.3	C	C	89-1961	19	18	87	0.080	4.11	P6222 (180)	4.921	4.921	5.416	3		42498
Magnesium manganese germanide	MgMnGe	6.0	C	C	87-0739	0	22	7	0.080	5.05	P4/nmm (129)	3.963	3.963	6.550	2		66952
Iron hexathioduo-diphosphate	Fe2P2S6	6.0	C	C	74-1501	0	52	5	-0.060	2.71	C2/m (12)	5.930	10.280	6.720	2		27307
Poly(pyromellitimide phenyl ether)	(C22H10N2O5)n	6.0	+	C	54-2400	0	3	10	-0.100			6.580	4.750	31.200			
Bijvoetite (Y)	(Y4.22Nd3.78)(H2...	7.2	?	C	70-3479	0	90	5	0.080	7.65	B21 (4)	21.234	12.958	44.911	4		89853
Iron Phosphorus Sulfide	FePS3	7.8	C	C	78-0496	0	49	5	0.000	2.69	C2/m (12)	5.947	10.300	6.722	4		61392
Boron Nitride	BN	8.0	C	C	73-2095	0	7	46	-0.040	2.16	P-6m2 (187)	2.504	2.504	6.661	2		24644
Microcline, intermediate	KAlSi3O8	8.8	+	F	19-0932	0	79	50	0.120		C-1 (2)	8.560	12.970	7.210	4		
Sanidine, potassian, disordered, syn	(Na,K)(Si3Al)O8	10.0	+	D	10-0357	1	17	50	-0.040		C2/m (12)	8.335	12.970	7.159	4		
Cadmium iron hexathioduo-diphosphate(IV)	CdFe(P2S6)	10.2	C	C	78-2069	0	75	5	-0.060	4.01	C2/m (12)	6.080	10.478	6.801	2		63274
Sanidine	K0.42Na0.58Ca0.0...	10.2	C	C	77-0982	0	103	55	0.040	0.60	C2/m (12)	8.360	12.997	7.162	4		39748
N,N'-Dimethyloxamide	C4H8N2O2	10.8	+	D	54-1488	0	30	10	0.100		P1 (1)	5.069	6.898	4.764	1		
Silver Vanadium Phosphorus Sulfide	Ag0.5V0.5PS3	10.8	+	C	40-0939	0	37	9	0.040		P2/a (13)	5.921	10.684	6.752	4		
Feldspar (Na-component)	Na(AlSi3O8)	12.3	C	C	89-8575	0	106	17	-0.080	0.55	C-1 (2)	8.126	12.996	7.164	4		88899
Zinc hexathioduo-diphosphate	Zn2(P2S6)	12.5	C	C	84-0996	1	52	5	0.040	3.11	C2/m (12)	5.972	10.342	6.756	2		201933
Zinc trithiophosphate(IV)	Zn(PS3)	12.5	C	C	83-0467	1	52	5	0.040	3.10	C2/m (12)	5.972	10.342	6.756	4		79557
5-Methyl-1H-tetrazole	C2H4N4	12.6	+	D	54-2290	0	29	10	-0.100		Cc (9)	4.599	12.864	9.775	4		
Anorthoclase	(Na0.7K0.3)(Al1.02...	12.7	C	C	76-0803	1	143	50	-0.060	0.63	C-1 (2)	8.300	12.953	7.149	4		34742
Bismuth dimagnesium dioxide phosphate	BiMg2O2(PO4)	12.9	C	C	81-2431	0	60	10	0.080	5.79	Cmcm (63)	7.801	11.888	5.273	4		73894
Boron Nitride	BN	12.9	+	D	34-0421	0	6	28	-0.040		P63/mmc (194)	2.504	2.504	6.656	2		
Anorthoclase	(Na0.667K0.333)(A...	16.2	C	C	75-1630	1	138	55	-0.020	0.61	C-1 (2)	8.290	12.966	7.151	4		31180
Microline intermediate	K.871Na.120Rb.0...	17.2	C	C	76-0826	3	133	50	0.100	0.58	C-1 (2)	8.567	12.980	7.200	4		34785
Orthoclase sodian, syn	K0.58Na0.42AlSi3...	17.4	C	C	83-1253	0	104	46	0.080	0.60	C-1 (2)	8.434	13.015	7.172	4		100087
Feldspar potassian	K.5Na.5AlSi3O8	17.5	C	C	84-0710	0	139	51	0.080	0.60	C-1 (2)	8.529	12.945	7.189	4		201602
Microperthite	K0.96Na0.04AlSi3...	18.5	C	C	83-1895	0	128	51	0.080	0.58	C-1 (2)	8.583	12.975	7.208	4		100819
Microline intermediate	K.904Na.085Ca.00...	19.6	C	C	76-0827	2	146	50	0.080	0.59	C-1 (2)	8.564	12.984	7.201	4		34786
Antimony sulfide iodide - II	SbSI	20.3	C	C	88-0985	0	86	10	0.060	6.85	P212121 (19)	8.529	10.149	4.094	4		85298
Indium Phosphorus Sulfide	In2P3S9	23.1	C	C	71-0322	2	140	7	0.020	3.35	P21/c (14)	6.842	10.528	18.266	4		1700
Lead tecto-dialumodisilicate	Pb(Al2Si2O8)	24.0	C	C	87-1003	0	118	10	0.100	2.19	C2/m (12)	8.428	13.054	7.174	4		82739
Trilithium hexavanadate	Li3(V6O16)	25.9	C	C	86-2421	0	101	5	-0.100	2.84	P21/m (11)	12.030	3.600	6.680	1		40417
Lead tecto-dialumodisilicate	Pb(Al2Si2O8)	27.6	C	C	89-6433	0	143	10	0.040	2.38	I2/c (15)	8.402	13.043	14.308	8		87664
1-[$GA-(1-Phenethylamino)-2-ethoxybenzyl]-2-naphthol	C27H27NO2	29.1	+	D	54-1842	0	108	3	-0.100	1.75	P21 (4)	9.025	14.889	17.001	4		

St-XRD-4

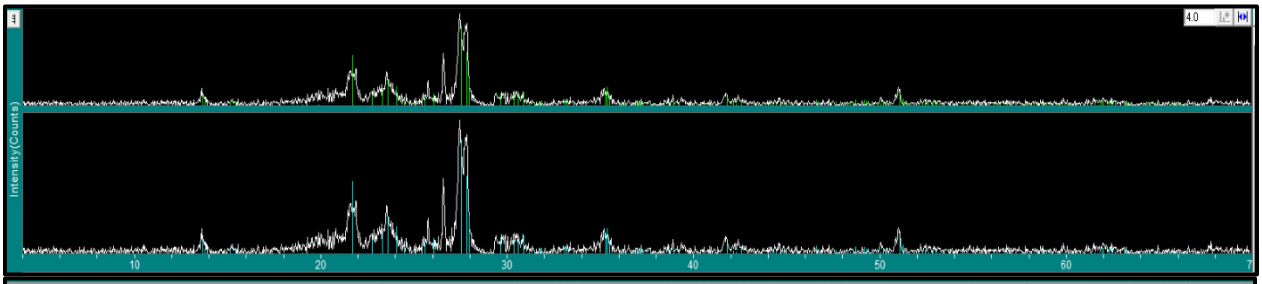

X 23 Hits Sorted on Figure-Of-Merit	Chemical Formula	FOM	J	D	PDF-#	Hits	#d/I	I%	2T(0)	RIR	Space Group	a	b	c	Z	G	CSD#
Anorthoclase	(Na0.75K0.25)(AlSi...	4.5	C	C	75-1632	1	146	81	-0.060	0.60	C-1 (2)	8.252	12.936	7.139	4		31182
Anorthoclase	(Na0.667K0.333)(A...	5.3	C	C	75-1630	1	138	93	-0.020	0.61	C-1 (2)	8.290	12.966	7.151	4		31180
Albite high (K-bearing)	(K0.22Na0.78)(AlSi...	5.5	C	C	83-1658	1	146	83	-0.080	0.62	C-1 (2)	8.144	12.989	7.160	4		100558
Anorthoclase	(Na0.7K0.3)(Al1.02...	5.5	C	C	76-0803	1	143	72	-0.080	0.63	C-1 (2)	8.300	12.953	7.149	4		34742
Albite high	K0.2Na0.8AlSi3O8	5.6	C	C	83-2215	1	146	83	-0.080	0.62	C-1 (2)	8.144	12.989	7.160	4		200359
Cesium-doped polyacetylene	[(CH)Cs0.167]n	5.7	+	D	46-1879	1	15	14	-0.100		P41212 (92)	9.093	9.093	7.952	24		
Albite high	Na(AlSi3O8)	6.4	?	C	83-1608	0	151	75	-0.100	0.61	C-1 (2)	8.208	12.933	7.133	4		100499
Anorthoclase	(Na0.85K0.14)(AlSi...	6.7	C	C	75-1634	4	145	64	-0.060	0.60	C-1 (2)	8.217	12.917	7.126	4		31184
Ethylenediammonium pentafluoroferrate	C2H10F5FeN2	6.9	+	D	43-1637	1	30	7	0.000	1.60		9.092	9.092	7.944	4		
Tetramethylammonium chromate	C8H24CrN2O4	7.0	+	D	54-2408	0	17	7	-0.100		Fm-3m (225)	11.039	11.039	11.039	4		
Anorthite	Ca(Al2Si2O8)	7.4	C	C	89-1459	0	127	62	0.000	0.54	P-1 (2)	8.175	12.873	14.170	8		86317
Microcline maximum	KAlSi3O8	8.0	C	C	72-1114	0	143	61	-0.060	0.59	C-1 (2)	8.560	12.964	7.215	4		16597
Albite calcian low	(Na0.75Ca0.25)(Al...	8.1	C	C	76-0926	1	141	73	-0.060	0.58	C-1 (2)	8.169	12.851	7.124	4		34916
Methyl p-hydroxybenzoate	C48H48O18	8.1	+	D	51-2329	0	64	10	0.000			12.485	16.973	11.024			
Andesine	Na0.622Ca0.368Al...	9.1	C	C	83-1938	1	146	67	-0.120	0.57	C-1 (2)	8.178	12.865	7.109	4		100867
Sodium Molybdenum Oxide	Na0.93Mo6O17	10.0	C	C	71-2170	0	47	18	0.040	9.55	P-3m1 (164)	5.510	5.510	12.950	1		14362
Albite (Ge-exchanged), syn	Na(AlSiGe2O8)	12.0	C	C	80-2296	0	148	33	0.080	1.02	C-1 (2)	8.331	13.156	7.266	4		71107
MAPO-39	AlPO4	13.1	+	C	50-1704	0	29	10	0.080		I-4 (82)	13.090	13.090	5.180			
Sanidine, potassian, disordered, syn	(Na,K)(Si3Al)O8	13.5	+	D	10-0357	1	17	77	0.100		C2/m (12)	8.335	12.970	7.159	4		
Feldspar potassian	K.5Na.5AlSi3O8	14.0	C	C	84-0710	0	139	67	0.100	0.60	C-1 (2)	8.529	12.945	7.189	4		201602
Microline maximum	K0.94Na0.06Al1.0...	16.2	C	C	76-0831	0	138	81	0.120	0.58	C-1 (2)	8.561	12.972	7.223	4		34790
Anorthite	Ca (Al2 Si2 O8)	18.5	+	C	99-0012	0	200	50	0.020	0.28	P-1 (2)	8.177	12.877	14.169	8		12
Indium Phosphorus Sulfide	In2P3S9	23.1	C	C	71-0322	2	140	7	0.000	3.35	P21/c (14)	6.842	10.528	18.266	4		1700

St-XRD-5

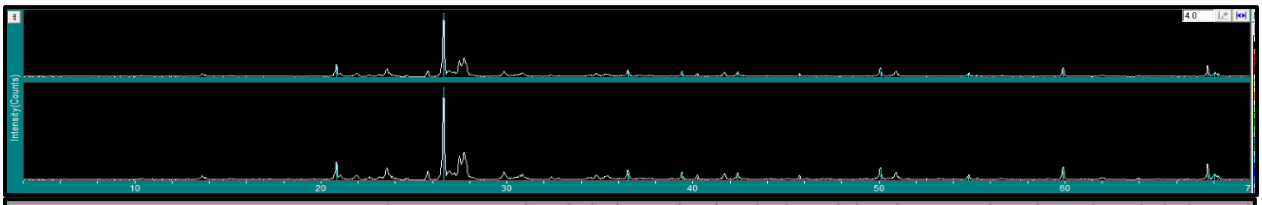

X 13 Hits Sorted on Figure-Of-Merit	Chemical Formula	FOM	J	D	PDF-#	Hits	#d/I	I%	2T(0)	RIR	Space Group	a	b	c	Z	G	CSD#
Quartz	Si O2	0.7	+	C	99-0088	17	18	93	-0.020	2.11	P3221 (154)	4.913	4.913	5.405	3		88
Quartz, syn	SiO2	0.7	+	D	46-1045	5	18	93	0.000	3.41	P3221 (154)	4.913	4.913	5.405	3		
Quartz	SiO2	1.0	C	C	86-2237	0	18	93	-0.020	3.02	P3121 (152)	4.913	4.913	5.404	3		40009
Silicon oxide - $-alpha	SiO2	1.0	C	C	77-1060	12	20	93	0.000	1.04	P1 (1)	4.916	4.917	5.407	3		39830
Quartz low, dauphinee-twinned	SiO2	1.3	C	C	89-1961	19	18	83	0.060	4.11	P6222 (180)	4.921	4.921	5.416	3		42498
Sanidine low	(K.93Na.07)(AlSi3...	7.9	C	C	87-0684	0	114	7	0.080	0.74	C2/m (12)	8.578	12.978	7.204	4		64961
Adularia	K(AlSi3O8)	7.9	C	C	71-1543	0	110	7	0.020	0.75	C2/m (12)	8.545	12.967	7.201	4		10273
Adularia	K4Al4Si12O32	8.2	C	C	71-0956	0	111	7	0.040	0.75	C2/m (12)	8.554	12.970	7.207	1		9543
Sanidine	K0.65Na0.35AlSi3...	9.1	C	C	83-1657	0	122	7	0.020	0.68	C2/m (12)	8.558	12.997	7.179	4		100557
Orthoclase	(K.88Na.10Ca.009...	9.1	C	C	76-0825	0	103	7	0.080	0.58	C-1 (2)	8.563	12.990	7.210	4		34784
Feldspar (K-component)	K(AlSi3O8)	9.4	C	C	89-8573	0	107	7	0.000	0.59	C-1 (2)	8.544	12.998	7.181	4		88897
Orthoclase	(K.931Na0.055Ca....	10.7	C	C	76-0824	3	106	7	0.060	0.59	C-1 (2)	8.583	12.988	7.202	4		34783
Sanidine low	(K.86Na.14)(AlSi3...	11.0	C	C	87-0682	0	111	7	0.020	0.73	C2/m (12)	8.543	13.019	7.183	4		64959

St-XRD-6

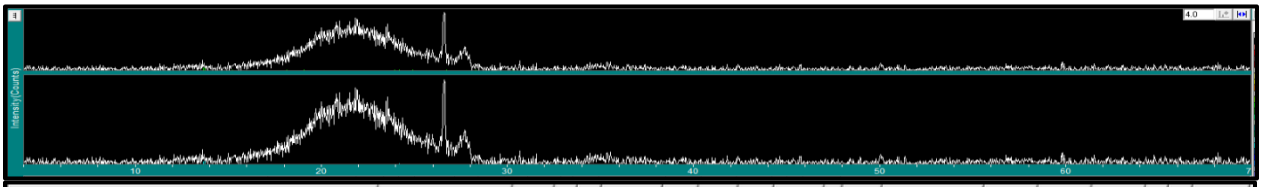

X 19 Hits Sorted on Figure-Of-Merit	Chemical Formula	FOM	J	D	PDF-#	Hits	#d/I	I%	2T(0)	RIR	Space Group	a	b	c	Z	G	CSD#
$GB-Hexanitrohexaazaisowurtzitane	C6H6N12O12	10.1	+	D	52-2432	3	30	3	0.000		Pca21 (29)	9.652	11.644	13.002	4		
7,14-dioxo-5,7,12,14-tetrahydroquinolino[2,3-b]acridine	C20H12N2O2	15.2	+	D	48-2094	0	12	3	0.060			14.010	12.950	11.660			
Quartz	SiO2	18.2	C	C	85-0797	3	18	100	0.000	3.31	P3221 (154)	4.914	4.914	5.404	3		27833
Quartz	SiO2	19.6	C	C	79-1906	3	18	100	-0.020	4.75	P3121 (152)	4.913	4.913	5.405	3		67117
Bismuth Chloride Fluoride	BiClF8	21.9	+	X	45-1253	0	24	66	0.040		P-1 (2)	5.649	10.533	5.339			
Silicon oxide - $-alpha	SiO2	22.0	C	C	77-1060	12	20	100	0.000	1.04	P1 (1)	4.916	4.917	5.407	3		39830
Quartz	Si O2	22.4	+	C	99-0088	17	18	93	0.000	2.11	P3221 (154)	4.913	4.913	5.405	3		88
Iron Hydroxide Phosphate	Fe4(OH)3(PO4)3	22.5	C	C	84-2019	0	140	79	-0.120	1.26	C2/c (15)	19.555	7.376	7.429	4		203049
Indole-2-carboxylic acid-5-nitroquinoline	C18H13N3O4	23.1	+	D	54-2358	0	8	94	0.100		P-1 (2)	8.229	12.828	15.335	4		
Iodyl disulfate	(IO2)2S2O7	24.3	+	X	52-0159	0	16	83	0.100		P21/a (14)	8.850	10.373	9.158	4		
Cadmium Silver	CdAg	28.1	+	C	28-0198	0	6	5	0.020		P63/mmc (194)	2.987	2.987	4.825	1		
2,6-Dichloro-4-nitrophenol	C6H3Cl2NO3	29.2	+	X	54-1619	2	29	93	-0.060		P-1 (2)	8.169	16.637	7.440	4		
2,4-Dichlorophenoxyacetylhydrazide	C8H8Cl2N2O2	30.3	+	D	51-2075	0	47	79	-0.040			7.340	8.110	8.530			
Cyanuric chloride	C3Cl3N3	37.0	+	F	36-1673	0	54	51	-0.060		I2/a (15)	11.278	7.471	7.606	4		
2,3-dichloro-1,4-napthoquinone	C10H4Cl2O2	37.5	+	D	22-1689	2	39	43	-0.100	2.50	P-1 (2)	18.170	8.280	7.330	4		
Lithium tetraiodoindate	LiInI4	44.0	C	C	76-2098	0	146	100	0.060	2.80	P21/c (14)	8.389	7.512	15.267	4		36599
Oxotitanium sulfate	(TiO)(SO4)	46.6	C	C	86-0647	0	73	62	-0.060	2.38	Pnma (62)	10.953	5.152	6.426	4		81348
Bis(oxoniobium) tetraphosphate(V)	(NbO)2P4O13	46.7	C	C	78-1318	0	136	74	-0.020	1.66	P1 (1)	6.586	8.400	10.842	2		62471
Trisodium pentaantimony fluoride	Na3Sb5F18	49.6	C	C	77-1853	0	125	85	0.100	2.49	P21/n (14)	5.459	24.089	12.119	4		60000

St-XRD-7

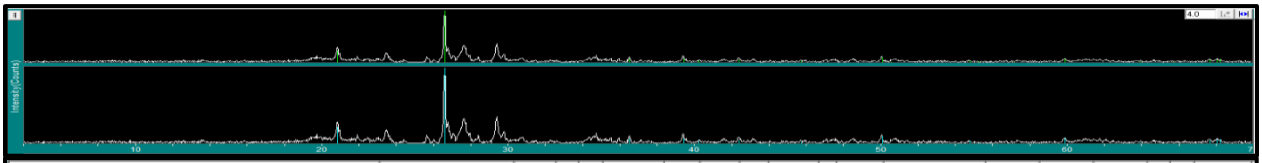

X 36 Hits Sorted on Figure-Of-Merit	Chemical Formula	FOM	J	D	PDF-#	Hits	#d/I	I%	2T(0)	RIR	Space Group	a	b	c	Z	G	CSD#
Quartz	SiO2	0.7	C	C	75-0443	2	18	99	-0.020	3.04	P3121 (152)	4.913	4.913	5.405	3		29122
Silicon Oxide	SiO2	0.8	C	C	85-0695	0	18	99	-0.020	3.04	P3221 (154)	4.913	4.913	5.405	3		26429
Quartz	Si O2	0.9	+	C	99-0088	17	18	99	-0.020	2.11	P3221 (154)	4.913	4.913	5.405	3		88
Quartz low, dauphinee-twinned	SiO2	0.9	C	C	89-1961	19	18	99	0.040	4.11	P6222 (180)	4.921	4.921	5.416	3		42498
Silicon oxide - $-alpha	SiO2	0.9	C	C	77-1060	12	20	99	0.000	1.04	P1 (1)	4.916	4.917	5.407	3		39830
Calcite, syn	CaCO3	1.9	C	C	72-1214	2	19	34	0.000	3.20	R-3c (167)	4.989	4.989	17.062	6		16710
Calcite, magnesium, syn	(Mg0.03Ca0.97)(C...	2.9	C	C	89-1304	24	19	34	-0.100	3.12	R-3c (167)	4.978	4.978	16.988	6		86161
Calcite	Ca C O3	3.2	+	C	99-0022	25	19	34	0.000	1.49	R-3c (167)	4.989	4.989	17.062	6		22
Molybdenum Carbide	MoC	6.0	C	C	89-2868	0	3	5	0.100	10.27	Fm-3m (225)	4.270	4.270	4.270	4		43523
Titanium Vanadium Carbide	TiVC2	6.0	C	C	65-7931	0	3	7	-0.040	3.88	Fm-3m (225)	4.255	4.255	4.255	2		
Zinc Oxide	ZnO	6.0	C	C	65-0682	0	3	5	0.100	5.83	Fm-3m (225)	4.270	4.270	4.270	4		
Osbornite, syn	TiN	6.0	C	C	65-0414	0	3	7	0.000	4.08	Fm-3m (225)	4.260	4.260	4.260	4		
Cobalt Oxide	CoO	6.0	+	C	43-1004	0	3	7	0.000	4.55	Fm-3m (225)	4.260	4.260	4.260	4		
Manganese Titanium Nitride	Mn0.4Ti0.6N0.88	6.6	C	C	89-4816	0	3	7	-0.060	4.17	Fm-3m (225)	4.253	4.253	4.253	4		76067
Stishovite	SiO2	6.6	C	C	82-0513	0	8	7	-0.060	1.91	P42/mnm (136)	4.095	4.095	2.708	2		74531
Vanadium Hydride	VH2	6.6	+	V	39-1326	0	3	7	0.020		Fm-3m (225)	4.260	4.260	4.260	4		
Nickel Titanium	Ni4Ti3	7.2	C	C	65-3957	0	31	5	-0.080	5.39	R-3 (148)	11.240	11.240	5.077	6		
Titanium Carbide Nitride Hydride	TiC0.25N0.22H0.19	7.8	C	C	85-1165	0	3	5	0.120	4.96	Fm-3m (225)	4.272	4.272	4.272	4		39956
Titanium Carbide Nitride	C0.3N0.7Ti	7.8	+	D	42-1488	0	3	7	0.060		Fm-3m (225)	4.264	4.264	4.264	4		
Chromium Titanium Hydride	Cr1.8TiH5.3	7.8	+	C	42-1124	0	3	7	0.100		F	4.268	4.268	4.268	2		
Vanadium Hydride	VH2.01	7.8	+	V	39-1172	0	3	5	0.100		Fm-3m (225)	4.271	4.271	4.271	4		
Calcite, magnesian	(Mg.064Ca.936)(C...	8.2	C	C	86-2335	20	19	34	-0.120	3.05	R-3c (167)	4.967	4.967	16.963	6		40108
Scandium Titanium Nitride	Sc0.1Ti0.9N0.9	8.4	C	C	89-5190	0	3	7	-0.100	3.98	Fm-3m (225)	4.249	4.249	4.249	4		76450
Sanidine, disordered	K(Si3Al)O8	8.4	+	D	25-0618	0	83	31	-0.040		C2/m (12)	8.604	13.035	7.175	4		
Magnesium ferrous oxide - in contact with iron	(MgO)0.593(FeO)0....	9.0	C	C	77-2367	0	3	7	0.060	3.82	Fm-3m (225)	4.265	4.265	4.265	4		60695
Sodium Chromium Titanium Sulfide	Na0.9Cr0.9Ti0.1S2	9.6	C	C	84-0202	0	20	7	-0.020	5.31	R-3m (166)	3.558	3.558	19.510	3		200982
Microcline intermediate	KAlSi3O8	10.6	C	C	83-1604	4	144	28	-0.060	0.59	C-1 (2)	8.643	12.929	7.190	4		100495
Betaine maleic acid	C5H11NO2I(CH2)2...	10.7	+	D	44-1588	2	76	99	-0.020		Pnma (62)	26.505	6.687	6.378	8		
Iron Titanium Vanadium	Fe0.1Ti0.135V0.765	10.8	C	C	65-9143	0	3	7	0.060	7.41	Fm-3m (225)	4.264	4.264	4.264	4		
Copper Oxide	Cu2O	10.8	C	C	65-3288	0	7	7	0.020	8.63	Pn-3m (224)	4.260	4.260	4.260	2		
Magnesium Vanadium Molybdenum Oxide	Mg2.5VMoO8	10.8	+	X	49-0679	2	23	69	-0.020			10.344	17.468	5.057			
Orthoclase	K4Al4Si12O32	10.9	C	C	71-0957	4	113	15	-0.040	0.75	C2/m (12)	8.561	12.996	7.192	1		9544
Microline intermediate	K.904Na.085Ca.00...	11.0	C	C	76-0827	2	146	23	0.000	0.59	C-1 (2)	8.564	12.984	7.201	4		34786
Sanidine ferric	KFe0.28Al0.72Si3O8	11.3	C	C	77-0992	3	124	25	0.100	0.82	C2/m (12)	8.639	13.065	7.221	4		39759
Magnesium Hafnium Oxide	Mg2Hf5O12	11.4	+	D	33-0862	0	23	7	0.000		R	9.391	9.391	8.704			
Cobalt Dysprosium Holmium Terbium	Co2Dy0.5Ho0.125...	11.7	C	C	65-5838	0	8	5	-0.040	9.85	Fd-3m (227)	7.183	7.183	7.183	8		

St-XRD-8

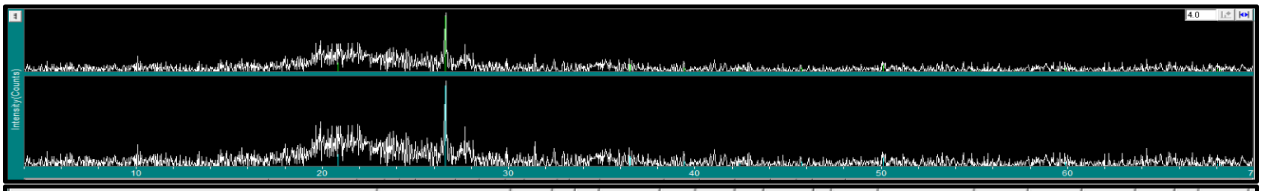

40 Hits Sorted on Figure-Of-Merit	Chemical Formula	FOM	J	D	PDF-#	Hits	#d/I	I%	2T(0)	RIR	Space Group	a	b	c	Z	G	CSD#
Quartz	SiO2	12.1	C	C	85-0798	0	18	89	0.000	3.34	P3221 (154)	4.914	4.914	5.405	3		27834
Quartz	Si O2	13.2	+	C	99-0088	17	18	89	-0.020	2.11	P3221 (154)	4.913	4.913	5.405	3		88
Quartz low, dauphinee-twinned	SiO2	13.3	C	C	89-1961	19	18	89	0.040	4.11	P6222 (180)	4.921	4.921	5.416	3		42498
Silicon oxide - $-alpha	SiO2	14.0	C	C	77-1060	12	20	82	0.020	1.04	P1 (1)	4.916	4.917	5.407	3		39830
5-(4-Methoxyphenyl)tetrazole	C8H8N4O	14.9	+	D	54-2179	0	33	89	0.100		P-1 (2)	8.349	8.815	5.897	2		
Poly-[6-[4-[4-methoxyphenyl)phenoxy]hexylmethacrylate]	(C23H28O4)n	15.6	+	V	53-1878	0	9	7	0.080			8.040	5.450	25.800	2		
Niobium Titanium Carbide	(Nb,Ti)C	16.8		D	47-1418	0	3	14	-0.020		Fm-3m (225)	4.427	4.427	4.427	8		
Indium Zirconium	InZr	19.2	C	C	65-6482	0	3	15	0.080	15.51	Fm-3m (225)	4.418	4.418	4.418	2		
Niobium Carbide	NbC	20.4	C	C	65-8783	0	3	10	0.100	9.86	Fm-3m (225)	4.428	4.428	4.428	4		
Niobium(III) nitride	NbN	21.0	C	C	74-1218	0	3	14	-0.020	9.00	Fm-3m (225)	4.410	4.410	4.410	4		26951
Tantalum Tungsten Carbide	Ta7W3C10	21.0	C	C	65-8801	0	3	15	0.000	17.91	Fm-3m (225)	4.410	4.410	4.410	4		
Lead Indium Sulfide	Pb3In6.67S13	21.0	+	F	35-1068	0	28	70	0.100		C2/m (12)	38.132	3.864	13.763	4		
Barium Iron Sulfide	Ba16Fe8S29.33	21.1	+	C	31-0147	0	49	89	0.060	2.10	P-1 (2)	9.002	6.709	24.658	1		
Ammonia Nickel Cyanide	Ni(CN)2(NH3)	21.6	C	C	74-1079	0	44	34	-0.060	3.69	I41/amd (141)	7.222	7.222	17.420	8		26788
Tantalum Carbide	CTa	21.6	C	C	65-8264	0	3	11	0.000	17.75	Fm-3m (225)	4.413	4.413	4.413	4		
Potassium tartrate bis(1,4,7,14,17,20,28,35-octaoxa[2(3.29)...	C56H60O16IC4H4...	21.9	+	X	31-1856	0	33	10	0.000	0.20	C2 (5)	26.079	14.575	16.758	4		
Hafnium Vanadium Nitride	Hf3V2N5	22.2	C	C	65-9260	0	3	14	0.040	10.90	Fm-3m (225)	4.415	4.415	4.415	8		
4-Chloro-2-methyl-isonitroso-acetanilide	C9H9ClN2O2	22.2	+	D	19-1511	0	21	82	-0.100		P21/c (14)	9.770	15.340	7.366	4		
Moganite	SiO2	22.7	+	X	52-1425	1	26	72	-0.100		I2/c (15)	8.758	4.869	10.717	12		
Indium Hafnium	HfIn2	23.0	C	C	65-7664	0	19	15	0.020	18.60	P4/mmm (123)	4.360	4.360	4.510	1.33		
Tantalum carbide nitride - $-delta	TaC0.275N0.218	23.4	C	C	89-3691	0	3	15	0.060	19.43	Fm-3m (225)	4.416	4.416	4.416	4		44356
Taxinine	C35H42O9	23.6	+	X	50-1999	0	30	37	0.100		P212121 (19)	9.859	29.179	11.352	4		
Betaine maleic acid	C5H11NO2I(CH2)2...	29.9	+	D	44-1588	2	76	89	-0.020		Pnma (62)	26.505	6.687	6.378	8		
Cobalt guanidinium sulfate hexahydrate	C2H12CoN6O8S2I...	30.9	+	D	52-2095	2	55	82	-0.060	1.20	P21/c (14)	10.079	7.654	12.021	2		
Dichloroglyoxime	C2H2Cl2N2O2	34.4	+	D	54-1590	3	78	89	0.020		P-1 (2)	5.998	9.947	5.131	2		
Magnesium Vanadium Molybdenum Oxide	Mg15V6Mo6O48	34.8	+	C	44-0607	0	151	89	-0.040	1.86	Pnma (62)	5.051	10.345	17.468	1		
Barium heptaoxodivanadate	Ba2V2O7	35.3	C	C	76-0612	0	146	89	-0.020	1.60	P-1 (2)	13.571	7.320	7.306	4		34320
Magnesium Vanadium Molybdenum Oxide	Mg2.5(VMo)O8	37.8	C	C	82-2074	0	128	89	-0.040	2.43	Pnma (62)	5.051	10.345	17.468	6		78186
Tamarugite	NaAl(SO4)2I6H2O	37.8	+	D	19-1186	0	53	34	-0.100		P21/m (11)	7.353	25.225	6.097	4		
Guanidinium nitrate(III) hemihydrate	CH6N4O2I0.5H2O	38.1	C	C	87-1452	0	115	89	-0.100	1.03	Fdd2 (43)	18.854	23.938	4.789	16		83191
Dibarium copper catena-phosphate	Ba2Cu(PO3)6	40.7	C	C	70-0858	0	139	89	-0.120	2.04	P21/a (14)	21.382	7.286	9.520	4		1868
3-t-Butyl-5-(2,4-dichlorophenyl)-1-phenyl-4-(1,2,4-triazol-1-yl)	C21H21Cl2N5	41.8	+	D	50-2022	0	76	37	0.120	1.31	P212121 (19)	9.509	18.241	24.459	8		
Zinc molybdate	ZnMoO4	42.9	C	C	72-1486	0	143	70	-0.120	1.88	P-1 (2)	9.625	6.965	8.373	6		17030
Sodium Borate	Na2B6O10	43.7	C	C	70-1446	0	145	82	0.100	0.57	P21/c (14)	8.990	11.033	12.107	6		2777
Sulfamerazine	C11H12N4O2S	45.9	+	X	43-2000	0	74	25	-0.060		Pbca (61)	9.145	11.704	22.884	8		
Sodium dichromate(VI)	Na2Cr2O7	47.3	C	C	70-1304	0	150	82	-0.080	0.81	A-1 (2)	7.820	10.360	9.540	4		2534

St-XRD-9

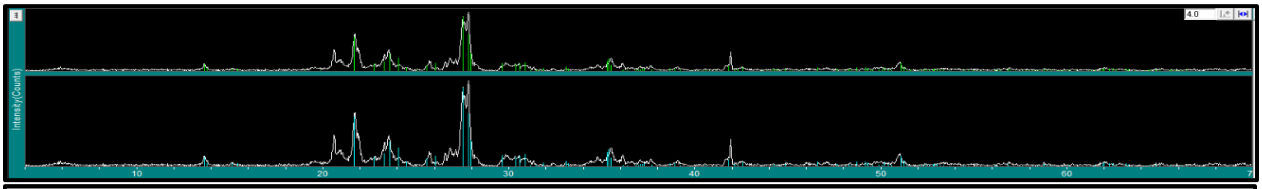

25 Hits Sorted on Figure-Of-Merit	Chemical Formula	FOM	J	D	PDF-#	Hits	#d/I	I%	2T(0)	RIR	Space Group	a	b	c	Z	G	CSD#
Anorthoclase	(Na0.75K0.25)(AlSi...	4.9	C	C	75-1632	1	146	87	-0.060	0.60	C-1 (2)	8.252	12.936	7.139	4		31182
Poly(pyromellitimide phenyl ether)	(C22H10N2O5)n	6.1	+	C	54-2400	0	3	10	-0.080			6.580	4.750	31.200			
Albite high (K-bearing)	(K0.22Na0.78)(AlSi...	6.3	C	C	83-1658	1	146	94	0.000	0.62	C-1 (2)	8.144	12.989	7.160	4		100558
Albite high	K0.2Na0.8AlSi3O8	6.4	C	C	83-2215	1	146	94	0.000	0.62	C-1 (2)	8.144	12.989	7.160	4		200359
Anorthoclase	(Na0.85K0.14)(AlSi...	6.4	C	C	75-1634	4	145	80	-0.040	0.60	C-1 (2)	8.217	12.917	7.126	4		31184
Tungsten Selenide	WSe2	6.4	+	D	38-1388	0	17	7	-0.020		P63/mmc (194)	3.286	3.286	12.983	2		
Albite (heat-treated)	Na(AlSi3O8)	6.9	C	C	89-6430	0	141	77	-0.100	0.66	C-1 (2)	8.152	12.831	7.110	4		87661
Albite calcian low	(Na0.75Ca0.25)(Al...	7.0	C	C	76-0926	1	141	70	-0.040	0.58	C-1 (2)	8.169	12.851	7.124	4		34916
Cesium-doped polyacetylene	[(CH)Cs0.167]n	7.2	+	D	46-1879	1	15	10	-0.060		P41212 (92)	9.093	9.093	7.952	24		
Anorthite sodian	Na0.48Ca0.52Al1....	7.3	C	C	85-0878	0	133	68	-0.060	0.59	C-1 (2)	8.176	12.841	14.207	8		30124
Andesine	Na0.622Ca0.368Al...	7.5	C	C	83-1938	1	146	75	-0.020	0.57	C-1 (2)	8.178	12.865	7.109	4		100867
Labradorite	Na0.45Ca0.55Al1....	7.6	C	C	78-0433	1	146	74	-0.100	0.58	C1 (1)	8.170	12.860	7.110	4		61328
Anorthoclase	(Na0.667K0.333)(A...	7.6	C	C	75-1630	1	138	87	0.020	0.61	C-1 (2)	8.290	12.966	7.151	4		31180
$GB-Hexanitrohexaazaisowurtzitane	C6H6N12O12	7.6	+	D	52-2432	3	30	9	-0.020		Pca21 (29)	9.652	11.644	13.002	4		
Andesine	Na0.685Ca0.347Al...	7.7	C	C	83-1939	1	144	75	-0.020	0.59	C-1 (2)	8.178	12.865	7.109	4		100868
Labradorite	Ca0.64Na0.35(Al1....	7.7	C	C	83-1371	0	144	75	-0.080	0.57	C-1 (2)	8.151	12.829	7.103	4		100236
Labradorite	Na0.45Ca0.55Al1....	7.9	C	C	78-0434	0	146	74	-0.100	0.58	C-1 (2)	8.170	12.860	7.110	4		61329
Cristobalite low	SiO2	8.0	C	C	71-0785	0	31	36	-0.020	5.07	P41212 (92)	4.978	4.978	6.948	4		9327
Anorthoclase	(Na0.7K0.3)(Al1.02...	8.1	C	C	76-0803	1	143	72	0.020	0.63	C-1 (2)	8.300	12.953	7.149	4		34742
Iron Phosphide Sulfide	FePS3	9.7	C	C	65-1227	0	73	7	0.040	2.75	C2/m (12)	5.934	10.280	6.772	4		
Andesine sunstructure	(Ca.38Na.62)(Al1.3...	10.7	C	C	79-1254	0	144	81	-0.060	0.58	C-1 (2)	8.151	12.829	7.103	4		66240
Labradorite	Na0.45Ca0.55Al1....	11.2	C	C	78-0435	1	146	68	-0.060	0.59	C-1 (2)	8.170	12.860	7.110	4		61330
Microcline, intermediate	KAlSi3O8	13.1	+	F	19-0932	0	79	81	0.120		C-1 (2)	8.560	12.970	7.210	4		
Tridymite, syn	SiO2	13.2	C	C	86-0681	0	109	31	0.100	1.34	C1 (1)	15.021	8.600	16.434	48		81382
Indium Phosphorus Sulfide	In2P3S9	23.1	C	C	71-0322	2	140	5	0.020	3.35	P21/c (14)	6.842	10.528	18.266	4		1700